Smart Thinking. New Materials. Sustainable Future.

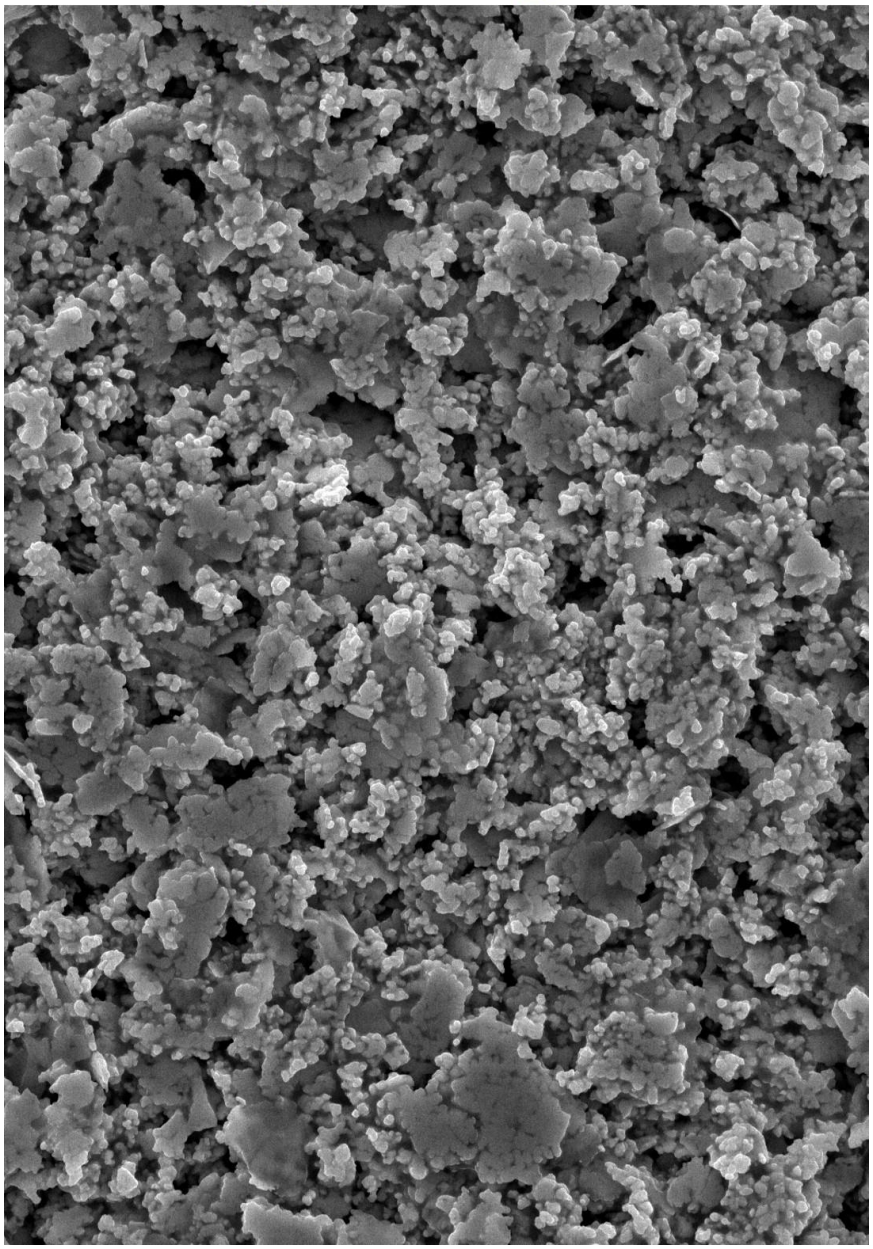

GREEN CONDUCTIVE INKS FOR FLEXIBLE ELECTRONICS

ABSTRACT

Sensors in healthcare, manufacturing, and other control systems have helped modernize, secure, and interconnected society. Machine learning, artificial intelligence, and robotics are the fastest-growing sensor sectors. In wearable electronics, biosensors, and soft robotics, high production costs, inflexible and expensive materials, and insufficient sensitivity have limited their use. Designers can use inks to create cutting-edge products for 5G communications, cars, advanced packaging, and healthcare devices. Green chemistry and biomaterials enable eco-friendly, printable, elastic, stretchy, and biodegradable materials for fabricating sensors that can be recovered and reused, lowering the amount of e-waste.

This thesis creates bio-based conductive inks for flexible electronics. The best features of the inks presented are their excellent electrical conductivity, adaptation to various printing method designs, good shelf life stability, noticeable adhesion to a wide range of substrates, and excellent durability, aiming to improve sustainability, reduce costs and fabrication complexity, and enhance mechanical, electrical, and thermal properties.

Maedeh Najafi

PHD PROGRAM IN BIOENGINEERING AND ROBOTICS

UNIVERSITY OF GENOVA

PHD PROGRAM IN BIOENGINEERING AND ROBOTICS

Green Conductive Inks for Flexible Electronics

By

Maedeh Najafi

Thesis submitted for the degree of *Doctor of Material Sciences* (35° cycle)

February 2023

Supervisor: Athanassia Athanassiou/ **Co-Supervisor:** Ilker s. Bayer

Head of the PhD program: Paolo Massobrio

Dibris

Department of Informatics, Bioengineering, Robotics and Systems Engineering

iit SMARTMAT ISTITUTO ITALIANO DI TECNOLOGIA SMART MATERIALS

Italian Institute of Technology, Smart Materials Group

I would like to dedicate this thesis to women in science who are leading ground-breaking research across the world. It is my sincere wish that one day we will live in a world where girls are inspired to pursue science, where women have adequate support to balance the commitments of research and motherhood, and where scientists are judged purely on the merit of their discoveries and the potential of their work to change the world. The world requires science, and science requires women.

And with honour to all the brave women of Iran...

Maedeh Najafi
February 2023

Abstract

The widespread use of sensors in healthcare, manufacturing, and other control systems has attributed to the path towards a modern, safe, and interconnected society. Among the various sectors where sensors are gaining prominence, machine learning, artificial intelligence, and robotics are the most rapidly expanding ones. To date, however, issues including high production costs, inflexible and expensive materials, and insufficient sensitivity have limited their use in fields like wearable electronics, biosensors, and soft robotics. Inks enable designers to make cutting-edge goods in a wide variety of industries and fields, from 5G communications and automobiles to advanced packaging and healthcare devices. Biomaterials and green chemistry manufacturing have opened up a world of eco-friendly, printable, elastic, stretchy, and biodegradable possibilities. In addition, sensors are undergoing a significant transformation toward materials that can be recovered and reused, lowering the amount of e-waste.

This thesis aims to create novel conductive inks from bio-based materials that could be applied in the flexible electronics field. The best features of the inks presented are their excellent electrical conductivity, adaptation to various printing method designs, good shelf life stability, noticeable adhesion to a broad range of substrates, and excellent durability, aiming to improve sustainability and reduce costs and fabrication complexity as well as enhance mechanical, electrical, and thermal properties.

Key-words: Flexible electronics, Green electronics, Wearable electronic, Strain sensor, Bio polymer, Vitrimer, Conductive fillers

Table of Contents

List of Figures

List of Tables

List of Abbreviations

- EEE: electrical and electronic equipment
- WEEE: waste of electrical and electronic equipment
- PE: printed electronic
- R2R: roll to roll
- SEM: scanning electron microscope
- SEM-FIB: focused ion beam-scanning electron microscope
- EDS: energy dispersive X-ray spectroscopy
- FTIR: fourier transform infrared
- TGA: thermogravimetric analysis
- DTG: derivative thermogravimetry
- DTA: differential thermal analysis
- DSC: differential scanning calorimetry
- DMTA: dynamic mechanical thermal analysis
- BOD: biochemical oxygen demand
- DLS: dynamic light scattering
- XRD: X-ray diffraction
- NMP: N-Methyl-2-pyrrolidone
- DMF: Dimethylformamide
- DMSO: Dimethyl sulfoxide
- THF: Tetrahydrofuran
- IPA: 2-propanol
- Span 65: sorbian tristearate
- Span 20: sorbitan monolaurate
- Tween 65: polyoxyethylenesorbitan tristearate
- Tween 85: polyoxyethylenesorbitan Trioleate
- Tween 80: polysorbate 80
- Span 85: Sorbitane trioleate
- ESO: epoxidized soybean oil
- DBEDT: diboronic ester dithiol
- AgF: Silver flakes

Statement of Original Authorship

I hereby declare that except where specific reference is made to the work of others, the contents of this dissertation are original and have not been submitted in whole or in part for consideration for any other degree or qualification in this, or any other university. This dissertation is my own work and contains nothing which is the outcome of work done in collaboration with others, except as specified in the text and Acknowledgements. This dissertation contains fewer than 65,000 words including appendices, bibliography, footnotes, tables and equations and has fewer than 150 figures.

Signature: Maedeh Najafi

Date: 27/02/2023

Acknowledgements

First and foremost, I must express my wholehearted thanks to my parents and family for their assistance and support. Without their patience and kindness, I am assured that this work would never have materialized.

I am grateful to my supervisor, Dr. Athanassia Athanassiou, who has always been generous during all phases of the research. I greatly appreciate the efforts made by Dr. Ilker S. Bayer, Dr. Pietro Cataldi, and Dr. Arkadiusz Zych. I am grateful to those who worked hard with me throughout the entire process of the current research.

I would like to take this opportunity to express my sincere gratitude to all of my dear friends for their unwavering support along the way in doing my Ph.D.

I also would like to give my sincere appreciation to Milad Safarpour and Dr. Leyla Najafi for the kind assistance they gave me throughout my life, notably during the process of obtaining my Ph.D. Their unconditional love gave me the opportunity to finish this thesis.

Chapter 1: Introduction

1.1 OVERVIEW

Technology and product development in the electronics industry has influenced society, markets, and the environment over the last decade. Electrical/electronic equipment manufacturing is one of the world's fastest-growing production domains[1]. The development of the integrated circuit in 1959 by Jack Kilby and Robert Noyce ushered the electronics industry into a new area, recognized as the primary foundation for the growth of the modern solid-state electronics industry. Since then, Moore's Law[2], which states that every 1.5 years the speed of electronics doubles, is valid and, thus, our electronics device performances are constantly improving and with that, the frequency with which we change them. This factor, together with the use of electronic chips in many industrial, medical, space, and military applications and with the growing demand for electronic devices in developing countries, increased the volume of electronic products drastically. This super rapid and uncontrollable growth of electronics, the ever-increasing needs of consumers, and, as a result, the ever-increasing obsolescence of electronic and electrical equipment on the one side, and the wide variety of chemical elements and materials used in their construction have increased natural resource consumption.[3] In other words, the development and growth of the electronics industry, despite improving people's quality of life, lead to increase in electronic waste (e-waste) and pollution. This issue has adverse environmental and humans effects due to the incorrect and complicated disposal of electrical and electronic waste.[4–7].

In more detail, waste of electrical and electronic equipment (WEEE) consists typically of organic materials, metals, and ceramics with more than 1000 "hazardous" and "non-hazardous" materials. **Figure 1** shows a typical combination of metallic and non-metallic components in a printed circuit board. Apart from non-hazardous metals, high concentrations of toxic substances such as polychlorinated biphenyls (PCBs), polycyclic aromatic hydrocarbons (PAHs), brominated flame retardants (BFRs), dioxins, and heavy metals such as lead, mercury, cadmium, and selenium are all present in a significant amount.[8] Such substances harm the environment and human

health after disposal in a standard landfill or even worse in the environment[8]. Moreover, these wastes include ferrous and non-ferrous metals and plastic, which are 50%, 13%, and 21%, respectively, while the rest is constituted mainly by glass, wood, and ceramics. Metals inside WEEE are basic and precious; as electronic equipment is designed today, it is difficult to separate them. Considering this, scientists have highlighted the opportunity for e-waste recycling. Moreover, since e-waste is rich of precious metals , their recycling can be profitable[9]. In addition, e-waste recycling also can diminish the need to extract new materials and damage the environment[9].

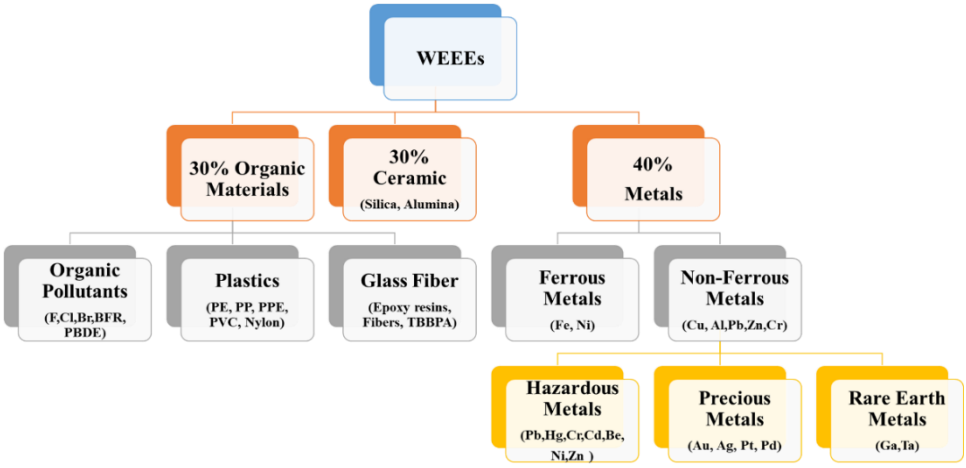

Figure 1. Components of electrical and electronic equipment discarded as waste. PBDES (Polybrominated Diphenyl Ethers) and BFR (brominated flame retardants) are classified as persistent organic pollutants and used as fire retardants.

The production of e-waste is projected to continue to grow at the fastest rate among wastes, with a projected average production of 120 million metric tons per year by 2050[10]. Currently, the worldwide e-waste generation is approximately 53.6 million tons with a production of 4000 tons per hour, which was 49.8 million tons in 2017 divided among continents as shown in **Figure 2**. This issue becomes tangible when we take a glance at our living environment and realize that we use many electronic and wearable devices in our daily life. According to the 2020 United Nations e-waste Global Examiner report, Asia leads internationally with 24.9 million tons, followed by the Americas with 13.1 million tons, Europe with 12 million tons, Africa with 2.9 million tons, and Oceania with 0.7 million tons[8]. In Asia, China and India are the first and the second countries with the most considerable amount of producing electronic waste per year, while their contributions are growing excessively. As an example to this excess and to the growing contribution to the e-waste coming from the developing

countries, India currently produces eighteen times more discarded mobile phones than it did in 2007[8,11,12].

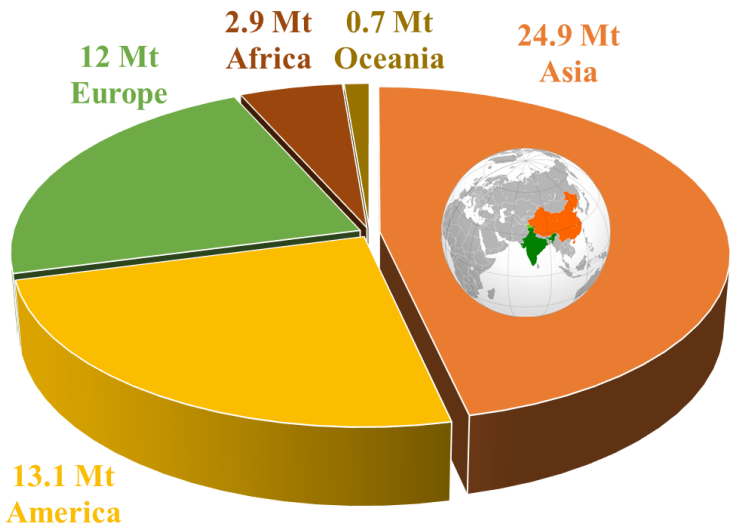

Figure 2. Statistical chart of countries' share in electronic waste production.

In order to raise awareness about the damage caused by the disposal of electronic devices, Joe Rush sculpted the G7 leaders' "Mount Recyclemore" from electronic waste in Cornwall prior to the 2021 G7 summit (**Figure 3**). This increasing amount of electronic waste around the world due to the lack of suitable recycling technology requires serious attention to the methods of dealing with this problem. Therefore, it requires fast and correct planning as well as national determination to respond appropriately to electronic waste and correct disposal[6,7,9].

Figure 3. The sculpture is constructed from electronic waste[13].

Given the nature and complexity of electrical/electronic product materials, their energy consumption, and the e-waste they generate, their design and innovation should

incorporate sustainability[14]. In such context, eco-friendliness is becoming a must for electrical and electronic equipment. Looking into the literature, eco-friendly electronics can be defined in its multiple meanings: equipment made with "green" processes, electronics made with materials that reduce environmental and health risks, devices that can be repaired, power-saving devices, end-of-life impact attenuators, etc[15].

In recent years, a significant revolution has started trying to invert the non-sustainable trend that was being established in the electronic industry, where not only enormous amounts of resources are consumed and hazardous substances produced, but also, devices are updated every year, causing the old ones to be discarded and, thus, vast quantities of non-recyclable e-waste to be produced[16,17]. Fortunately, several innovative strategies from a circular economy perspective have been developed, trying to give new life to e-waste through environmentally sound recovery processes[3,18]. Inks enable designers to make cutting-edge products in a wide range of industries and fields, from 5G communications and automobiles to advanced packaging and medical devices. Bio-material production and green chemistry have made it possible to make things that are green, printable, flexible, stretchable, and degradable in the environment.

1.2 GREEN ELECTRONICS

The considerable demand for electronic devices is causing an energy consumption imbalance and a progression of harmful outcomes: (i) the production of an enormous amount of e-waste; and (ii) an exponential rise in the utilization and depletion of natural elements, like indium and gallium. Both of these problems are exacerbated by the fact that the need for electronic devices is increasing. The toxic substances in e-waste are not only causing damage to the environment but are also harmful to humans. Reducing, reusing, and recycling are three of the most common approaches to managing electronic waste[19]. The diversity of electronic wastes, which are currently considered as one of the most complex waste streams, has largely hindered progress in finding a solution towards the e-waste problem. This is due to the wide variety of products on the market, where the recovery of electronic waste is a difficult issue because of variances in product models, sizes, compatibility problems, and other specifications, as well as variations in the materials and components

used[20,21]. In spite of the fact that recycling can positively affect the economy and tackle the issue of scarcity of raw materials through the reuse of the metals in e-waste, it is not a long-term solution. In other words, recycling can be accomplished for e-waste issues only to a certain extent[20]. As the world moves toward a more sustainable future, despite the fact that technologies have progressed rapidly in terms of miniaturization and computing power, the materials used in electrical and electronic equipment have remained unchanged over the past three decades[22]. As a result, it suggests a need to develop a new electronics class that is environmentally safe, low-cost, and disposable[23,24]. Here is where green electronics enter the picture. Green electronics are a more viable solution to compensate for the issues that cannot be solved by recycling alone, and they contribute to making the world more sustainable. "Green" electronics expresses not only a novel scientific term, but it is also an emerging area of research focused on finding compounds of natural origin and trying to establish economically efficient paths for producing synthetic materials that possess pertinency in environmentally safe (biodegradable) and/or biocompatible devices[19,25–28]. The term "green" electronics was coined in 2005 by a group of researchers at the University of California, Santa Barbara[24].

The field of green electronics tries to deliver on its original goal of making devices through materials with minimal cost and high efficiency in terms of energy use while also working toward accomplishing various functionalities for electronics that help interface them with the real world[29,30].

Moreover, green electronic products in developed or developing countries that are facing the e-waste management problem, can be an excellent solution to increase human health and prevent environmental damage[31].

Biodegradable electronics are a new type of "green" electronics that can be used for a certain length of time and then broken down into harmless components. More specifically, the EN13432 standard defines biodegradability as the property where fungi or microorganisms can turn at least 90% of the compound into water, carbon dioxide, and biomass in six months under certain temperature conditions, humidity, and oxygen. With this quality, such systems can be safely integrated into the surrounding environment or the human body in the future[32].

The biodegradable properties of the electronics will not only solve the problem of electronic waste but also allow them to be used in a wide range of areas, such as

packaging and biomedical implants[33]. When biodegradable electronics decompose after their intended life span, the costs and health risks associated with managing and recycling hazardous waste streams decrease[3]. Many devices on the market today need new technologies that can decompose physically or stop working at the end of their operational term. So, developing biodegradable electronics could also make a massive difference in the quality of the technologies which designers use today[34]. In the biomedical field, for instance, electronics are not utilized much in vivo because of the risks that come with long-term implants. Even though they have a lot of potentials to solve many medical problems, such as by acting as implanted sensors, the long-term health risks of permanent implants and the need for surgery to remove them are still significant problems[32,35]. To overcome this problem, more work must be done to make green electronics so that living organisms can decompose. Because these devices are only there briefly, they can work as electronic medical diagnostic and therapy devices that can be implanted. This means they lack the long-term side effects that arise with permanent implants[32]. Moreover, some biodegradable electronics, like those made of paper and silk, are more flexible than traditional electronics[36,37].

Biodegradable components and environmentally friendly manufacturing techniques make green electronics efficient in managing electronic waste. Greenization, along with micro miniaturization, integration, and multi-functionalization, is one of the most basic movements affecting the future e-market. Fortunately, research communities are conscious of the significance of eco-friendly electronics and have taken steps to achieve this objective[3].

1.3 FLEXIBLE ELECTRONICS

Flexible electronic devices are required for applications involving unusual interfaces, such as soft and curved biological systems, where traditional silicon-based electronics encounter mechanical mismatches[36]. Flexible electronics, also known as printable or organic circuits, are made by depositing electronic devices onto flexible substrates[38]. Flexible and wearable electronics devices have recently demonstrated considerable application potential in the Internet of Things (IoT), sensor, energy, biomedical systems, artificial intelligence (AI), and smart robots. Flexible electronics have many advantages over traditional electronic equipment, such as portability, flexibility, extensibility, low manufacturing cost, unique deformability, and so on[39].

Flexible electronics are attractive for a new generation of electronic devices such as smartphones, soft robotics, touch sensors, or bionic devices[9]. This thesis elaborates on the preparation materials and fabrication of wearable and flexible sensors and their applicability while discussing the ideas of sensory mechanisms based on strain or pressure.

Flexible and wearable sensors are designed to be integrated into daily life. Researchers can use flexible sensors to convert external forces into electrical signals, perform signal processing, and incorporate flexible sensors into wearable products to monitor human body indicators in real time and accurately[40,41].

The widespread use of sensors in healthcare, manufacturing, and other control systems has contributed to the path toward a modern, safe, and interconnected society[3,18,24]. Sensors are becoming increasingly crucial in numerous fields, especially those overgrowing, like machine learning, artificially intelligent systems, and robots[42–47]. Traditional and flexible sensors are made using entirely different materials and techniques. Flexible substrates must be used with flexible sensors. They have strict requirements for electrical conductivity, cannot be processed at high temperatures, and need to maintain stable performance when bent, folded or exposed to continuous cyclic strain/pressure. Flexible sensors have unique properties depending on the fabrication methods. They also operate differently from conventional sensors regarding factors like changing the conductive network between overlapping nanomaterials, the tunnelling effect, crack propagation, and other aspects[48,49]. To date, however, their use in areas like wearable electronics, biosensors, and soft robotics has been limited so far because of aspects such as high production costs, inflexible and expensive materials, and insufficient sensitivity[50–54].

Conductive inks are one of the most promising methods for the production of flexible sensors due to their potential low cost, high throughput, completely additive nature, relatively low-temperature processes, and the creation of complex patterns without plating, masking, or etching. The use of biomaterials such as regenerated proteins, hydrogels, and biopolymers in flexible electronic devices can increase their compatibility with environmental requirements. This research is designed to create novel conductive inks from bio-based materials that could be implemented in the flexible electronics field. The best features of the inks presented are their excellent electrical conductivity, adaptation to various printing method designs, good shelf life

stability, noticeable adhesion to a broad range of substrates, and excellent durability, aiming to improve sustainability and reduce costs and fabrication complexity as well as enhance mechanical, electrical, and thermal properties.

1.4 GREEN FLEXIBLE ELECTRONICS

Green flexible electronics are electronic devices that are both environmentally friendly and flexible[37]. These devices are typically created from flexible, sustainable materials like biodegradable polymers such as polylactic acid (PLA), poly hydroxyl alkanoates (PHA), and polybutylene succinate (PBS) or organic materials like conductive polymers that can be printed or moulded into various shapes[39,55,56]. They can be used a wide range of applications, including wearable electronics, solar panels, and energy storage devices. They are appealing to manufacturers who want to create more sustainable and innovative products because they are flexible and can be easily integrated into a wide range of products[31].

Green flexible electronics have a lower environmental impact than traditional electronics, which is one of their main advantages. They are usually made of renewable or biodegradable materials, which means they can be easily recycled or disposed of without causing any environmental damage[57,58].

Furthermore, green flexible electronics are frequently designed to be energy-efficient, reducing the amount of electricity required to power the device. This contributes to the conservation of natural resources and the reduction of greenhouse gas emissions[17].

Green flexible electronics typically include a number of components, such as: the foundation layer on which electronic components are constructed is known as a substrate. The substrate for green flexible electronics is typically made of flexible and sustainable materials, like organic or biodegradable materials. Conductors are materials that permit the flow of electricity through them. Conductors are typically made of materials like silver, copper, or carbon nanotubes in green flexible electronics. Semiconductors are materials that can conduct electricity under certain conditions. Semiconductors used in green flexible electronics are typically made of organic materials like polymers or small molecules. Dielectric materials are compounds that can shield electronic components from interfering with one another. Dielectric materials are typically created from renewable resources like cellulose or

nanocellulose in green flexible electronics. Materials for encapsulation are used to protect electronic components from environmental factors like moisture and dust. Encapsulation materials for green flexible electronics are typically created from sustainable resources like glass or biodegradable polymers[59–61].

1.5 CONDUCTIVE INKS

Structurally, Conductive ink is a medium- to low-viscosity thermoplastic paste used to carry electricity from point A to point B. The ink is usually made up of three or four parts. The binder keeps everything together and serves as the product's backbone. The conductor is the functional component of the ink and allows electricity to flow through; the solvent dissolves the ink and determines the material's drying and working conditions; optionally, surfactants are added to the material to make it more compatible with the printing process and substrates. In greater detail, conductive ink acts as an interface to connect conductive paths. In particular, these materials are known as suspensions of conductive nanomaterials in water or a solvent medium, produced by adding a surfactant or polymer, and have a stabilizing role. Conductive inks evaporate quickly after deposition and do not dry rapidly in the print head nozzles when idle for a short period[62–67]. These nanomaterials should be smaller than hundreds of nozzle sizes to prevent clogging of the print head. As mentioned before, conductive inks have different types that should have characteristics such as ideal conductivity, simple formulated, low cost, good printability, low viscosity, good stability, good adhesion to the substrate, and high electrical conductivity after printing and processing. Apart from this, to have a uniform coated layer, conductive ink needs to be compacted and dried on the surface of the substrate. Conductive inks are widely used in various electronic applications such as organic light-emitting diodes (OLEDs), organic and inorganic photovoltaics, touch interfaces (HMI), soft machines and robots, bendable circuits, flexible NFC tags, flexible displays, radio frequency identification (RFID), health devices, thin film transistors, solar cells, sensors, smart textiles, batteries, memory components, and antennas are used. Due to the comprehensive capabilities of these materials, it is expected that the market value share of these materials will increase by 2026[67].

1.5.1 Required properties of conductive inks

Stretchable circuit fabrication is generally difficult since it includes patterning electrically conductive lines on a stretchable substrate and connecting the sensor with circuits for power transmission, signal conditioning, and data collecting from the device's surface. Although more improved techniques for patterning electrical lines on flexible and stretchable substrates have recently been developed, a fully stretchy device is still not feasible[68].

Because of the role that conductive inks play in integrating the various components of the devices, they are considered to be of utmost significance in fabricating any stretchy, flexible, and wearable electronic applications[69]. The conductive substance is widely regarded as the single most critical component in the production of conductive ink. The selection of conductive materials is determined by the physical properties of the pattern that will be printed, such as its level of adhesion with the substrate, and the desired physiochemical properties of the inks, including their level of compatibility with the printing procedure. This includes limitations on the size of the nozzle used for printing nanoparticles and restrictions on aggregation (to avoid clogging), stability, rheology, and electrical and mechanical properties[70]. The essential requirements for conductive inks are outlined in **Figure 4**.

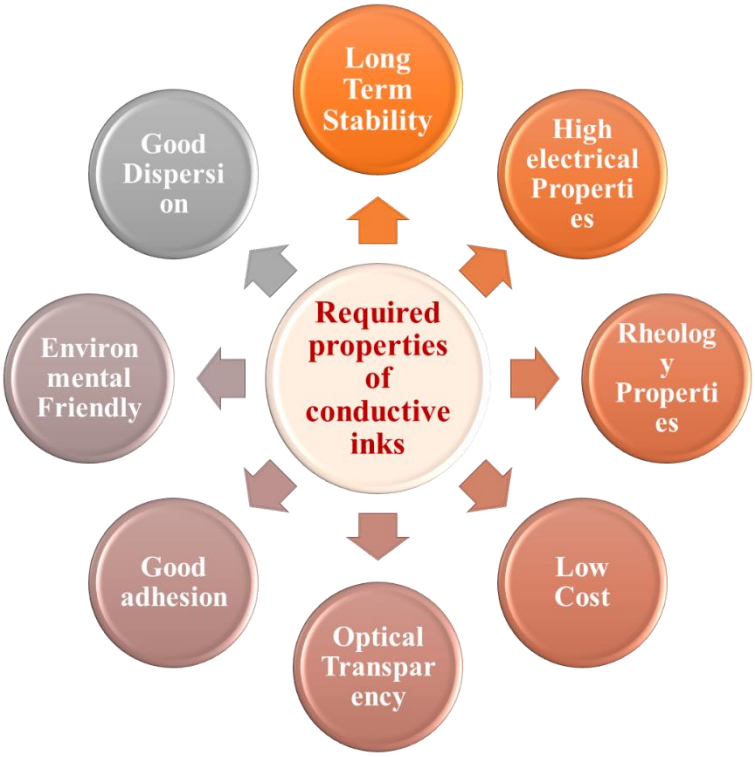

Figure 4. The essential requirements for conductive inks.

A stable ink is an ink whose properties remain constant over time. For inks that do not have undissolved substances, instability is usually caused by interactions between ink components, sedimentation, and phase separation. The effect of changing the solubility (for instance, changing the temperature during transportation and storage) and even the interaction with the walls of the container containing the ink, for example, the penetration of the wetting agent from the ink to the polymer walls of the container can lead to an increase in surface tension or partial polymerization of monomers during be stored, which can lead to an increase in ink viscosity[71].

It should be emphasized that to achieve a stable ink dispersion; one must evaluate the various suspending agents and find their optimal concentration. The quality of the suspending agent is essential; there is an optimal concentration of the suspending agent, which is determined through measurements of dimensions and viscosity. The viscosity of the suspension system usually decreases with the increase in the concentration of the suspending agent, of course, up to a certain concentration; after that concentration, the viscosity increases. This increase can result from the dissolving of the free polymer suspension in the liquid medium[72]. Nevertheless, one possibility for improving the ink stability is using a high viscosity at room temperature to prevent particle settling.

Surface tension or surface energy expresses the characteristic that any liquid surface imposes mechanical stress on the environment or another phase or medium to minimize the dimensions of the interface with that environment. The reason for the formation of liquid drops is the same tendency to minimize the contact surface, because a spherical shape has a minor character among conditions of the same volume. Therefore, the ink's surface tension is a primary factor in determining the formation of an ink droplet and its spreading on the substrate. As we know, with the reduction of the dimensions of a particle, the ratio of its surface area to its volume increases as the ratio R (the radius of the sphere) increases, so we expect surface effects to be more visible in these particles. One of these features is surface energy, which increases with decreasing particle dimensions. That is, even though by reducing the dimensions we expect that the suspension of these particles in the solvent will be easier, due to the increase in surface energy, the particles will attract each other and stick to each other, making the suspension difficult. The surface tension can be controlled by using surface activating agents or surfactants and choosing the appropriate solution composition. For

example, adding propanol to water results in a drastic decrease in surface tension from 72.8 dyne/cm to 30 dyne/cm. A significant decrease in surface tension by adding co-solvents is usually achieved at high co-solvent concentrations[73,74].

1.6 SUBSTRATES IN FLEXIBLE ELECTRONICS

As a result of the demand for flexible and wearable electronic applications, there has been a rise in interest in application systems that are bendable, foldable, lightweight, and smart. Scientists are focusing more on inventing various manufacturing techniques for mass producing high-quality electronic devices on low-cost and flexible substrates that can be stable when folded, bent, or twisted[75]. Every substrate that is used for flexible and wearable sensors needs to comply with certain necessary characteristics. These characteristics include being thermally stable, having a low coefficient of thermal expansion, having a low cost, being flexible, being resistant to moisture and gas, having transparency, and having a high volume area[76].

To date, flexible and elastic substrates for printed electronics have been made out of thin glass, metal foils, paper, polymer, and textile fabrics, among other materials. In spite of the fact that thin glass structures that are capable of good bending are taken into consideration to be viable possibilities for substrates, the brittle nature of glass prevents it from being utilized in the production of stretchy and flexible electronic devices. On the other hand, metal foils and tapes have the ability to withstand high temperatures and have good flexibility; however, due to their cost, they are not suited for use in electronics that are both cheap and flexible[77]. The main advantages of utilizing polymer, paper, and textile substrates in flexible and stretchable electronic are summarized in **Figure 5**.

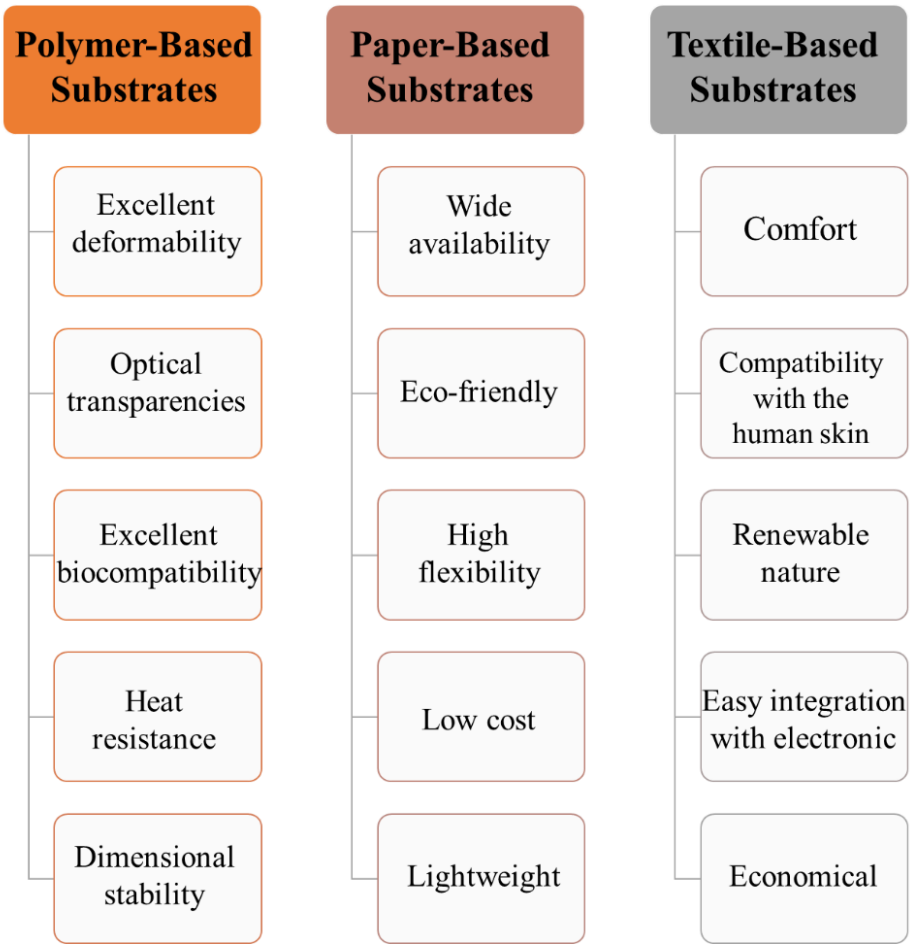

Figure 5. The main advantage of using polymer-, paper- and textile-based substrates in the flexible and stretchable electronic.

1.7 PRINTING AND DEPOSITION TECHNIQUES

For flexible, elastic, and wearable electronic applications, numerous printing processes have been developed. Deposition and patterning technologies are the most amazing achievements for advanced lean development. Apparently, coating and patterning are the two main deposition and patterning techniques that have been used to create flexible electronic devices. The choice of deposition processes is reliant on numerous variables, including the uniformity of the deposited film or the consideration of material waste. It depends on the thickness as well. For instance, organic solar cells require a thickness in the range of a few hundred nanometres, whereas dye-sensitized solar cells can have a thickness in the range of micrometres, and there are a variety of thicknesses that can be obtained depending on the technique.

Aside from this, consideration must be given to the choice of deposition technique, as the morphology of the deposited film can vary depending on factors such

as the rate of solvent evaporation in the case of solvent-based techniques such as spray coating, the deposition rate, and post-processing steps such as annealing for metal-based conductive fillers. The solubility and polarity of the material, as well as whether the system is composed of a single or hybrid material, must be taken into account while selecting the appropriate procedures. In the case of deposition techniques, the form and dimensions of the substrate, as well as its surface characteristics such as roughness and wettability, might also influence our selection[78–80]. From such a perspective, **Table 1** provides a summary of benefits and drawbacks of main techniques that used in this thesis.

Table 1. Different used deposition methods, their advantages and limitations[78–80]

Types of techniques	Pros	Cons
Rod Coating	Very simple and efficient approach that can cover a large area, produces no waste, has good uniformity, is fast, and is compatible with the roll to roll technique. Because of the spiral winding, directional printing is possible.	It is not possible to deposit extremely thin films; the thickness is determined by the number of windings of spirals on the rod. The thickness of the deposited layer is determined by a number of variables such as surface tension, wetting, viscosity, and coating speed.
Spray Coating	Air pressure, solvent viscosity, gun tip geometry, solvent properties (evaporation temperature), and the distance between the nozzle and the substrate can all be used to control film thickness and morphology. Depending on whether one or more passes are sprayed, the thickness can be adjusted, and the process is fast and R2R compatible. It is possible to cover 3D surfaces on a wide range of substrates.	The requirement for solvent-based inks can make this method relatively limited. Droplets may dry independently during multilayer coating passes, creating a rough, uneven surface. Material waste is a significant problem with this technology.
Screen Printing	Low setup costs, a very wide variety of materials including fabrics may be utilized, a variety of manufacturing processes can be used, stencils can be easily produced, and flat or curved surfaces can be printed on.	Long drying times, high costs for large runs, and the requirement for a specialized method (UV) to dry ink quickly are among the problems associated with printing ink through this method.

* "Roll to Roll" (R2R) processing has the potential to revolutionize large area electronics production including mass producing solar roofing panels, large area solid state lighting devices, x-ray imagers, and flexible flat panel displays[81].

1.8 APPLICATIONS

In flexible and wearable electronic systems, printed electronics has certain significant applications, as presented in **Figure 6**. Electrochemical cells, antennas, photodetectors, electrochemical sensors, solar cells, strain sensors, wearable skin sensors, flexible light-emitting electrodes, and super capacitors are some of these[82–89]. Electrical conductivity, high flexibility, stretchability, high durability, biocompatibility, lightweight, and eco-friendliness are only a few of the desirable

qualities for flexible and stretchable electronics, which were discussed in greater detail in earlier chapters[90]. Therefore, the following specific elements need to be carefully considered while printing: (1) the use of a flexible and stretchable substrate that will assist in linking the personal devices with the human body; (2) the use of low-toxicity, soluble, chemically stable, and lower temperature-producible inks for post-treatment and fast printing; and (3) designs that are even and high-resolution for improved electrical characteristics and the integration of lightweight electronics. (4) A unique structure design for the item that helps to prevent it from breaking and slipping about, which contributes to its high use endurance. Controlling these printing processes appropriately and purposefully will, without a doubt, make it easier to design high-performance electronics that are flexible and stretchable[86,91,92].

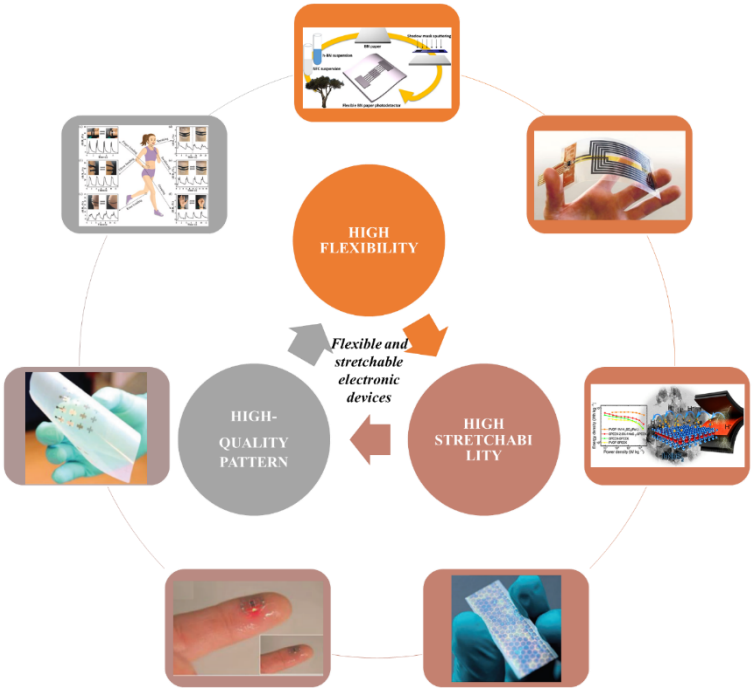

Figure 6. Applications of printed electronics in flexible, stretchable, and wearable electronic devices[82–89].

Considering what was said about the importance of conductive inks in green and flexible electronics and considering that the use of these materials still faces challenges in the electronics industry, in this research, an attempt is made to use biopolymer to improve the performance of conductive inks. Biopolymers can be used in flexible electronic devices due to their biocompatibility with environment, stability, reasonable cost, as well as the ability of the solution process. On the other hand, if biopolymers are used in producing conductive inks, they can be used directly and immersed in a solution as spraying or as a coating on the substrate.

1.9 THESIS SCOPE AND CONTRIBUTIONS

Flexible electronics are electronic devices that can be bent, twisted, or stretched without compromising their functionality. They have applications in areas such as wearable electronics, biomedical devices, and flexible displays.

Green flexible electronics refers to the design and production of flexible electronic devices and systems that are environmentally sustainable and have minimal impact on the natural world. These devices are made using eco-friendly materials that are non-toxic, biodegradable, and/or recyclable. To be considered "green", flexible electronics should also incorporate features that enable efficient use of resources, such as power-saving modes, energy-efficient components, and smart power management systems. By reducing the environmental impact of electronic devices, green flexible electronics can contribute to a more sustainable future.

Green flexible electronics designed with conductive inks offer a more sustainable and versatile option for electronic device manufacturing, with several advantages, including:

Reduced environmental impact: Conductive inks are often made from eco-friendly materials, such as silver nanoparticles or graphene, which are non-toxic, biodegradable, and recyclable. This makes them a more environmentally friendly option compared to traditional electronic manufacturing methods that rely on toxic chemicals and metals.

Flexibility: Conductive inks can be printed on various flexible substrates, such as plastics, paper, and textiles, allowing for the creation of flexible electronic devices that can bend, fold, and stretch without breaking. This opens up new possibilities for wearable devices, medical sensors, and smart packaging.

Lower cost: Printing with conductive inks is more straightforward and cost-effective than traditional manufacturing methods, such as lithography or etching. This makes producing electronic devices in smaller quantities or for niche applications more accessible and affordable.

Faster production time: Conductive inks can be printed quickly and easily using screen printing, inkjet printing, or spray coating techniques. This reduces the time and

resources required for manufacturing, allowing for faster product development and commercialization.

This thesis cover:

1) Development of innovative conductive ink from bio-based materials for use in green flexible electronics.

2) The best features of all formulated inks are their excellent electrical conductivity, adaptability to different printing methods and designs, good stability, noticeable adhesion to a broad range of substrates, and excellent durability.

3) Remarked features are meant to improve sustainability, reduce costs and fabrication complexity, and boost mechanical, electrical, and thermal properties.

Chapter 2: Literature Review

In this chapter, we introduce the state of the art of 1) flexible electronic architectures and materials, 2) flexible strain/pressure sensors, 3) green electronics, and 4) conductive ink.

2.1 FLEXIBLE ELECTRONIC ARCHITECTURES AND MATERIALS

The first steps toward making flexible electronics were taken in the 1960s. The first flexible solar cell arrays were made by making single-crystal silicon wafer cells thinner than ~100 μm and then putting them on a flexible plastic substrate[93]. In the past few decades, the electronics industry has become familiar with a new concept called flexible electronics. Flexibility is generally seen in thin and very long materials such as cables and wires. But the concept of flexible electronics is much more complicated than cables and wiring[94]. Flexible electronics incorporate all the functional properties of conventional rigid electronics in forms modified to survive mechanical deformation. Therefore, understanding the evolution of device performance during bending, stretching or other mechanical operations is essential for research efforts in this field. Recently, the development of flexible electronics has attracted considerable attention. Most researchers are trying to develop devices or techniques that pave the way to adaptive sensors for healthcare applications, electronic skins for versatile and adaptive robots, or flexible analogues of common consumer electronics such as e-readers, cell phones, or televisions. **Figure 7** shows a number of flexible electronic devices such as pressure sensors, a piezoelectric energy harvester, and LED, and skin mountable medical device[94].

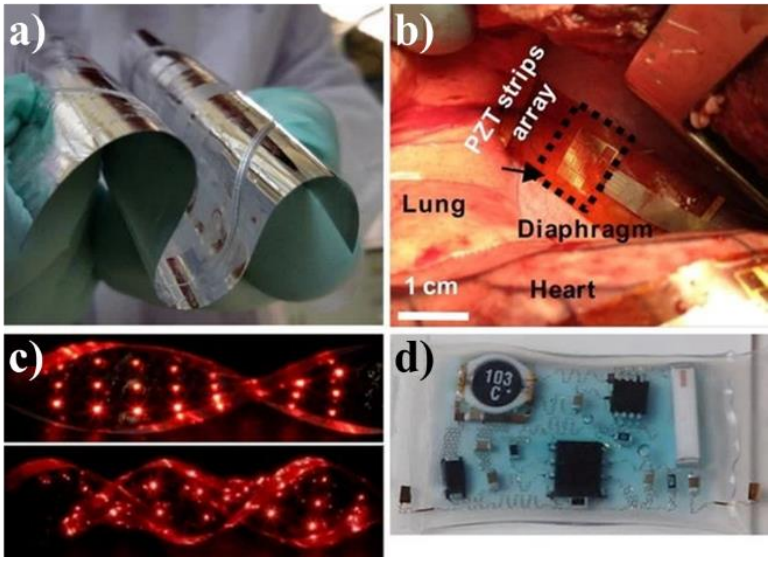

Figure 7. Examples of flexible electronic devices: a) a set of flexible pressure sensors (reproduced with permission), b) an integrated piezoelectric energy harvester, c) a rotatable LED array, and d) a stretchable skin-mountable physiological measurement device[94].

Flexible electronic devices apply electronic materials (organic or inorganic) to flexible substrates[95]. Electronic components, flexible substrates, cross-linked conductors, and sealing layers are the four most common components found in flexible electronic devices[79]. The flexible substrates are the most significant difference between flexible and rigid electronics. Flexible substrates also need to be inexpensive and insulating. As such, the development of flexible electronics puts strong limits on the choice of materials and the manufacturing process of the substrate[96]. Cross-linked conductors link the electronic components to create completely flexible circuits. Each electronic component exists as an isolated device island. Metal conductors are currently the most popular conductors; copper foil is the most common among them due to its low cost, good conductivity, and good ductility. The two most popular kinds of copper foil are electrolytic and rolled, with rolled copper foil having superior conductivity and ductility[97]. The sealing layer protects flexible electronics from dust, water, gases, and mechanical forces. The sealing layer must maintain electrical stability under large bending deformations, and this requirement limits material choice. Acrylic resin, epoxy resin, and polyimide are commonly used, but their chemical stability is insufficient for flexible devices to have acceptable durability[98]. The stretchability and flexibility of flexible electronic devices are also impacted by the sealing layer. Therefore, the sealing layer's structural design needs to be optimized in order for the electronic components to be placed on the sealing

layer's mechanically neutral surface. In the island-interconnect structure, for instance, the proper design of the sealing layer's structure can reduce stress on the edge of the cell island to increase the mechanical toughness of the flexible device and protect the separation of electronic components and flexible substrates from reducing the life span of flexible devices[99]. Different applications for flexible electronic devices have various requirements for the sealing layer. For instance, liquid crystal displays (LCDs) and thin film transistor (TFT) devices have low sealing requirements compared to organic light-emitting diodes (OLEDs), which have high sealing requirements[100].

Flexible or stretchable electronic devices can be produced using different techniques. For example, electrical conductors are deposited by physical vapour deposition (PVD) processes (i.e., evaporation or sputtering), and patterned by shadow mask or simple optical lithography. If a suitable solvent can be identified, the semiconductors are spin coated from solution, or deposited in PVD or chemical vapour deposition (CVD) processes. Insulators are spin-cast from solution or deposited by PVD. In some cases, spin coating is replaced by techniques such as drop casting, rod coating, or guided assembly, and evaporation/sputtering processes are replaced by metal ink casting, CVD, or atomic layer deposition (ALD)[61,94,101–103].

The use of organic materials and nanoscale materials are the best option for increasing the efficiency of flexible and stretchable electronic devices due to their high processing and flexibility[104]. Choi et al[105] stated that high-performance stretchable conductive nanocomposites are ideal options for soft electronics, optoelectronics, and energy harvesting devices. Also, Kamyshny and Magdassi[92] investigated the effect of integrating conductive nanomaterials with inkjet-based production processes in order to increase the performance of flexible electronic devices. Kagan[106] developed perovskite-VI, IV-VI, I-III-VI2 and perovskite metal halide semiconductors for thin film based on how to precisely control the synthesis and assembly of semiconductor nanocrystals for flexible electronic devices.

In particular, Sun and Bao[107] stated that the materials used in flexible electronic devices should have excellent mechanical properties to withstand strain in addition to the main properties such as energy generation, energy storage, and signal sensing / tension or geometric deformation are also large. According to the articles by Wang et al[108,109] the use of innovative structural designs that originate from the existing natural structure and the resulting function can bring new concepts for intelligent functions.

As stated by Chun et al[110], high adhesion and water resistance for wearable electronic devices that can be attached to the skin are requirements of the materials used in these devices. For this purpose, an artificial patch with an octopus-like pattern with high adhesion capability in dry and wet conditions on different surfaces for skin sensors to monitor in vitro and in vivo biological signals can be inspired by the protrusion or infundibulum in octopus suckers.

The study of flexible electronic equipment is the pinnacle of science, mechanical electronic materials and production methods in the field of making circuits on flexible substrates (**Figure 8**). Flexible electronic equipment has the potential to be better than its traditional and rigid counterpart in terms of weight, price and flexibility. The potential applications of flexible electronic devices briefly include paper video displays, such as pseudo-skin smart prostheses and printable thin film solar cells. Flexible displays can be rolled into small volumes, which saves both space and weight[111]. This equipment can reduce the need for bulky and large traditional screens. Rollable screens save space by using them on TV screens, computer monitors and solar panels. A traditional solar panel is usually shaped like a large rigid rectangle; Compared to the flexible solar panel that can be folded into a tube. In addition, the flexibility of the solar panel allows it to take different forms (such as the roof of houses or cars). Also, flexible electronic equipment can be simulated as a sheet of paper. By electronic media which are easily available one can get daily news books and other reading material through wireless communication. Flexible electronic sensors allow the prosthetic skin to bend and straighten like natural skin while providing electrical feedback based on temperature, pressure and humidity[112–116].

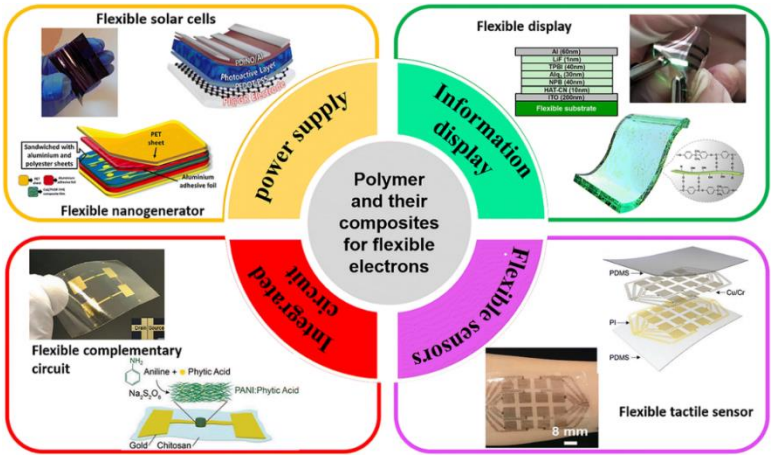

Figure 8. Range of applications for flexible electronic[117]

The above examples show a set of uses of flexible electronic equipment. Flexible electronic equipment differs from traditional electronic equipment in terms of its ability to change shape. Flexible electronic devices tend to use more flexible materials as building blocks, with circuits such as polymers and elastomers that can withstand large deformations without cracking or breaking. Flexible electronic equipment usually includes a large number of microelectronic components integrated on large areas such as display screens. Finally, flexible electronic components have thin profiles to achieve better flexibility and reduce weight[118].

2.2 FLEXIBLE STRAIN/PRESSURE SENSORS

Flexible strain and pressure sensors are a type of flexible electronic device that can detect mechanical deformations such as bending, stretching, and compressing. These sensors have gained significant attention in recent years due to their numerous potential applications, such as in wearable health monitoring[58,119–121], robotic skin[122,123], and human-machine interfaces[124].

The most common materials used in the fabrication of flexible strain and pressure sensors are divided into four categories:

1. Polymers: polymers are widely used as the base material for flexible strain and pressure sensors due to their excellent mechanical properties, low cost, and easy process ability[125,126]. The polymer material can be combined with conductive materials or additives to enable sensing properties, making it possible to detect mechanical changes in the sensors. Apart from this, using polymers as substrate comprises flexibility and therefore overcomes the limitations of conventional rigid electronics. Examples of polymers used in flexible sensors include polydimethylsiloxane (PDMS), polyurethane (PU), polyethylene terephthalate (PET), and polyimide (PI)[127–129].

2. Carbon-based materials: carbon-based materials, such as carbon nanotubes (CNTs), graphene, and carbon black, are also commonly used in flexible sensors. These materials offer high sensitivity, low hysteresis, and excellent mechanical flexibility. They can be easily incorporated into the polymer matrix to form composites with enhanced sensing properties[130–132].

3. Metals: metals, such as copper, gold, and silver, are used in flexible strain and pressure sensors due to their excellent electrical conductivity and good mechanical

properties. They can be deposited on flexible substrates, such as polyimide, by various techniques, including sputtering, evaporation, and printing[131,133,134].

4. Ceramics: ceramic materials, such as zinc oxide (ZnO), aluminium nitride (AlN), and silicon carbide (SiC), are also used in flexible strain and pressure sensors. These materials offer high sensitivity and stability at high temperatures and harsh environments. They can be deposited on flexible substrates by various techniques, including chemical vapour deposition (CVD) and inkjet printing[135,136].

To fabricate flexible sensors, special techniques, and materials should be used to have the same performance and efficiency as conventional sensors[137]. The types of technologies used in the construction of flexible sensors can be surface acoustic wave[138], infrared[139], tensiometry[140], optical imaging (image processing)[141], signal propagation technology, resistive and capacitive sound pulse detection[142]. In the resistive type of these sensors, the touch screen comprises several layers, the most important of which are two metal layers of pressure-sensitive resistive layers separated by a small distance[143].

Several techniques have been employed to fabricate flexible strain and pressure sensors, such as screen printing, inkjet printing, and micro contact printing. These techniques allow for the precise patterning of conductive materials on the flexible substrate, resulting in sensors with high sensitivity, accuracy, and repeatability[144,145].

The performance of flexible strain and pressure sensors has been improved by developing novel sensor designs that enhance their sensitivity, selectivity, and durability. One approach to improving sensor performance is modifying the sensing materials' structure and composition. For instance, researchers have developed composite materials that combine multiple types of conductive materials to achieve superior sensing performance. These composites may include carbon nanotubes, graphene, silver nanowires, and conductive polymers, among others[144].

Another strategy for improving sensor performance is by designing the sensor's architecture. For example, some researchers have developed sensors with multiple layers, each with a different function, such as an electrode layer, an insulating layer, and a sensing layer. This approach can enable a more robust and sensitive sensor with enhanced mechanical properties and environmental stability[146–148].

Furthermore, several advanced signal processing techniques have been employed to enhance sensor performance. Machine learning algorithms, for example, can help to improve sensor selectivity and enable the detection of subtle mechanical deformations that may be missed by traditional sensors. Additionally, smart materials such as shape-memory alloys and ferroelectric materials can be incorporated into sensor designs to enable adaptive sensing capabilities[149–151].

Developing novel sensor designs and integrating them with advanced signal processing techniques has dramatically improved the performance of flexible strain and pressure sensors, enabling their use in a broad range of applications.

2.3 GREEN ELECTRONICS

The concepts of eco-friendly or green electronics encompass various dimensions of this electronic-environmental relationship and have been loosely used for countless initiatives. These concept refer to I) the production process through the use of environmentally friendly processes and avoiding hazardous components or chemicals; II) Waste generation (avoidance) by reducing the effects of e-waste through the use of cleaner materials, longer product life, introducing programs to raise awareness and promote reuse/recycling; III) Using sustainable performance (green computing), through responsible use of computer resources, for example, by turning devices off and on as needed, reducing energy consumption during inactivity. IV) Design is applied by developing more efficient components that require less energy to run, reduce carbon emissions, and generate less heat[152].

Under such a perspective, green electronics, as a rapidly evolving field, has recent developments in different areas, for instance;

1. Development of biodegradable and recyclable electronic materials: Researchers have been exploring new materials for electronic devices that are biodegradable and recyclable. For example, a recent study described the development of a biodegradable polymer-based electronic material that can be recycled and used to make new devices[153].

2. Use of nanomaterials for energy-efficient electronics: Nanomaterials such as graphene and carbon nanotubes are being used to develop energy-efficient electronic

devices. A recent study reported the development of a graphene-based transistor that uses less energy than conventional silicon-based transistors[132].

3. Green manufacturing techniques for electronic devices: Researchers are developing new manufacturing techniques that reduce the environmental impact of electronic devices. For example, a recent study reported the use of a solvent-free printing technique to fabricate organic photovoltaic cells, which reduces the amount of waste generated during production[154].

4. Development of eco-friendly batteries: Researchers are exploring new materials for batteries that are environmentally friendly and sustainable. For example, a recent study reported the development of a sodium-ion battery that uses non-toxic and abundant materials, making it a more sustainable alternative to traditional lithium-ion batteries[155].

Among the new trends in green materials used in green electronics, a new class of advanced electronics, called biodegradable electronics and transient electronics, may represent new and promising strategies for developing environmentally friendly devices[31]. Biodegradable electronics refer to electronic devices or components that are designed to be biodegradable, meaning they can decompose naturally and safely in the environment after their useful life has ended. These devices are typically made from biocompatible and biodegradable materials, such as silk, cellulose, or chitosan[18,23,37]. Transient electronics, on the other hand, are electronic devices or components that are designed to dissolve or disintegrate upon exposure to certain environmental stimuli, such as heat, light, or moisture. These devices are typically made from materials that are soluble or biodegradable, such as magnesium or zinc[156–159].

While both biodegradable electronics and transient electronics are designed to reduce the environmental impact of electronic waste, they have different mechanisms and objectives. Biodegradable electronics are designed to be environmentally sustainable throughout their lifecycle, from production to disposal, while transient electronics are designed to have a limited lifespan and disappear completely once their usefulness is over[37].

From material perspective, as a biodegradable and renewable synthetic material, polylactic acid (PLA) has attracted attention as a potential alternative to conventional petroleum-based plastics in various applications, including green electronics[160–162].

PLA is a biodegradable and biocompatible thermoplastic polyester derived from renewable sources such as corn starch, sugarcane, or tapioca roots[163].

In the field of electronics, PLA has been explored for use in both biodegradable electronics and transient electronics, but its use is more common in biodegradable electronics[164,165]. For example, PLA-based materials have been used to create biodegradable circuit boards[166], sensors[167,168], and batteries[169]. PLA has several advantages, making it a promising material for green flexible electronics. It has good mechanical strength, flexibility, and thermal stability, which are essential properties for flexible electronic substrates[160,162]. It is also transparent, which makes it suitable for use in displays and touchscreens[170]. Moreover, PLA is biodegradable and biocompatible, making it suitable for biomedical applications[171].

Recent research has focused on developing PLA-based materials for various applications in green flexible electronics.

Substrates for flexible electronic devices: PLA has been used as a substrate material for various flexible electronic devices, such as organic light-emitting diodes (OLEDs), thin-film transistors (TFTs), and sensors. The mechanical properties of PLA, such as its flexibility and tensile strength, make it a suitable material for use as a flexible substrate. PLA can also be easily processed into thin films using methods such as spin-coating, dip-coating, or roll-to-roll processing[162,172,173].

Conductive composites: PLA has been used as a matrix material for conductive composites, which can be used as electrodes in flexible electronic devices. Conductive nanoparticles, such as carbon nanotubes, graphene, or silver nanoparticles, can be dispersed in the PLA matrix to improve its electrical conductivity. In addition to improving electrical conductivity, the addition of conductive nanoparticles can also enhance the mechanical properties of the composite material[174,175].

PLA-based conductive polymers: PLA can be combined with other conductive polymers, such as polyaniline, to form PLA-based conductive polymers. The resulting materials have improved electrical conductivity and can be used as electrodes in flexible electronic devices. The use of conductive polymers can also improve the adhesion between the electrode and the substrate, which is important for maintaining the integrity of the device during bending or stretching[176–178].

Biomedical applications: PLA is biodegradable and biocompatible, which makes it suitable for use in biomedical applications. PLA-based materials have been used for the fabrication of flexible sensors for medical monitoring, such as temperature sensors, pressure sensors, and glucose sensors. PLA-based materials have also been investigated as scaffolds for tissue engineering and drug delivery applications[171,179].

Although PLA is a promising material for green flexible electronics due to its biodegradability, biocompatibility, mechanical strength, and transparency, because of the insulated nature of this polymer, it is necessary to be mixed with other conductive polymers or particles. Nevertheless, these approaches can increase the material cost and processing complexity. Another challenge is the limited thermal stability of PLA, which can limit its use in high-temperature applications. Further research is needed to optimize its electrical properties and to develop new PLA-based materials for specific applications in green flexible electronics.

In line with green electronic development, another alternative material with recyclability properties is a new polymer called vitrimers. The term "vitrimer" is derived from the words "vitreous" (meaning glassy) and "polymer." A vitrimer is a type of polymer that exhibits a unique property known as dynamic covalent behaviour. This means the bonds between the polymer chains can break and reform in response to external stimuli, such as heat, light, or mechanical stress[180,181].

Vitrimeric polymers are similar to conventional thermosetting polymers in that they can form a solid, three-dimensional network structure. However, unlike conventional thermosets, vitrimers are not permanently cross-linked and can be reprocessed and reshaped multiple times without losing their mechanical properties[182].

Vitrimers have potential applications in various fields, including coatings, adhesives, and composites. For example, vitrimeric coatings could create self-healing materials that can repair damage in response to external stimuli. In electronics, vitrimers could be used to develop flexible and self-healing electronic devices[182].

2.4 PRINTABLE INKS

Printable inks are typically liquid and are classified as conductive, semiconductive, or dielectric. **Table 2** shows the primary materials for the conventional

approach and bio absorbable alternatives for conductors, semiconductors, and dielectrics[152].

Table 2. Conventional and bio absorbable materials for conductors, semiconductors and dielectrics[152].

Materials	Conductors	Semiconductors	Dielectrics
Conventional	AU	GaAs	Lead zirconate titanate (PZT)
	Ag	SiGe	$BaTiO_3$
	Cu	Si	SiO_2
	Other metals	Ge	
	Conductive polymers	GaN	
		SiC	
		AlN	
Bioresorbable	Zn	ZnO	SiO_2
	Fe	Mono-Si; poly-Si; a-Si	MgO
	Mo	Ge	Si_3N_4
	Mg	$InGaZnO_4$	Spin-on-glass (SOG)
	W	SiGe	Silk

Semiconductive inks have a significant impact on the final device's performance. Semiconductive inks can be inorganic, such as metal oxide based, or organic, used in active devices like Organic Photo Diodes, Organic Light Emitting Diodes (OLEDs), Organic Field Transistors, organic solar cells, and so on[183]. Zinc oxide (ZnO), magnesium oxide (MgO), and silicon nitride (Si_3N_4) are all recognized as having potential as semiconductors to replace more traditional materials[184,185].

Dielectric inks play an essential role in electronics, protecting and enhancing the functionality of conductive materials, allowing for energy storage and operation under a biased voltage. Dielectric inks typically contain organic polymers or ceramics in solvents, insulating 2D nanomaterials such as hexagonal boron nitride and improving thermal and electrochemical stability, which is required for solid-state batteries, field effect transistors, and neuromorphic systems[63].

Conductive inks form the fundamental structure of all printed electronic devices and circuit boards, as well as integrated low-resistance circuit interconnects, antennae, contact electrodes within transistors, and so on. Conductive inks and pastes are also appealing for the fabrication of medical biosensors, such as disposable glucose sensors for diabetic patients and conductive patterns found in photovoltaic cell configurations for the electrodes exposed to light[186]. Conductive inks could contain a wide range of

conductive materials, including conductive polymers, carbon, organic and metallic compounds, metal precursors, and metal nanoparticles, as well as combinations of composite materials[187]. Organic inks are made of organic materials such as polymers[183]. Conductive polymer-based inks have good stretch ability and biocompatibility, essential for printing flexible patterns and making bioelectronics, but their resistivity is relatively high[188]. Conductive polymer-based inks are thus used in batteries, capacitors, resistors, inductors, sensors, electromagnetic shields, and other electronic devices. Carbon nanomaterials like graphene nanoplatelets and carbon nanotubes are also popular because of their unique surface area, chemical stability, and electrical, optical, and mechanical properties[67]. However, they are less conductive than metal particles, making them more appealing for use as electrode materials in printed batteries, supercapacitor, stretchable bioelectronics, and wearables. Metal nano- or microparticles-based inks are the most popular conductive ink category due to the unique electrical properties of metallic species and the high surface-to-volume ratio of nano- or microparticles. These particles have a resistivity similar to that of the bulk material (two to three times higher)[187].

Nan et al[189] developed an environmentally friendly soft ionic actuator using cellulose acetate (CA), graphene Nano powders (GN), ionic liquid (IL), and poly(3,4-ethylene-dioxythiophene)-polystyrene sulfonate (PEDOT: PSS) as an electrode. Ba et al[190] used cotton fabrics coated as a peeling agent to produce a highly dispersed multi-layer graphene solution, which is very efficient from an environmental and economic point of view, and to obtain flexible folding electronic devices. It uses paper as a substrate and consists of simple or brush coating followed by low-temperature heat treatment. Liu et al[62] produced a highly concentrated graphene powder-based conductive ink. The ink is compatible with multiple substrates and can be used in a roll-to-roll production process. The ink can be used as a screen printing ink and is suitable for applications such as RFID tags, microwave antennas, and healthcare monitors. Several research showed that graphene production significantly impacts environmental and human toxicity and increases energy consumption. As these articles highlight, the use of ultrasound in manufacturing results in fewer negative impacts on the environment across the board. Inorganic reagents, such as diethyl ether and acidic solvents, can be recovered and used again to lessen these effects[191,192].

2.5 CONDUCTIVE INKS

Inks have gained significant importance in electronics due to their unique properties, such as flexibility, low cost, and ease of processing, which make them suitable for various electronic applications. Inks are used in electronic devices for printing circuits, displays, sensors, and energy storage devices[57]. As mentioned earlier, one of the most significant recent progress in ink technology is the development of conductive inks, which can be used to print conductive traces and patterns on various substrates, including flexible materials. These inks consist of conductive particles, such as silver, copper, and graphene, dispersed in a solvent, which can be printed using various printing techniques. Developing conductive inks has enabled the production of flexible and stretchable electronic devices, which are finding applications in wearable devices, healthcare, and automotive industries[193]. Traditional conductive inks, on the other hand, often have metals or solvents that are harmful to humans and the environment. Researchers have been developing green conductive inks made from eco-friendly materials to address this issue. These inks can potentially reduce the environmental impact of electronic device manufacturing while maintaining high levels of functionality and performance[193].

In general, conductive inks are divided into two general categories.

1. Organic conductive inks such as PEDOT or some of its derivatives.
2. Inorganic conductive inks such as conductive nanoparticle inks.

Each of these types of inks has its own advantages and disadvantages, which are mentioned in .Considering the important advantages of inorganic inks made with conductive nanoparticles, such as high stability and electronic characteristics closer to the current bulk materials technology, as well as the greater availability of these inks, this category has been chosen for the experimental part of this thesis, and our explanations are based on this type of ink[63,194,195].

Table 3. Advantages and disadvantages of organic and inorganic materials for printed electronics

General categories	Advantages	Disadvantages
Organic conductive inks	Ability to design organic molecules	Low load mobility
	Low cooking temperature	Low environmental stability
	flexible	Poor printability of small molecule materials
	Better printing capability of polymer materials	The heterogeneity of the produced devices
Inorganic conductive inks	High inherent load mobility	Difficulty in ink formulation (separation and suspension problems)
	Environmental sustainability	Impurity caused by surfactants
	Maturity of mass production technology	High post-process temperature
	Abundance	Coffee ring effect
	Homogeneity of manufactured devices	Weaker properties compared to bulk material

2.6 INORGANIC CONDUCTIVE INKS

Developing low-cost, functional inks with desired printability and possibility to coat different substrates is critical to realizing printed electronic (PE) and large area coatings and exploring various electronics applications. The ink and its physical properties, such as viscosity and surface tension, are the most vital aspects of printing and coating techniques, affecting both printing conditions and pattern resolution. Because a variety of functional nanomaterials are obligated for PE fabrication, such as high conductivity metals for electrode and inter-connectivity, high capacitance/low leakage gate dielectrics for supercapacitor and TFTs, and high-mobility n-type and p-type semiconductors for complementary, low-power logic circuits and solar cells, developing and integrating innovative PE materials has become a core activity. Metallic NPs, carbon nanomaterials, semiconductor nanomaterials, and reactive inks are the most common printable inorganic nanomaterials among the aforementioned inorganic materials. Furthermore, printing ink is a unique combination of ingredients blended in a specific formulation to meet the desired properties of the ink's printing application. In general, inorganic nanomaterials serve to provide electronic properties for PE devices. To formulate the inks, resins, oils or carriers, additives, and solvents are also added. The resin is frequently used as a binder to affix the nanomaterials to the print substrates, the oil or carrier is the medium for transferring the functional nanomaterials and resin through the press, and the additives and solvents are used to control the rheological properties of the ink. In terms of ink formulation, the choice of solvents is critical, and there is a push to use water as a non-toxic, inexpensive, and

environmentally friendly solvent. However, because the surface energy of typical plastic substrates is much lower than that of water, water-based inks have difficulty wetting these materials. Much effort has gone into optimizing various ink parameters, allowing for using many functional inorganic nanomaterials in printed electronics[196,197].

So far, it has been shown that a number of different materials can be synthesized and used as functional inks, including conductive polymers[198–200], carbon[72,201], and metallic NPs[202–206]. These functional inks have become a focal point of study in the field of printed electronics due to their widespread use in the development of PE devices based on plastic, textile, and paper substrates.

2.6.1 Inks based on metallic nanoparticles

Various metallic NPs-based inks, including Au, Ag, Pd, Cu, Sn, and Ni NPs and their alloys or composite NPs, have been proposed and used in printed electronics[207,208]. Because metallic NPs have a lower melting temperature than the bulk material, the ease of achieving a printable functional ink is an important factor in deciding which metallic NPs to use[197].

The four metals that are mostly used as printable conductors are silver, copper, gold, and aluminium, with conductivity value of 6.30×10^7, 5.96×10^7, 4.10×10^7 ,and 3.5×10^7 (S/m) respectively at 20 °C[209]. Since their conductivity is slightly different, other parameters are the deciding factors. Gold appears to be a perfect conductor for printing ink. Its environmental stability is high and its conductivity at low process temperature is close to the conductivity of its bulk form, but the price of gold is high for use in cheap printed electronics and large area conductive coatings[210]. One good alternative to gold is silver because its price is lower compared to gold but has the highest conductivity, and a low chemical reactivity. Silver inks can be easily processed at ambient temperature to reach conductivity close to bulk form with a processing temperature below 200°C (even in some cases close to room temperature)[210]. Copper is a metal about 100 times cheaper than silver, but its ink preparation is more difficult due to its high tendency to oxidize. Aluminium has the same problem, with the difference that it is more chemically active. Like other useful metals, there are many challenges in the preparation of inks and their printing processes that limit their use to specific applications[211,212]. Gold and silver inks are comparable in terms of their high conductivity and thermal stability, but silver has a clear advantage over gold. As

mentioned, its price is lower. Silver and gold inks with a high solid content (for example, 50% by weight) are easily available in the market and can even be prepared in the laboratory, whose typical resistance after the modification process (not above 200°C) is only several times that of the bulk metal[213]. Printed silver and gold conductive lines have been successfully used in some devices, such as transparent conductive film-based grids of transistors and solar cells. Despite the maturity of silver ink features such as high conductivity and stability, its high relative price and the phenomenon of electrical migration of silver atoms cause circuit failure in high humidity and limit its wide industrial use. Copper ink is a promising alternative to silver and gold due to its much lower price, comparable conductivity to competitors, and excellent electrical migration resistance. But oxidation of copper during the synthesis, maintenance, and transfer of electrical properties destroys it. First, traditional reduction methods make it very difficult to prepare copper nanoparticles without copper oxide when water and oxygen molecules are in the reaction medium. Secondly, copper particles require a high processing temperature due to copper's high melting temperature and copper oxide's presence[213–215].

Metals cannot be dissolved in standard aqueous or organic solutions. To make metals printable, the conventional way is to mix metal particles with viscous polymer solutions, specifically with thermoset resins, to form pastes. Conductive pastes can create good mechanical connections and have good reliability. Still, these materials can have poor electrical conductivity, two or three orders of magnitude lower than the mass state. Recent advances in nanomaterials and surface modification methods have made it possible to disperse metal nanoparticles in an organic or aqueous solution with only a small amount of surfactants without using resin, creating conductive inks. After printing the ink and drying, the metal nanoparticles are very close to each other to form a continuous layer containing only a small amount of residual surfactants and lubricants[216].

Metallic printed layers can have excellent electrical conductivity but can lack mechanical properties such as flexibility, or resistance to folding and stretch. Like soluble compounds, these nanoparticle-based solutions have very low viscosity, making them suitable for high-resolution printing and forming like inkjet printing forming a thin film. Metal compounds can also be soluble and form soluble model inks that are particle-free. They are usually called organic metal decomposition inks[207].

They differ significantly from the nanoparticle model inks mentioned above in ink properties and film formation. In the inks of metal compounds, the thin conductive layer is made by converting the implanted metal compound layer into a metal layer by post-modification. The particle-free nature of these types of inks can reduce nozzle clogging, remove colloidal stabilizers from the ink and create a denser layer that is always lower than the inks based on nanoparticles. The small size of metal nanoparticles can reduce their melting point and accelerate their processing at low temperature. In addition, the small dimensions, spherical shape and uniform distribution of nanoparticles make it easy to form a dense layer[187].

In general, nanoparticles tend to agglomerate due to their high surface energy. Usually, the addition of dispersing agents is necessary to: 1) improve the suspension and stability of nanoparticles in solution, 2) control the dimensions and shape of a nanocrystal during their synthesis, 3) control the homogeneity of the coating process, and 4) improve the binding energy to create a strong interaction between the nanoparticles and the coating agent. On the other hand, strong binding energy results in the need for high thermal energy to separate these coating agents from the surface of a nanoparticle after ink printing. The findings show that functional groups with oxygen, nitrogen, and sulphur atoms can interact well with metals such as gold, silver, and copper[217].

To resume, Ag is the most promising metal-based conductive nanofiller since it has the highest electrical conductivity of all metals, it costs less than Au, and has a better air stability compared to Cu.

2.6.2 Inks based on carbon nanomaterials

In a variety of chemical and physical environments, such as in acidic or basic media, as well as at high temperatures and pressures, carbon nanomaterials demonstrate noticeably more excellent stability. Since they are relatively inexpensive and have good electrochemical performance, carbon inks have been particularly appealing for printing electrochemical electrodes for sensing applications (low background currents and broad potential windows)[83]. Graphite particles, a polymer binder, and other additives are frequently found in inks (for the dispersion, printing, and adhesion tasks). Due to their distinct electrical characteristics and potential for a wide range of applications, carbon nanotubes (CNTs) have since been used to construct printed devices[218].

Recent promising commercial developments in CNT electronics have included low-cost TFT printing and RFID tags. SWCNT films with 90% transparency and a sheet resistivity of 100 Ω/sq have recently been developed commercially[219]. Graphite and CNTs are frequently printed using inkjet and screen printing. Kordás et al., for example, reported that an aqueous dispersion of functionalized CNTs could be inkjet printed onto the surface of paper and plastic substrates, allowing the fabrication of electrically conductive patterns[220]. Due to its small dimensions (diameter of about 12 nm), its surface without dangling bonds, and its excellent optical properties, along with its stunning mechanical properties, SWNTs have the potential to be used in a wide range of applications in electronic devices such as transparent films, conductive connections, transistors, and sensors. Baechler et al. used inkjet printing to create MWCNT electrodes for dielectric elastomer actuators. Thin film electrodes with conductivities greater than 30 S/cm were obtained after optimizing the printing parameters without any sintering process[221].

Graphene, as an unique type of 2D carbon material with a honeycomb structure one atom thick, is receiving attention in fundamental and experimental scientific research because of its extraordinary physical and chemical properties. Graphene can be rolled into 1D nanotubes, wrapped around 0D fullerenes, or stacked to form 3D graphite. Numerous studies have shown that a high-quality graphene sheet can be used to create transparent, flexible electronic devices with extremely high mobility[222,223]. Yang and Wang examined the development of graphene and graphene hybrid inks, paying close attention to their composition and characteristics. Inkjet-printed graphene inks were achieved by Secor et al. with conductive features having a low resistivity of 4 mΩ.cm after sintering at 250 °C for 30 min. The samples exhibit consistent morphology, are compatible with flexible substrates, and have excellent bending stress tolerance[224]. Huang et al. used single- and multi-layered graphene oxide (GO) aqueous solutions as inks to print patterns on various flexible substrates, such as paper, PET, and polyimide (PI). The printed patterns had a better image quality and were produced using an easy and affordable inkjet printing technique. The printed patterns on PI substrates, out of the three substrates, showed the highest electrical conductivity (~874 S/m) after thermal reduction[224]. The topic of printed graphene electronics has received increasing attention in recent years. For instance, Torrisi et al. created graphene-based ink by exfoliating graphite in N-methyl pyrrolidine during the liquid phase. They used

it to inkjet print conductive and transparent patterns with ~80 % transmittance and 30 kΩ.sq sheet resistance, as well as TFTs with mobility up to ~95 cm^2/V.s. Because they affect the electrical and mechanical properties of printed patterns, the characteristics of graphene or its derivatives are crucial for inks. Although high-quality graphene could be produced without oxidation using liquid-phase exfoliation, pristine graphene still has a low solubility in common solvents, which is the main barrier to the production of graphene-based PE devices[65,70].

However, the patterns printed from pure carbon nanomaterials as obtained still have a very low conductivity, which limits their application. Inks that combine metal and carbon may be a better way to realize high-conductivity applications. For instance, to create flexible PE devices, Zhang et al. prepared an Ag/RGO composite that worked well as conductive inkjet printing ink. The conductivity was increased from 800 to 2000 S/m by the attached Ag NPs, and their size and morphology could be easily tailored[225].However, more research and understanding are needed to fully comprehend the conductive mechanism of carbon/metal hybrid inks.

Chapter 3: Characterization techniques and analyses methods

3.1 CHARACTERIZATION

3.1.1 Morphology

An analytical (low vacuum) scanning electron microscope using a JSM-6490LA SEM (JEOL) at 10 kV acceleration voltage and at fixed magnifications was used to analyse top surface and cross-section morphologies. The samples were then secured to a proper stub using carbon tape before being sputter-coated with a 10 nm-thick layer of gold in the Cressington 208HR sputter coater to eliminate the effects of charging. In order to carry out the analysis of the cross-section view, the samples required to be examined were freeze-dried with liquid nitrogen to facilitate breakage and retain morphology, and then twisted until breaking. An Oxford X-Max system with an active area of 80 mm^2 was used to conduct the energy-dispersive X-ray spectroscopy (EDS) analyses.

Zeta-20 optical profilometer (Zeta Instruments, San Jose CA, US), working in the confocal mode, imaged the roughness analyses on the coating layer surface. The image size was chosen to be 1920×1440 pixels with an objective of 20X magnification, giving a field of view of 664×498 μm^2. Moreover, the z spacing in the vertical tomography with a maximum range of 25 mm and a resolution of 10 nm used to reconstruct the 3D surface profile.

3.1.2 Dynamic light scattering (DLS)

The dynamic light scattering method (DLS, Malvern Zetasizer Nano ZS) with a He/Ne laser was used to characterize solutions, emulsions, and conductive inks for average droplet size. Probe sonicated (Sonics, Vibra cell, USA) samples were analyzed from 0 to 6 hours.

The emulsion-based inks were imaged with a standard optical microscope (Nikon microscope Eclipse 80i, Nikon Corp., Japan) and NIS Elements F Image Processing Software. Before analysis, the emulsions were gently stirred in vials to

ensure uniformity. A drop of each emulsion was placed on a microscope slide, which was then covered with a cover slip. For each type of emulsion, over ten shots were taken.

3.1.3 Scotch-tape test

To test the adhesion of the coating to the substrate, a strip of Scotch tape with a known adhesive force of 2.5 mN/m for steel was placed on the coated substrate and ripped off after 10 seconds. This test was specifically developed to compare and assess the adherence of ink to various substrates.

3.1.4 Water contact angle (WCA)

The static water contact angles (WCAs) of the top layer of ink at room temperature were measured using a contact angle goniometer (OCA-20 DataPhysics, Germany). 5 μL of deionized water were dropped onto the surfaces of the samples with the assistance of built-in software, and the contact angle was calculated from the side view. To ensure that the results could be repeated, five measurements were taken for each sample.

3.1.5 Mechanical test

Using a dual-column tabletop universal testing system, the System 3365, stress-strain curves were generated to examine the mechanical characteristics of the coating. The samples were mechanically hollow-die punched into a dog-bone shape with a nominal width of 4 mm and an effective length of 25 mm, then stretched at different rates. Young's modulus was calculated from the engineering stress-strain curves at two places to account for the two stages of textile material deformation. The structural rearrangement of the thread bundles, which was the initial response, was measured as the segment's slope crossing the curves at 0% and 1% strain. With the tangent at 20% strain, the samples' actual deformation was taken into account. The curves were also used to compute tensile strength. Each sample receives an average of seven measurements, which are then presented along with standard deviations.

3.1.6 Electromechanical tests

3.3.6.1 Electrical characterization under static conditions

In order to record I-V curves using the two-point probe method, electrical properties were measured using a Keithley 2612A source meter (Tektronix, Inc., US)

linked to a Signatone 1160 probe station (Microworld, France). Samples having an area of 10 mm^2 were glued to glass slides for basic resistivity (sheet-resistance) measurements using double-sided adhesive tape. In order to reduce contact resistances, two electrodes were painted on the surface on opposing sides using silver conductive paint with a specified resistivity of ~0.001 Ω/cm. The electrodes were subjected to electrical voltages ranging from -2.0 V to 2.0 V and backwards.

3.3.6.2 Electrical characterization under deformations

A micro tensile stage (Deben Micro uniaxial stage) with a 2 kN load cell linked to the Keithley source meter was utilized for dynamic electromechanical measurements. The samples were stretched to a strain of 10% before being released (strain 0%) up to 400 times at a strain rate of 2 mm/min.

Tensile deformation up to break was further studied by Instron dual column table top universal testing system 3365 (USA) coupled with the Keithley 2612A source meter (Tektronix, Inc. US). The effect of a cyclic deformation on the resistance change for higher than 500 cycles, was studied through the same Zwick (ZwickRoell S.r.l. Genova)-Keithley coupling measurements.

3.1.7 Post-printing treatment

As a post-printing method, thermal sintering was done. As a result, the printed patterns have a high surface-to-volume ratio and improved self-diffusion of surface atoms of metal nanoparticles. The sample was heated inside the SH-262 Benchtop Atmospheric Chamber (ESPEC NORTH AMERICA, Inc.) for sintering by using precise ramps and rates as well as one-minute equilibration intervals to raise the temperature from ambient temperature to the desired temperature. The prepared samples' relative electrical resistance was examined under the impact of temperature in order to further examine how electrical characteristics are affected by temperature. In order to record the IV curves, a dog bone-shaped sample was taped inside a petri dish, and its two ends were linked to the Keithley source meter using crocodile clamps.

3.1.8 The flexural rigidity

A cantilever test (ASTM D1388) was used to quantify the flexural rigidity GPierce (Nm) in order to assess the effect of the coated layer on the bending characteristics and drapability. The coated samples and substrates without coating, both measuring 200 mm by 250 mm, were used for the test. In summary, the samples

were placed on the instrument's horizontal terrace underneath a rectangular piece of metal, then progressively pushed over the edge at nearly constant speed until the sample's front side reached a banding angle of 41.5° under his own weight. The formula (I), where w (g/m^2) is equal to each sample's weight density and C (mm) is the length of the bent sample during the cantilever test to reach the specific angle (41.5°), was used to calculate the average flexural rigidity from four measurements on each piece, the face and back of both ends. A higher value of the bending length indicates a stiffer fabric[226,227].

$$G_{Pierce} = 9.81 \times 10^{-12} wc^3 \quad \text{(I)}$$

3.1.9 Reusability and recycling

A mixture of 50% vol solution and 50% vol water was used to soak the inked-coated glass substrate overnight. The glass substrate was then taken out, cleaned with a little new solvent, filtered to remove any conductive particles that had accumulated on the filter paper, and allowed to air dry at ambient temperature.

3.1.10 Viscosity measurement

Viscosity is an essential property of ink that affects its printability and final quality. The viscosity of the ink can be measured using a viscometer. It is influenced by various factors, including the concentration and size of its components, such as particles, polymers, and solvents. Although the weight or volume percentage of the components cannot be used to determine the viscosity of ink directly, they can provide some insight into the potential viscosity behaviour of the ink. The weight percentage of a component in a conductive ink can be calculated using the formula:

Weight Percentage = (Weight of component / Total weight of ink) x 100% (II)

Similarly, the volume percentage of a component in a conductive ink can be calculated using the formula:

Volume Percentage = (Volume of component / Total volume of ink) x 100% (III)

However, it is recommended to test the viscosity of the ink at different concentrations to determine the optimal formulation. Ultimately, measuring the viscosity of the ink using a viscometer at a specific temperature and shear rate is necessary to determine its actual viscosity and to optimize the ink formulation for particular printing applications.

3.2 COMPLEMENTARY ANALYSES

3.2.1 FTIR

A Fourier transform infrared spectrometer (Equinox 70 FT-IR, Bruker) and MIRacle attenuated total reflectance (ATR) (PIKE Technologies) with a diamond crystal were used to obtain the infrared spectra. All spectra were captured at a resolution of 4 cm^{-1} with a total of 120 scans in the range of 4000 to 600 cm^{-1}.

3.2.2 XRD

The X-ray diffraction (XRD) pattern of conductive particulates was recorded using a PANalytical Empyrean X-ray diffractometer installed with a 1.8 kW Cu K ceramic X-ray tube and a PIXcel3D 22 mm^2 area detector. The diffraction pattern was produced utilizing a parallel-beam geometry, a symmetric reflection mode, and a step size of 0.05° over an angular range of 23°–70°. For phase detection, PANalytical's High Score 4.1 software was used.

3.2.3 Raman

A Renishaw micro Raman Invia 1000 mounted with a 50× objective, an excitation wavelength of 633 nm, and an incident power of 1 mW was used to perform the Raman spectroscopy observations.

3.2.4 TGA/DSC/DMTA

On a TGA Q500 system, thermogravimetric analysis (TGA) is conducted (TA Instruments USA). The tests were carried out on approximately 4.00 mg of samples heated from 30 to 800 °C at a rate of 10 °C/min under nitrogen at a constant flow rate of 50 mL/min in platinum pans.

With the use of Discovery DSC 250 TA Instruments, differential scanning calorimetry (DSC) was carried out. The measurements were performed using nitrogen as a cell purge gas at a rate of 50 mL/min and at a heating and cooling rate of 20 °C/min from 90 to 150 °C. From the second heating, glass transition temperatures were calculated. These observations have been made in order to figure out the glass transition and α-relaxation temperatures as well as to investigate how ink changes with temperature.

Through DMTA measurements in a DMA850-TA, the thermomechanical sensitivity and viscoelastic behaviour have been examined (Discovery). With a

constant frequency of 5 Hz, a temperature ramp from 30 °C to 150 °C has been run with a displacement amplitude of 100 µm and a heating rate of 5 °C/min. From the glassy plateau to the start of the α-relaxation, frequency sweeps have been performed at several temperatures. Based on the characteristics of the samples, 3-point bending clamp was found to be the best choice, especially for determining the temperature range at which peeled-off ink becomes softer. The three most widely investigated variables include storage modulus, loss modulus, and tanδ which provide details on the degrees of freedom of internal particles and the transition temperatures. This analysis aimed to check for the robustness of peel-off ink in the investigated temperature range, which is helpful to attest that it does not degrade during the combined test of resistivity and temperature.

3.2.5 Biochemical oxygen demand (BOD) in seawater

By measuring the amount of oxygen consumed in a closed respirometer, the biochemical oxygen demand (BOD), a simple method for assessing biodegradability, was used to evaluate the biodegradability of the samples. More specifically, 432 mL of seawater as a single carbon source were added to the approximate amount of 200 mg sample. In order to replicate real environmental conditions, seawater was chosen. It already has the salty nutrients and microbial consortiums required for its growth. The experiment was carried out at room temperature inside 510 mL dark glass bottles that were hermetically sealed with an OxiTop measurement head. In order to sequester the carbon dioxide created during biodegradation, a CO_2 scavenger was added, and the biotic consumption of the oxygen present in the system's free volume was monitored as a function of the pressure change. Samples were examined twice. The mean values of the blanks, which were generated by measuring the oxygen consumption of the seawater in the absence of any test material, were subtracted from the raw data of oxygen consumption (mg O_2/L). Following this subtraction, results were standardized based on the mass of the individual samples and expressed as 100 mg of the material (mg O_2/100 mg).

3.3 COATING METHODS

Rod coating: Conductive inks were speared to the substrate with a rod coating system (EZ coater EC-200, Chemsultants Intl., Inc.) to create a homogeneous coating surface. Rod number 5 was employed at a coating speed of 0.4 m/min. In order to

finish the evaporation of the solvent and water, the substrate was then placed under the fume hood at room temperature. Similarly, the coating procedure was performed three times overall, with a three-day gap between printing cycles. In order to enhance conductivity, compactness, and adhesion, the hot pressing was carried out using a Carver press (model 3853CE, USA). The obtained samples were subjected to a 9.3 kPa force press for five minutes at a temperature of 110 °C after they had completely dried. In the fourth chapter, the ink is spread throughout the substrate using this printing technique.

Spray Coating: Spray coating was carried out using an airbrush atomizer spray coater (VL Siphon feed, 0.73 mm internal nozzle diameter, Paasche airbrush, US) with a pressure of 2 bar with the nozzle positioned at a fixed distance of roughly 15-20 cm from the substrate. In the fifth chapter, the ink is spread throughout the substrate using this printing technique.

Screen Printing: To apply the ink to the substrate, a manual screen printing machine (NS101-S) with a frame chuck and 360° frame rotation was used. According to the needs investigated in various applications, manual screen printing gives fabrication-related characteristics that are easily manipulable to produce various film qualities for different applications. In the screen printing method, a metal mesh frame with a dog bone pattern was placed on the substrate, and the prepared ink was applied to the edge of the mesh. The paste was then forced through the mesh using a squeegee that had a rubber blade attached. Screen counting mesh, repeated printing time, viscosity, ink shape, and sintering temperature and time are only a few of the crucial factors that affect the screen printing process. These factors are covered in more detail in the following chapter. The number of wires overall per linear inch can be used to describe a screen's mesh count. A film thickness of 10 μm can be obtained by printing three times. In the sixth chapter, the ink is spread throughout the substrate using this printing technique.

Chapter 4: Polylactic acid/graphene emulsion conductive ink for textile-based strain sensor

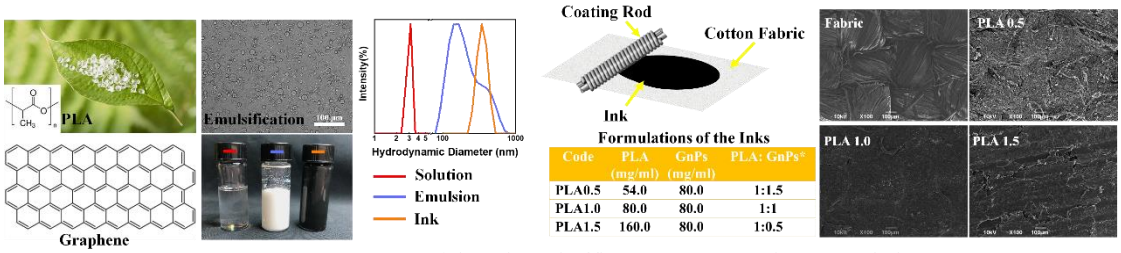

Formulations of the Inks

Code	PLA (mg/ml)	GnPs (mg/ml)	PLA: GnPs*
PLA0.5	54.0	80.0	1:1.5
PLA1.0	80.0	80.0	1:1
PLA1.5	160.0	80.0	1:0.5

*Final weight ratio of filler compare to polymer in the conductive inks

Nowadays, acquiring durable and reproducible electronics based on biodegradable and bio-based materials is demanded to confront electronic waste consequences. However, developing such sustainable materials with high conductivity remains a challenging task. Apart from this, in many cases, the use of toxic solvents may be unavoidable. Thus, in this chapter, a novel and efficient method founded on aqueous emulsion-based printable conductive ink is developed, which shows the feasibility of being used as fabric stretch sensors. Moreover, the influence of stretchability on the conductivity of the fabric-based sensor is investigated, and it exhibits high stability in cyclic strain tests suitable for wearable electronics.

Polylactic acid (PLA) is used as a bio-based binder to prepare the emulsion ink, and graphene nanoplatelets are used as a conductive filler. Spray-coated cotton fabric shows an encouraging electrical conductivity of 34.5 S/m. An additional improvement in the electrical conductivity of conductive cotton fabric is gained by hot pressing post-treatment. Additionally, the mechanical studies of the coated fabrics have been studied. The findings illustrate the enhancement of the mechanical properties of the cotton fabrics by increasing Young's modulus values almost twice compared to pristine fabric. This eco-friendly conductive ink can be used to coat a wide range of textile-based substrates and serve as a strain sensor for transforming specific electronic components into biodegradable versions.

4.1 OVERVIEW

Flexible electronics increasingly require wearable devices[228–231]. This is driving demand for flexible, lightweight, biocompatible, easy-to-fabricate, reasonably priced, and biodegradable electronic devices[232,233]. Wearable flexible hybrid electronics are widely used for continuous health monitoring, diagnostics, and human–machine interfaces, with development focusing on non-irritating, non-toxic materials and cost-effective processes[234–237]. Functional electronic materials must be biodegradable and biocompatible to meet health and environmental regulations and reduce electronic waste management risks[24]. After their effective service lives, biomaterial-based electronic devices should partially or completely biodegrade or disintegrate in physiological liquids or natural environments[238]. A new term, "green electronics", is addressing this biggest challenge[24,239].

The use of bio based materials, such as regenerated silk, hydrogels, and polylactic acid (PLA), offers decent potential for flexible electronic devices due to their biocompatibility, environmental friendliness, sustainability, reasonable cost, and solution process ability[3,175,240–243]. The biopolymer-based conductive inks can be directly applied to any substrate via solution immersion, coating rods, or spraying[244,245]. For example, Barreiro et al.[246] used solution casting to create a conductive, highly stretchable, flexible, and biocompatible silk-based composite with bio-based carbons derived from biomass via hydrothermal processing as filler. The authors used bio-based carbon fillers to reduce electrical resistivity on one side of the films by creating a carbon-rich layer. At lower concentrations of bio-based carbon, this layer aids in the formation of the conductive network. Although the resulting deformations after tensile stress could not be fully recovered due to relaxation in the silk fibroin chains, the authors concluded that these materials are still suitable for use as disposable ecofriendly strain sensors. Metal nanoparticles and metal oxide semiconductors[247], in addition to carbon-based nanomaterials[248], are widely used in flexible electronics[60]. Despite significant advancements in recent decades, their inherent mechanical properties, high cost, and uncertainties regarding biocompatibility and degradation limit their widespread use[249]. Lee et al. [250], for example, demonstrated printable bio/eco-resorbable conductive inks based on polybutane dithiol and molybdenum metal microparticles. The most significant benefit of this ink is its stability in water-soluble electronic devices. However, above a certain concentration

(800 µg/ml), molybdenum can be toxic[251,252], and producing this ink on a large scale may have environmental consequences. Madhur et al.[175] also created PLA-based, versatile, ready-to-use conductive inks to print biodegradable conductors with improved moisture stability. Tetrahydrofuran (THF) solutions containing tungsten powder were used for this.

In the production of conductive ink, solvents are crucial for maintaining the viscosity required for each type of printing method. The most common solvent for PLA in green flexible electronics and conductive inks is chloroform. Chloroform is a volatile organic solvent that can dissolve PLA at room temperature, making it an effective solvent for the processing of PLA-based materials. However, the use of chloroform is associated with safety and environmental concerns, as it is toxic and can contribute to the formation of ozone in the atmosphere. Therefore, researchers have also explored alternative solvents for PLA processing, such as acetone, tetrahydrofuran (THF), and 2-butanone. These solvents have lower toxicity and environmental impact compared to chloroform, but they may have different effects on the properties of the resulting PLA-based materials. To facilitate the dominance of bio-based polymers in flexible electronics, the use of toxic solvents must be minimized. This can be accomplished by utilizing biodegradable, halogen-free, and non-toxic solvents for solution processing in the development of electronic materials[253]. **Table 4** summarizes the most common used solvents for graphene conductive inks to date, with their chemical properties, advantages, and disadvantages.

Table 4. The most common used solvents for the graphene conductive inks[38,254].

Name	Formula	Boiling point (°C)	Surface tension (mJ/m²)	Pro	Cons
NMP	C_5H_9NO	202	40.8	High stability and good graphene dispersion	Not compatible with plastic substrate, costly, potentially toxic, hazardous, and heating of the substrate may need to accelerate the evaporation process and improve film morphology because of high boiling point.
DMF	C_3H_7NO	153	37.1		
DMSO	C_2H_6OS	189	43.5		
THF	C_4H_8O	66	26.4	Relatively low boiling point, less toxicity, and low cost	Low quality graphene dispersion; need to combine stabilizer
Toluene	C_7H_8	111	28.4		
Cyclohexanol	$C_2H_{12}O$	162	34.4		
Acetone	C_3H_6O	56	27.6		
IPA	C_3H_8O	83	23		
Ethanol	C_2H_6O	78	22.1		
Water	H_2O	100	72.8	Inexpensive, non-hazardous	Poor wetting properties, poor graphene dispersion with low stability, and need for surfactant to disperse

Given the importance of environmentally friendly conductive ink for humans and the environment, researchers are focusing on reducing the use of organic solvents and investigating the possibility of replacing them with eco-friendly alternatives in conductive ink formulations. As a result, selecting appropriate, environmentally sustainable solvents is a critical focus of evaluation[255]. Guidelines for choosing the proper solvent include good biopolymer solubility, low cost, lower hazards, and minimal environmental impact. Even so, finding a suitable solvent that is safe for the environment remains difficult[256]. Because of its non-toxicity and low boiling point, water is the most preferred solvent. It does, however, have a high surface tension of 72.8 mJ/m^2. Aside from that, the hydrophobic nature of graphite carbon makes graphene dispersion in water extremely difficult. As a result, surfactants are frequently used to improve graphene dispersion in graphene inks via van der Waals forces, hydrogen bonding, electrostatic activity, and π-π interactions. The presence of graphene electrons in the solution negatively charges the graphene layer surface. As a result, surfactants may get between graphene layers, thereby increasing the risk of aggregation. Surfactants used with water are thought to perform better than other toxic solvents such as NMP and DMF. As a matter of fact, several surfactants, including ionic, non-ionic, and polymeric surfactants, have been used to prepare graphene suspensions[257].

Butler et al.[258] created porous materials from hydrophobic biopolymers using emulsions for controlled release devices and biological tissue scaffolds. This method is critical because it is solvent-free during both the synthesis and purification steps. Similarly, stable PLA-based emulsions, such as oil-in-water, can be used to encapsulate electrically active components like graphene or carbon nanofibers. One advantage of emulsion-based green conductive ink is that it can be made using non-toxic and sustainable materials. For example, the solvent can be water-based and the surfactant can be made from renewable resources. In addition, emulsion-based inks can be printed using a variety of techniques, including screen printing, inkjet printing, and roll-to-roll printing. Emulsion-based green conductive inks have a variety of potential applications, including in the production of flexible and wearable electronics, sensors, and smart packaging. They offer a more sustainable and environmentally friendly alternative to traditional conductive inks that may contain hazardous materials or require harsh chemicals for processing.[259,260]. However, to date, no research has been conducted on PLA-based emulsions using green solvents for the fabrication of electrically conductive inks.

Several studies based on natural materials such as cotton have recently been reported to generate multifunctional devices such as strain sensors[261–264]. Our novel and efficient method, which uses aqueous emulsion-based printable conductive ink sprayed on cotton fabric, demonstrates high stability in cyclic strain tests, abrasion tests, and laundering tests and may be suitable for wearable electronics. In this chapter, we introduce an oil-in-water emulsion PLA-graphene-based printable conductive ink that is suitable for the development of functional coatings in consumable electronics[175,265–267]. Water and biodegradable solvents, such as anisole, were used to create emulsions. The inks were created by emulsifying various PLA binder ratios. Inks were rod-coated over the fabrics, reducing waste generation. For varying PLA binder ratios in the inks, the electrical and mechanical properties of the coated layers were monitored.

4.2 EXPERIMENTAL SECTION

4.2.1 Materials

Amorphous PLA pellets (Ingeo™ Biopolymer 6060D) were provided from Nature Works (USA), with a density of 1.24 g/cm^3. The glass transition temperature

(Tg) is 55 to 60 °C [45], which can be used as received. Sigma-Aldrich in Italy supplied sodium carboxymethyl cellulose (SCC). Graphene nanoplatelets (GnPs) were received from STREM Chemicals Inc. (USA). The average thickness is 6–8 nm, platelet width of 25 μm, surface area ~500 m^2/g, bulk density of 0.03 to 0.10 g/cm^3, an oxygen content of <1 %, and carbon content of ≥99 wt. %. Merck Life Science S.r.l. (Italy), was supplied Anisole (C_7H_8O) and was used as a solvent to prepare the polymer solution. Polyoxyethylene sorbitan Tristearate (Tween® 65), as a non-ionic surfactant, was provided by Merck Life Science S.r.l. Italy. Ultrapure Mili-Q water is utilized in making water-based GnPs dispersion. A plain woven and bleached cotton (100%) fabric was used as substrate with a mass density of 180 ± 5 g/m^2 and 24 threads/cm in warp and weft directions.

4.2.2 Preparation of PLA emulsion and GnPs dispersion

Prior to making PLA emulsion, the pellets were dissolved in anisole at three different concentrations of 53.3, 80.0, and 150.0 mg/mL with stirring at 70 °C for 3 hours and stored in a sealed bottle at room temperature. Following that, a concentration of 100 mg/mL of Tween® 65 in MiliQ-water was prepared in three vials at 50 °C while stirring for 15 min. Prepared PLA solutions were combined with these three vials and probe sonicated (Sonics, Vibra cell, USA) for 1 min. The final PLA-based emulsions were labelled as PLA 0.5, PLA 1.0, and PLA 1.5. To further homogenize, PLA emulsions were stirred overnight at 750 rpm at room temperature (RT), and for a few days, the PLA emulsions were stable. The GnPs dispersions were then prepared in the following step. In particular, 100 mg SCC were dissolved in 5 mL MiliQ-water at 40 °C for 3 minutes while stirring, and then 400 mg of GnPs were added and sonicated for another 3 minutes.

4.2.3 Conductive inks formulation

To make PLA-based conductive inks, the various PLA emulsions were mixed to the GnPs dispersions and sonicated in the ultrasonic bath at 59 Hz (Savatec, Strumenti scientifici, LCD Series, Italy) for 1 h. **Table 5** shows the final formulations with various GnPs to PLA weight ratios.

Table 5. The PLA and GnPs-based dispersions formulations.

Code	PLA (mg/ml)	GnPs (mg/ml)	PLA: GnPs*
PLA0.5	53.3	80.0	1:1.5
PLA1.0	80.0	80.0	1:1
PLA1.5	150.0	80.0	1:0.5

*Final weight ratio of filler compare to polymer in the conductive ink

4.2.4 Deposition of the conductive inks on cotton fabric

Rod coating, as described in the section 3.5, is used to create a conductive layer from different formulated PLA-based emulsion inks on the cotton fabric. Prior to coating, all vials were placed in an ultrasonic bath at 59 Hz for 2 hours to ensure ink homogeneity. After the solvent had completely evaporated, the as-prepared conductive cotton fabrics were hot pressed for 5 minutes at 110 °C under 9.3 kPa force. The hot-pressing temperature was lower than the melting temperature of PLA (220 to 240 °C) but much higher than its glass transition temperature (55 to 60 °C), so the PLA-coated samples were not melted. To protect the coated layer during the hot pressing process, the samples were covered with non-stick Teflon films. Cotton fabrics coated with conductive inks will be referred to as PLA 0.5, PLA 1.0, and PLA 1.5 in the following.

4.3 SIGNIFICANT FINDINGS

4.3.1 PLA-emulsion stability and particle size distribution

Emulsions are often composed of two different fluids, and intercalation between the phases is critical. Oil-in-water emulsions are typically composed of a lipid and an aqueous phase that have been homogenized by a water-soluble emulsifier[260,268]. Homogenization is the process of creating an emulsion by providing sufficient energy to the oil-water contact to break the bulk oil into smaller droplets[269]. An ideal emulsion is homogeneous throughout its volume[270]. As a result, it has small droplets with polydispersity and does not change greatly over time. An emulsion with these qualities has a prolonged "shelf life". Creaming, sedimentation, phase separation, or oil leakage are all signs of unstable emulsions[271].

To reduce the rate of breakdown in emulsions, tiny and equal droplets are preferred. After comprehensive screening, the necessary stability is reached with surfactants from the Tween series (ethoxylated or polyoxyethylene derivatives of sorbitan esters) in the current study. The hydrophilic-lipophilic balance (HLB) values of the surfactants in this series govern the selection of an emulsifier. Surfactants with high HLB are employed for oil-in-water emulsions when water-loving groups predominate[272–274]. To make a stable oil-in-water (O/W) emulsion, the HLB range should be 8-18 (10.5 in this study). **Figure 9** shows some images of PLA-based emulsions prepared with various surfactants; all of the photographs were taken after one day of preparation.

Figure 9. Prepared PLA-based emulsions using different surfactants from left to the right: Tween®80- Span®20- Tween®65- Span®65- Tween®85- Mixture of Span®20:Tween®80 in the total weight percentage of 60:40.

Although simple high-speed stirring can reduce enormous droplets of macro emulsion to a few micrometres in size, a larger amount of energy is required to further reduce droplet size. Rotor-stator, high-pressure, membrane, and ultrasonic systems are the most frequent breakdown techniques. Ultrasonic systems are employed to create emulsions in this study[275] . Optical microscopy is frequently used to image emulsions. **Figure 10**a and **Figure 10**b represents optical microscopy images of two PLA-emulsions using: (i) polyoxyethylenesorbitan tristearate (Tween®65); and (ii) sorbian tristearate (Span®65) respectively. The optical images were obtained after six hours of emulsion preparation under the conditions specified in section **4.2.2**. When oil droplets are completely covered with a proportional surfactant, they repel against each other and remain as individual particles[276,277]. (See **Figure 10**a). Storage time and emulsifier type are two important parameters that can influence emulsion stability. In unstable emulsions, dispersed droplets can aggregate into larger droplets called floccules, as shown in **Figure 10**b. Individual droplets become linked together in flocculation

phenomena to increase the degree of creaming in emulsions[278]. The results show that PLA emulsions in anisole/water prepared with Tween®65 as the emulsifier were much more stable than emulsions prepared with other surfactants. As a result, from this point on, the performance of Tween®65-prepared emulsions are investigated. **Figure 10**c depicts glass vials containing 5.0 wt.% PLA in Anisole, a PLA-based emulsion, and the final conductive ink, which includes graphene dispersed in the PLA emulsion (sample PLA1.0) (see **Table 5**). **Figure 10**d shows the dynamic light scattering (DLS) results for the droplet size distribution of the corresponding solutions and dispersions. It should be noted that samples were diluted in water 20 times before being measured. The average droplet size of the PLA-based solution is around 3 nm, with a narrow particle size distribution. The PLA-based emulsion, on the other hand, has an average droplet size of about 200 nm and a wide particle size distribution ranging from 80 to 800 nm. When the PLA-based emulsion was blended with GnPs to create conductive ink, the average droplet size increased to 400 nm and remained highly stable. The hypothesis is that the GnPs dispersed in the PLA-based emulsion aid in the stabilization of the emulsion, known as Pickering emulsion[279,280]. In comparison to regular surfactant-stabilized emulsions, the Pickering emulsion system has significantly higher deformation resistance due to the immutable adsorption of solid particles at the interfaces of two immiscible liquids[281–283]. As a result, the PLA-based conductive ink (with GnPs) has better stability and shelf-life.

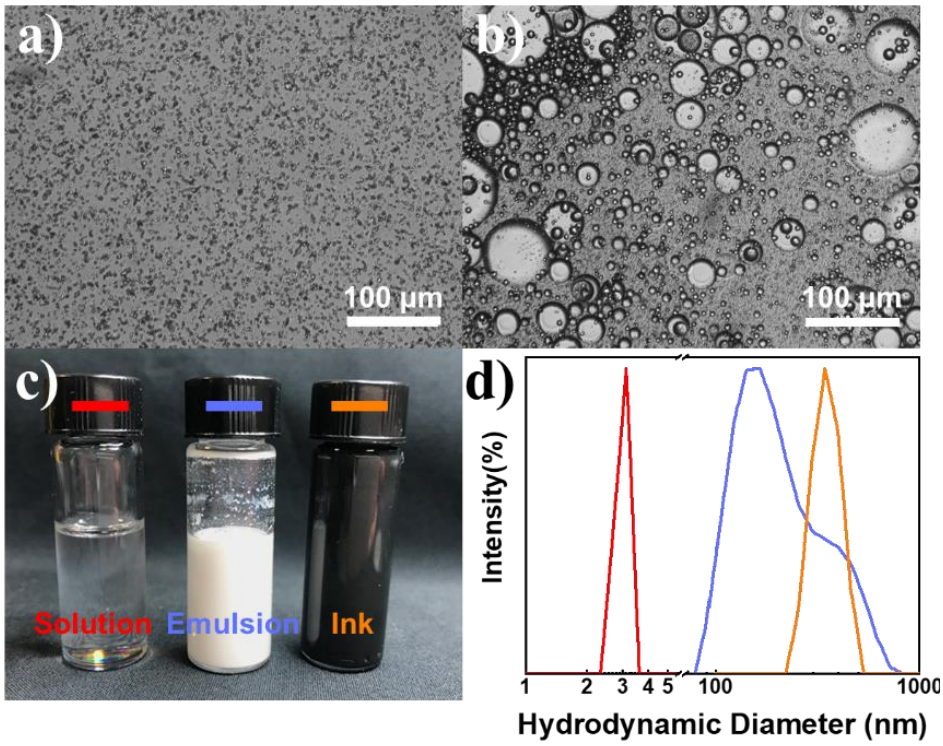

Figure 10. Optical microscope image PLA-emulsion, a) Made with Tween®65. b) Made with Span®65. c) Images of PLA solution (transparent liquid) and PLA-based emulsion (milky white) as well as conductive ink (black). d) The corresponding samples' droplet size distribution.

4.3.2 Morphological analysis of the coated fabrics

Figure 11 displays SEM images of the pristine cotton fabric (**Figure 11**a) and the cotton fabrics coated with conductive inks having different formulations. In particular, **Figure 11**b represents the surface morphology of sample PLA0.5 (see **Table 5** for formulation), revealing an irregular and partially filled surface. In contrast, the sample PLA1.0 displays a more uniform surface due to the presence of a higher amount of binder, i.e., PLA, see **Figure 11**c. Therefore, at this PLA to GnPs ratio (1:1), the binder creates a better coating of ink on the substrate. This implies that the GnPs can form networks throughout the substrate. **Figure 11**d shows the sample PLA1.5 where PLA to GnPs ratio is 1:0.5. Indeed; the surface appears wholly coated; nevertheless, the coated surface is uneven. It can be observed by comparing **Figure 11**c and **Figure 11**d that by increasing the amount of PLA near to 3 times, it is impossible to obtain a uniform thickness of the coating on the substrate using the rod coating setup because the binder dramatically increases the ink's viscosity.

The insets of **Figure 11**a-d show cross-sectional SEM images of the respective samples. The images observed in the cross-sections are comparable with those imaged

in top-view mode. Briefly, images demonstrate that in the ratio of 1:1, i.e., sample PLA1.0, the coating layer is more profound and more uniform on the substrate's surface (see inset of **Figure 11**c).

PLA and cellulose are highly compatible, and many reports in the literature show cellulose or cotton linters have been demonstrated as fillers or reinforcing agents for PLA, as shown by Wang et al.[284]. Several studies also show cellulose surfaces chemically modified to obtain better interfacial interactions with PLA[285] . Even certain polar solvents can be used to compatibilized PLA and cellulose interfaces[286]. Given this, the polarity of the anisole/water system[287] can be considered advantageous for better interactions between PLA and cotton.

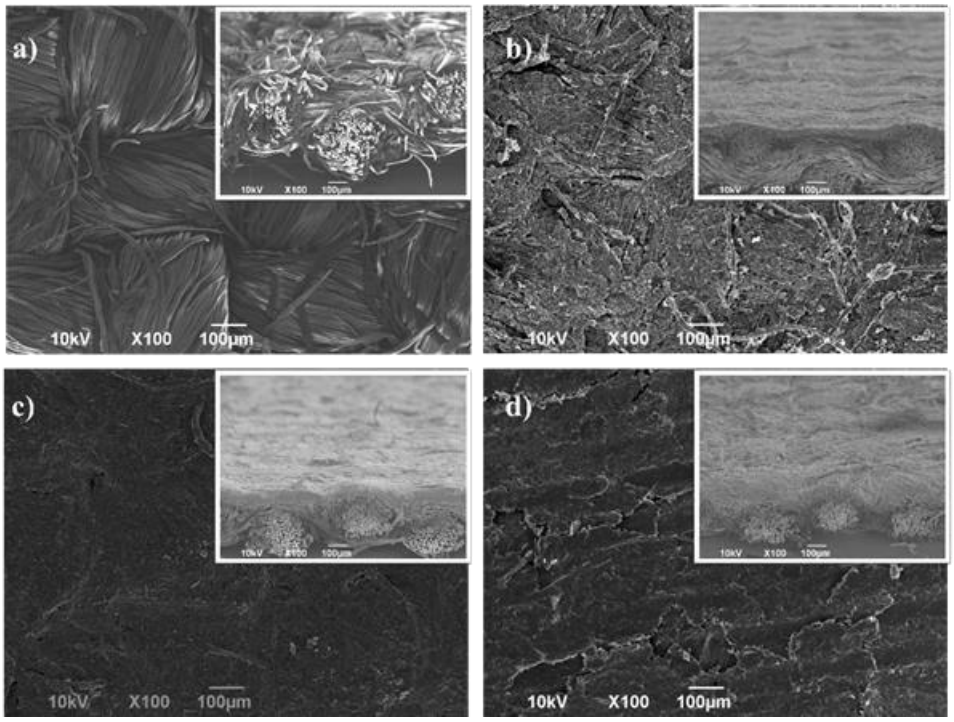

Figure 11. SEM images of the top-view of a) pristine cotton fabric and samples coated with conductive inks, particularly, b) sample PLA0.5, c) PLA1.0, and d) PLA1.5. No hot pressing is applied. The inset SEM images illustrate the cross-sectional view of the respective samples[226].

4.3.3 Mechanical characterization

The mechanical properties of the coating were investigated using stress-strain curves. The samples were cut in the shape of a dog bone and stretched at a rate of 10 mm/min. Young's modulus was measured at two points on the engineering stress-strain curves to capture the two phases of deformation of textile materials. The slope of the segment crossing the curves at 0% and 1% strain was used to evaluate the initial response, the structural rearrangement of the thread bundles. The actual deformation

of the samples was taken into account using the tangent at 20% strain. Tensile strength was also calculated using the curves. Each sample receives an average of seven measurements, which are reported with standard deviations.

The corresponding results are shown in **Figure 12**a. The characteristic stress-strain curve for freestanding PLA films (the black curve in **Figure 12**a), which had previously been prepared by hot pressing, demonstrates linear elasticity and relatively high rigidity, with a Young's modulus of 5.5 ±1.5 GPa, which agrees with previous reports[288]. In contrast, the stress-strain curves associated with the coated samples exhibit non-linear deformation, with a slow initial slope that gradually increases until fracture. This behaviour is typical of fabrics, with the first phase corresponding to weave stretching and the second to actual yarn deformation[65,289]. As a result, the former stiffness is an apparent modulus that is affected not only by the material but also by the weave design and crimp. The addition of a coating over the fibres is expected to change this modulus by decreasing the mobility of the woven structure.

The coating increases both moduli during initial stretching and final deformation (**Figure 12**a-c). Specifically, for any binder ratio, the increment of the weave apparent modulus is constant, whereas the intrinsic modulus increases linearly. After the hot-press treatment, the moduli, particularly the apparent modulus, increase further, which can be explained by better penetration of the PLA binder into the weave and, as a result, reduced structural mobility even in the fabric without any coating.

The slight increase in the Young's Modulus of the uncoated cotton fabric after hot pressing can be related to better alignment of the fibres of the woven structure, which gives the material greater rigidity; however, this increase is not statistically significant.

Flexural rigidity G_{Pierce} (Nm) was measured on coated samples and neat fabric without coating with dimensions of 200×250 mm. In the section **3.3.8** the testing procedure has been described. The flexural rigidity of the textile is also an important mechanical feature that specifies the bending stiffness of the coated fabric[290]. **Figure 12**d shows the results of the cantilever tests. The higher the binder ratio, the stiffer the fabric, according to the results, confirming the results of stress-strain mechanical tests.

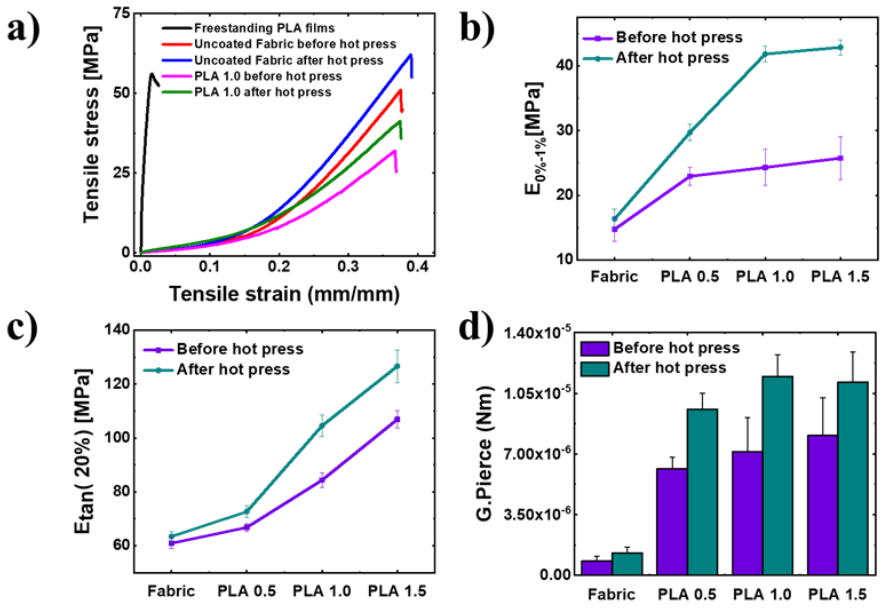

Figure 12. Mechanical properties of PLA-based conductive cotton fabrics. a) Stress-strain curves for PLA-coated fabrics; b) Young's moduli at segments 0%–1% ($E_{0\%–1\%}$, MPa), corresponding to weave stretching from the representative stress-strain curve; c) PLA-coated fabric Tangent Young's moduli (E_{tan}, MPa). The slope of the tangent to the stress-strain curve at a fixed point corresponds to 20% of the ultimate strain d). Estimated flexural rigidity via the G. Pierce cantilever test.

4.3.4 Thermochemical characterization

The FTIR spectra of pristine PLA films prepared by hot press, PLA/anisole solution, and PLA emulsion are shown in **Figure 13**a. Using PLA-based conductive ink, a conductive freestanding film is also created. Stretching frequencies for -CH3 asymmetric, -CH3 symmetric, and C=O groups in pristine PLA film are 2997, 2943, and 1724 cm^{-1}, respectively. C-O is linked to two stretching frequencies at 1075 and 1198 cm^{-1}. The bending frequencies of -CH3 asymmetric and -CH3 symmetric are related to two separate peaks detectable at 1468 and 1368 cm^{-1} [291]. All of the other films' spectra show roughly the same absorption peaks as the hot-pressed pristine PLA film, implying that no new bonds or other strong chemical interactions have been detected between the PLA and GnPs or as a result of the solvent presence.

Figure 13b and c show the thermogravimetric analysis (TGA) and first derivative of the thermogravimetric curve (DTG) of the hot-pressed pristine PLA film, the fabric substrate before and after hot pressing, and the coated sample PLA1.0 before and after hot pressing. During only one decomposition stage, all samples exhibit primary weight loss in the range of 275 to 325°C. These curves reveal the nature and extent of the substrate's degradation prior to coating, as well as the effect of the coating on the

substrate. **Table 6** summarizes the detailed measurements of the thermograms. The average percent weight lost for all samples from 0 to 230 C is between 0.5 and 2.5%. The results show that the thermal properties of the graphene-ink-coated samples improved, which can be attributed to the GnPs' inherent thermal properties. In general, when nanoscale fillers such as GnPs are dispersed inside polymeric films, the geometry and concentration of the nanoscale fillers have the greatest influence on the films' gas solvability and diffusion coefficients [292,293]. GnPs act as a barrier to the release of compounds during or after decomposition[174]. Furthermore, the hot-press process causes a uniform arrangement of the fillers within the coating, which improves the gas barrier properties[293].

Table 6. TGA and DTG result related to all samples.

Sample name	T_{on} (°C) (St.dev.±0.5 °C)	T_{max} (°C) (St.dev.±0.5 °C)	T_{80} (°C) (St.dev.±0.5 °C)
Freestanding PLA film	276.60	334.80	314.18
Fabric before hot press	298.84	363.52	340.11
Fabric after hot press	298.84	362.77	339.52
PLA1.0 before hot press	271.26	364.44	338.3
PLA1.0 after hot press	273.25	364.44	339.02

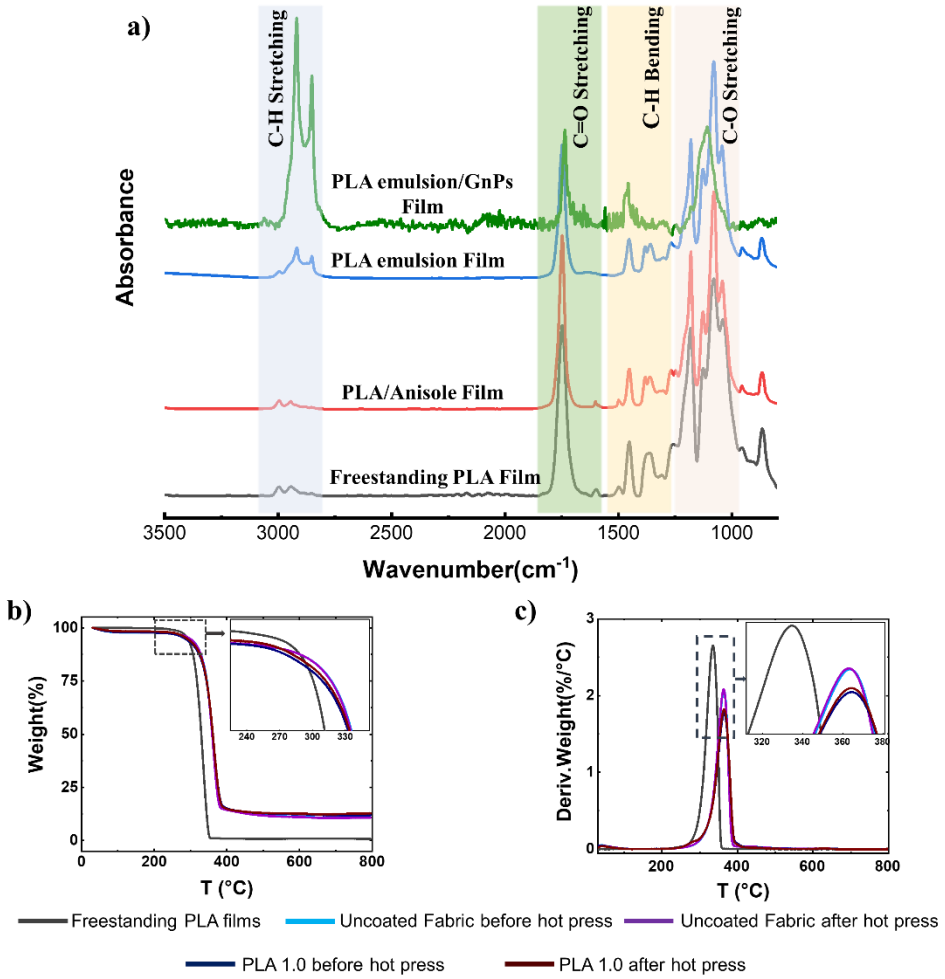

Figure 13. a) FTIR spectra of hot-pressed PLA film, PLA/Anisole solution film, PLA emulsion film, and final ink (PLA emulsion/GnPs blend Film). b) Thermogravimetric analysis (TGA) curves of freestanding PLA film, fabric without coating and coated with GnPs-PLA ink before and after hot-press. c) Derivative thermogravimetric analysis (DTG) freestanding PLA film, fabric without coating and coated with GnPs-PLA ink a before and after hot-press. The insets in (b) and (c) illustrate the magnified curves of the main images[226].

4.3.5 Electrical characterization

The Probe station measurement setup is depicted schematically in **Figure 14**a. The measured current-voltage curves are in accordance with Ohm's law (**Figure 14**b). The sample PLA1.0 has the most conductive curve with the highest Ohmic slope with a binder to filler weight ratio of 1:1, indicating that the binder causes a better coating of ink on the substrate at this ratio. As a result, the GnPs can form electrically conductive networks across the substrate[294]. Such conductivity is obtained without the use of hot pressing.

Conductivity is associated with the electrical properties of bulk uniform materials such as metals or semiconductors, whereas sheet resistance (Rs) is

commonly used to specify the electrical properties of conductive or semiconductive coatings. The sheet resistance (Rs) multiplied by the film thickness (t) yields the bulk resistivity (Ω) [295]. Our findings for the PLA1.0 hot-pressed samples confirmed that by reducing overall sample thickness (**Table 7**), conductivity improved while sheet resistance decreased (see **Figure 14**c). **Figure 14**d and **Figure 14**e show the coating surfaces prior to and after compression molding. The defects on the coated surface are clearly reduced after hot pressing.

Table 7. Coating thickness was averaged in 10 random points from each sample with a ±0.001 mm error.

Sample	Thickness Before hot press	Thickness After hot press
PLA0.5	0.295 mm	0.265 mm
PLA1.0	0.300 mm	0.280 mm
PLA1.5	0.305 mm	0.298 mm

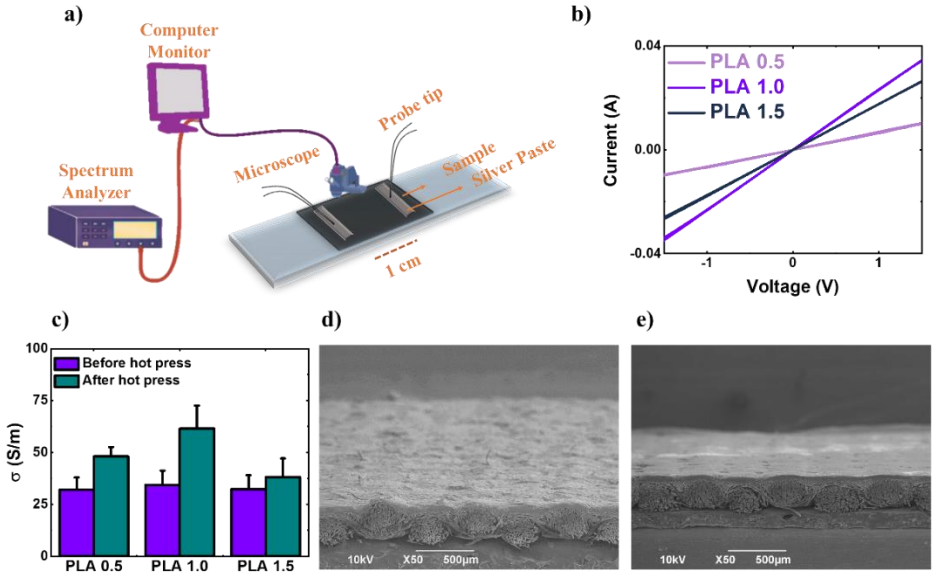

Figure 14. a) Schematic of the setup for conductivity measurements of the samples using the Probe station instrument. b) I-V curves of the different prepared inks coated on the substrate (see **Table 5**). c) The electrical conductivity measurements of the different prepared inks coated on the substrate. Coating surface sample PLA1.0; d) before hot-pressing, e) after hot-pressing.

Annealing at temperatures above the binder polymer's glass transition temperature (Tg) causes the filler (GnPs) within the composite to densify. This results in an inevitable rearrangement of the GnPs within the polymer network, increasing contact between GnPs and, as a result, increasing conductivity throughout the

samples[250,296–298]. To assess the effect of hot pressing on the electrical conductivity of the samples, isothermal curing at various times was investigated separately and compared to the hot press results. For this, the best sample, PLA1.0, is chosen and oven-treated at 110 °C for 5 minutes, 12, 24, 36, and 48 hours (**Figure 15**a). Only after 24 hours do the results show an increase in electrical conductivity. The latter can be likened to the solvents completely evaporating. Crack formations on the coating layer were observed when the sample was exposed to 110 °C for more than 24 hours (36 and 48 h). This effect was time-dependent, and after 24 hours, the crack's depth, length, and width increased with exposure time (highlighted by yellow arrows). Indeed, increased crack parameters cause defects in the polymer network, resulting in a decrease in electrical conductivity (**Figure 15** b, c, and d)[299].

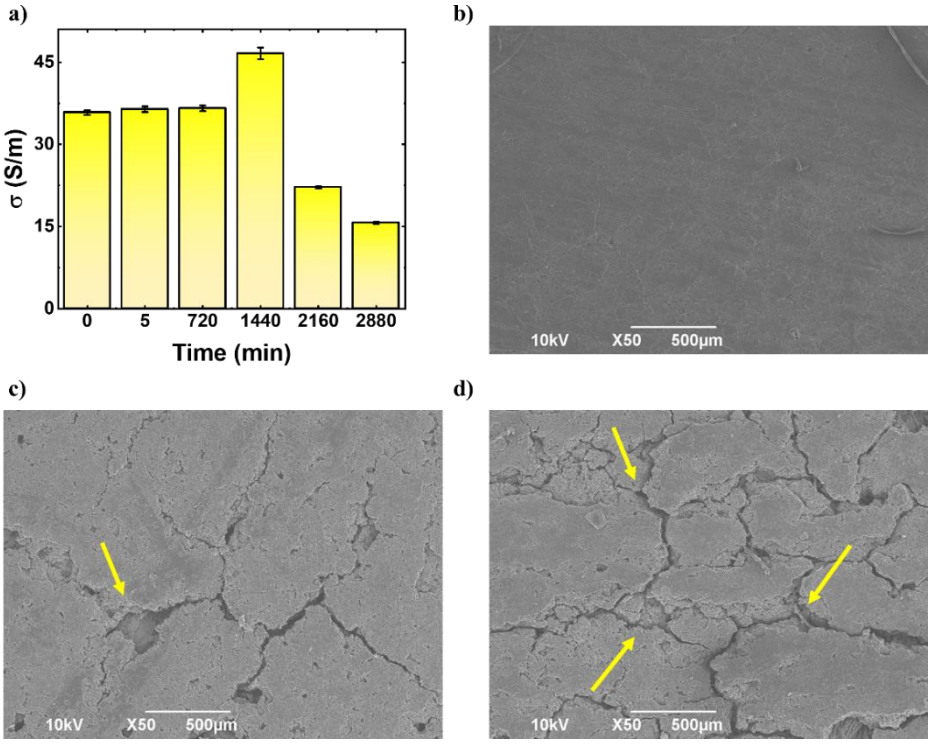

Figure 15. a) The effect of isothermal curing at various times on the electrical conductivity of the PLA1.0 sample. Surface state of the coating after b) 24 hours. c) 36 hours and d) 48 hours.

4.3.6 Electromechanical characterization

The durability of the coated layer is one of the most important parameters in wearable electronics because it affects long-term functionality[300]. Simultaneously, the weak interactions between the textile substrate and the conductive coating layers result in electrical conduction instability and low durability after repeated cyclic

deformation, rubbing, and washing[301]. Hu et al.[302] proposed a green method for producing ultra-durable conductive textiles. The adhesive force produced by crosslinking water-borne bio-based SWNTs with GA-chitosan organic salt increased the durability of the conductive textiles. The conductivity of the fabric decreased by approximately 13% after multiple bending and by 17% after 20 cycles of washing. Despite the high durability of this conductive polymer composite, it is preferable to develop a simple method for producing conductive textiles for practical applications. **Figure 16**a depicts cyclic strain tests of the pristine sample PLA1.0 at a strain rate of 2 mm/min for 100 cycles with a maximum elongation of 10%. Inset **Figure 16** depicts the state of the sample in the Deben micro-test setup used for the cyclic tests. Plastic deformations in the rigid parts inside the polymer structure cause the small peaks (**Figure 16** b) that appear in each cycle when the substrate reaches 10% stretching[303,304]. The polymer matrix deforms at maximum elongation, causing the conducting network formed by GnPs inside the PLA matrix to collapse. As a result, by the end of the repeated cycles, the electrical conductivity had dropped from 34.5 to 26.4 S/m[305,306]. The number of cycles was increased from 100 to 400 to further demonstrate that the fabric's electrical conductivity is stable under harsh conditions (**Figure 16** c and **Figure 16**e). According to the cyclic test results, the hot-pressed sample nearly retains approximately 70% of its initial conductivity value after 400 cycles, with no significant change after 50 cycles. The results show that the hot-press process improves cotton fabric filling with the conductive coating layer, resulting in a better conductive network. Furthermore, as previously stated, adequate PLA binder penetration into the weave due to compression molding results in reduced structural mobility and demonstrates remarkable structural retention and fatigue resistance during the applied tensile strain.

Cracks initiate and grow at the stress-concentrated areas in the coated layer over the surface of the textile upon stretching due to their mechanical mismatch with the material that is supporting them, as seen in images captured by a scanning electron microscope (**Figure 16** d and **Figure 16**f). In graphene-based strain sensors and their derivatives, this phenomenon has already been reported[307,308]. Even though cracks are undesirable for structural designs, several long-lasting devices and strain sensors with such microcracks in their conductive thin layers have been successfully implemented[309,310]. This is despite the fact that cracks are a common source of failure

for structural components. Because of the rapid separation of conductive materials at the microcrack edges, there is a dramatic reduction in the number of electrical conduction paths within the conductive layer. This leads to a significant increase in the electrical resistance of the strain sensors when the tensile strain is applied. The reconnection of microcrack edges may be responsible for the rise in conductivity that was observed in both samples after being released.

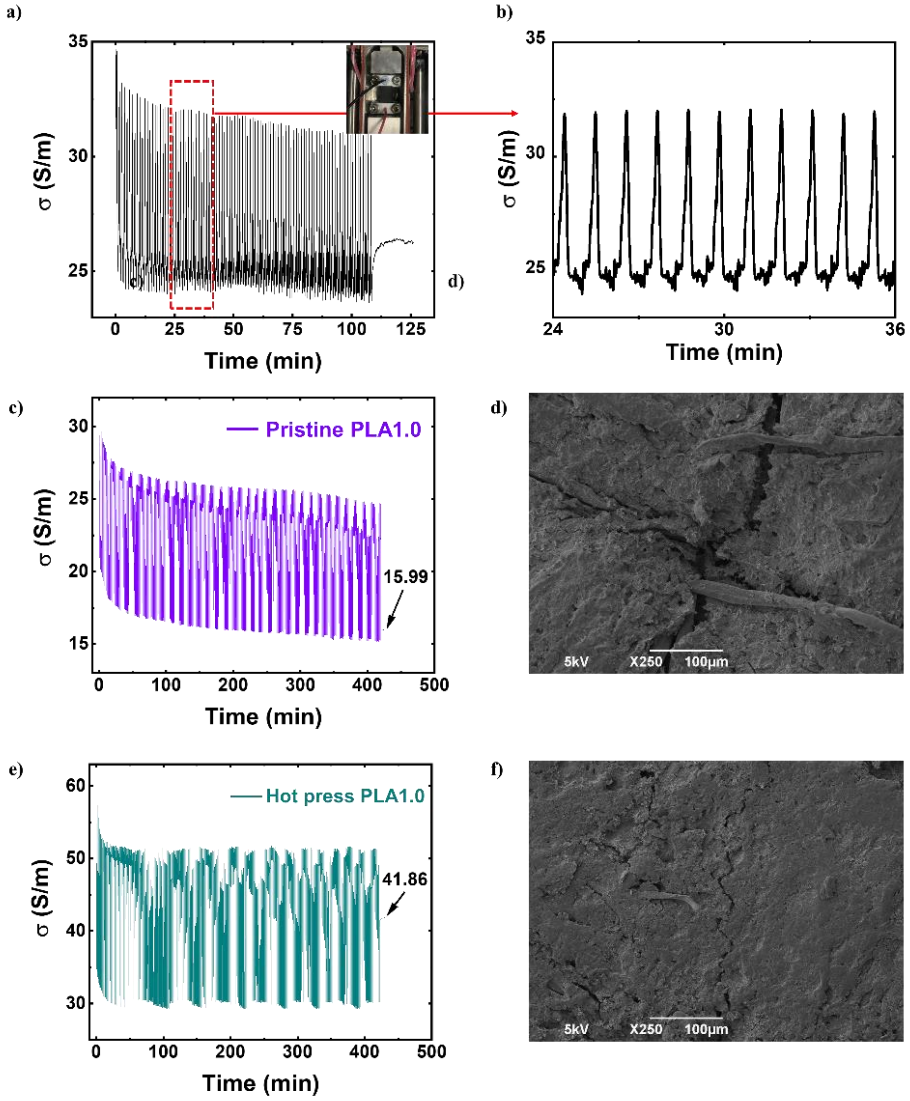

Figure 16. a) Electrical conductivity changes in pristine PLA1.0 during a 10% maximum elongation cyclic test. The photograph inset shows the sample's placement status in the Deben micro-test setup. b) An illustration of a similar magnified graph. Changes in electrical conductivity during 400 cycles of tensile strain c) Pristine PLA1.0, and d) Pristine PLA1.0 coating surface states at the end of 400 strain cycles. Changes in electrical conductivity during 400 cycles of tensile strain on e) hot-pressed PLA1.0 and f) hot-pressed PLA1.0 coating surface state at the end of 400 strain cycles.

The washing test is performed in MiliQ water to estimate the durability of conductive coatings during laundering. Five 5×5 cm^2 samples of hot-pressed and

pristine PLA1.0 were cut and placed in two separate 500 ml beakers at room temperature. The coated samples were washed with detergent and water under stirring conditions in order to assess their durability during the washing process. The total washing time for one laundry cycle begins at 0 minutes and gradually increases by 10 minutes on each cycle; in this way, the shortest washing cycle was assumed to be 10 minutes, and the most extended cycle was 60 minutes. At the end of every 10 minutes, when the washing cycle was completed, all five samples were removed from the beakers, and new samples were placed (**Figure 17**a).

The effect of laundering time on the electrical conductivity of pristine and hot-pressed sample PLA1.0 is shown in **Figure 17**b. Surface conductivity of pristine and hot-pressed samples decreased from 35 to 7 S/m and 63 to 40 S/m, respectively, after laundering for 60 minutes, as shown in this graph. After 10 minutes of laundering, the electrical conductivity of the pristine sample was reduced by 5 times. After one hour of continuous laundering, the hot-pressed sample (at 110 °C) retained more than half of its initial conductivity value with almost no significant variation. As the laundry time increases, more conductive fillers are detached from the surface, and a visible coating inhomogeneity with exposed underlying cotton begins to form. In addition, the results show that compression molding improves the quality and robustness of the coated layers by allowing the ink to penetrate deeper into the fabric warp. For each laundry cycle time, electrical conductivity is reported for an average of five washed pieces. Repeating the hot press after the washing test has no effect on conductivity.

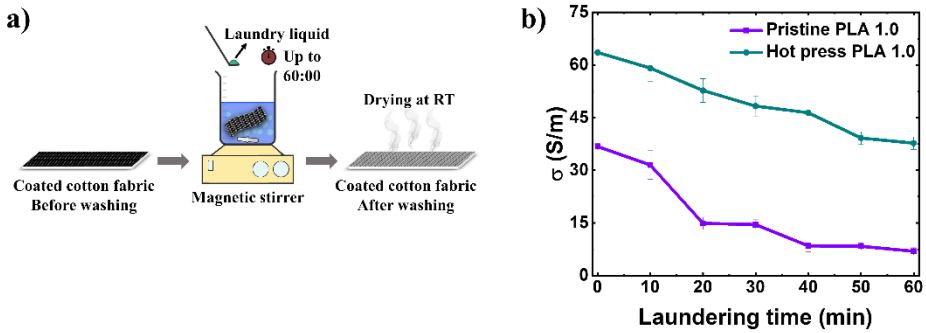

Figure 17. a) Schematic of the washing process for the sample PLA 1.0. b) The electrical conductivity measurement for the evaluation of washing durability of the coated layer in pristine PLA1.0 and hot-pressed PLA1.0.

Abrasion tests were performed on the pristine and hot press PLA1.0 samples using a linear abrasion method. The schematic of the abrasion tests for these samples

with 200 g loading over 500 grit abrasive paper is shown in **Figure 18**a. Before beginning the test, a 5×5 cm^2 area of the sample PLA1.0 was stuck to an appropriate glass frame. A 200 g weight was glued on top of the frame to ensure the coated surface was in contact with abrasive paper. Each abrasive cycle was 10 cm forward and 10 cm back to the start. The thickness of the samples decreased by 10 to 15 micrometres at the end of each cycle. The same test was performed on the hot-pressed PLA1.0 sample. The electrical conductivity values were measured after the fabric's surface was damaged by abrasion every ten cycles up to 100 cycles, as shown in **Figure 18**b. Although abrasion reduced conductivity in all samples, hot-pressed conductive fabrics maintained significantly higher electrical conductivity values than pristine fabrics. The abrasion cycles remove all unconsolidated material, even in the hot press sample, demonstrating that the hot-pressed coating has relatively high conductivity, with a slight decrease in conductivity observed with the increasing number of rubbing cycles up to 50 cycles. Wearing away the loose materials appears to aid in the contact of the GnPs, which are actually fixed within the conductive layer and connected to the percolation paths within the coating. While high friction between abrasive paper and coated layer demolishes the coated layer and the conductive electrical network after 60 cycles, significantly reducing conductivity. Apparently, the coating layer in pristine conductive fabrics can be removed, resulting in coating thinning and negatively impacting electrical conduction. In both samples, however, the primary damage is maintained by the conductive network generated by the polymer-bound GnPs.

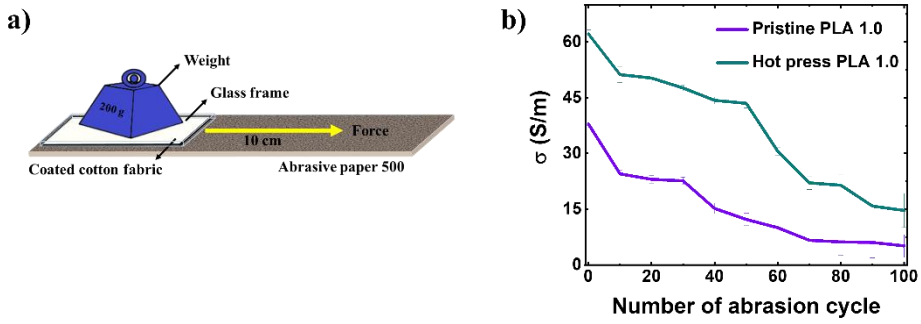

Figure 18. a) Abrasion test schematic for sample PLA1.0 at 200 g loading on Abrasive paper 500. b) Rubbing test for different cycles of graphene/PLA pristine and hot-pressed coated cotton fabric.

4.4 CONCLUSIONS

In summary, bio-based conductive inks made from graphene nanoplatelets and PLA-based aqueous emulsions in three different weight ratios were evaluated in this chapter. To form emulsions with water, a biodegradable solvent such as anisole was used, and PLA was used as a binder for connecting conductive particulates of GnPs. In general, PLA is soluble in chloroform. The primary goal of this chapter was to discourage the use of such hazardous solvents. Anisole is a non-petroleum-based sustainable solvent with high biodegradability[311]. Emulsifying ensures that water replaces a significant portion of the solvent. If the solvent is not biodegradable, this means lower solvent emissions and, of course, lower solvent costs. The only disadvantages of anisole are its flammability and high boiling point, which complicate sample drying time. The dynamic light scattering and optical microscopy studies of the emulsion and ink revealed a very well-dispersed oil-in-water emulsion with dispersed PLA and GnPs. With the rod coating technique, the inks were spread into the cotton fabrics. Their structural morphology revealed that inks with a PLA: GnPs ratio of 1:1, sample PLA1.0, covered the fabrics in the most uniform manner, yielding the best conductivity and mechanical properties in comparison to the other inks prepared. The results showed that the samples' electrical conductivity was improved twofold after being hot pressed. Furthermore, the hot-pressed samples demonstrated improved mechanical performance due to improved PLA binder penetration into the weft of cotton fabric. It is worth mentioning that, regardless of being subjected to a series of stretch-release cycles during strain testing, coated samples maintained electrical conductivity. The collapse of the conductive networks formed by GnPs can explain the decrease in electrical conductivity observed near the end of the 100 cyclic strain test, from 34.5 to 26.4 S/m. Printed inks were also resistant to washing and abrasion while remaining conductive. Future research might explore the possibility of using alternative polar green solvent-water emulsions in the formulation of such inks with biopolymers, which was the inspiration for an idea for the next chapter.

Chapter 5: Environmentally friendly, electrically conductive, and versatile emulsion-based ink for distributed tactile sensing

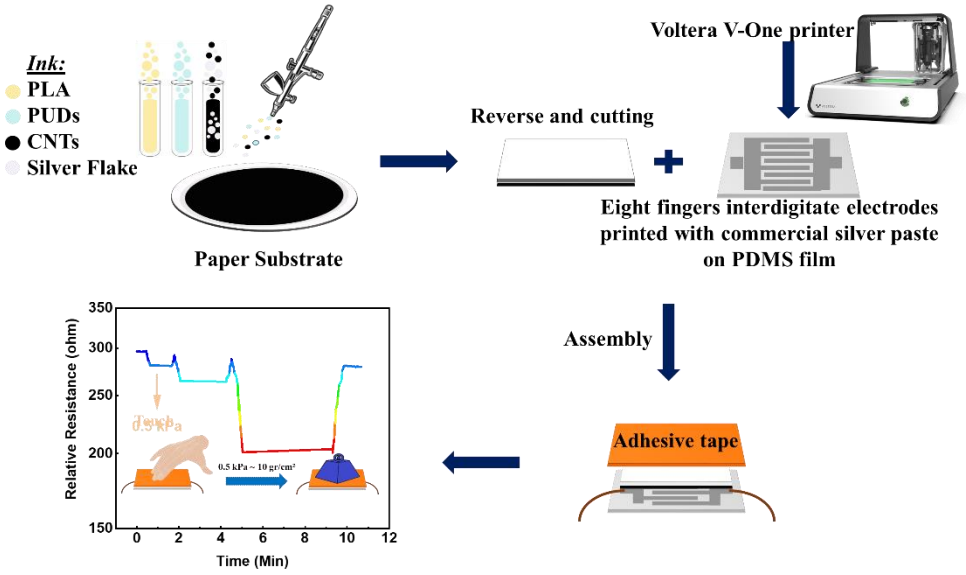

Polylactic acid (PLA), a synthetic polymer that is both renewable and biodegradable, has garnered a lot of interest as a potential approach to reducing the negative effects of electronic waste in environmentally friendly flexible electronics. The fact that PLA-based electrical devices can last even after being submerged in water or buried underground for three years is a significant limitation on their development. Under such a perspective, in this chapter, another conductive ink that is based on PLA-emulsion and hybrid conductive fillers such as silver flake and carbon nanotubes is formulated using a variety of methods in order to determine its morphology, electrical properties, and mechanical performance. In order to improve the electrical characteristics, thermal sintering is done as a post-treatment. After being annealed isothermally at temperatures up to 110 °C for varying amounts of time, the self-diffusion of surface atoms of conductive filler, in particular metal particles, at the printed patterns is increased, resulting in an improvement in the sheet resistance value and reach to 290±2.23 Ω/sq after the improvement. When hybrid conductive fillers are utilized, the ink's percolation threshold and production costs are both reduced, while the ink's excellent electrical properties are preserved. Additionally,

CNTs that are used as conductivity fillers have the ability to bridge adjacent silver flakes, which increases the amount of electron transport. To satisfy the ever-increasing demand for environmental protection, the ink exhibited noticeable adhesion to a wide variety of substrates, including biodegradable nitrile gloves, cotton fabric, and paper. Moreover, a sensor that is constructed out of paper demonstrates high-pressure sensitivity (0.3 kPa) along with an operational range (0.1- 500 kPa). In addition, ink is capable of biodegradation in marine environments, which leads to a gradual reduction in the accumulation of the substance within the ecosystem.

5.1 OVERVIEW

The widespread use of sensors in healthcare, manufacturing, and other control systems has opened the door to a more modern, secure, and interconnected society. However, factors such as high production costs, rigid and expensive materials, and insufficient sensitivity have prevented their broad acceptance in industries such as wearable electronics, biosensors, and soft robotics[152,312,313]. While developers working in such an area can use inks to create cutting-edge products in a variety of industries and fields, including 5G communications and automobiles, as well as advanced packaging and healthcare devices, Because of recent developments in biomaterials and green chemistry, environmentally friendly, printable, flexible, stretchable, and degradable options are now available[314,315]. Printed electronics are created by registering thin functional material (ink) layer combinations on a low-cost substrate that can be recycled and/or naturally degraded in nature, and they offer a number of benefits that conventional electronics manufacturing does not[23,316]. As a result of recent advances in printed electronics, long-term goals include developing conductive inks made from recycled and/or bio-based materials to create interesting elements with excellent electrical conductivity that might be investigated for the fabrication of a broad range of stretchy and flexible electronic devices[90,317].

Because of their function in connecting the devices' components, conductive inks are considered critical for creating all types of stretchy, flexible, and wearable electronic devices[69,312]. The material that conducts electricity is thought to be the primary ingredient in the process of producing conductive ink[318–320]. The physical properties of the pattern to be printed, such as its adherence to the substrate, as well as

the desired physiochemical features of the inks, such as their compatibility with the printing procedure, influence the selection of conductive materials[70].

Carbon-based nanoparticles have been discovered to preserve great promise for use in printed and flexible electronics, making them one of many nanomaterials discovered to date[321–323]. CNTs are electrically heterogeneous in comparison to other nanomaterials, which is one of the primary reasons for their widespread interest (metallic or semiconducting)[324]. However, the stability of CNT dispersion in water remains a concern because the nanoparticles frequently appear to agglomerate rapidly as a result of their strong van der Waals attraction[325,326]. Despite the numerous benefits provided by carbonaceous fillers, the maximum conductivity achievable with their nanocomposites is significantly lower than the values required for many applications. While adding more fillers may increase conductivity, it may also increase cost and viscosity, resulting in poor applicability and, in some cases, diminished mechanical qualities[327,328].

Silver-based materials (nanoparticles, micro- and nanoflakes, nanospheres, etc.) are more promising metal nanoparticles for flexible and stretchable electronics than carbon-based materials because silver possesses the highest electrical conductivity [195,329]. Silver-based conductive ink is the preferred option for printed electronics among the numerous nanoparticle-based conductive inks investigated due to its superior oxidation resistance, electrical conductivity, and other relevant physical features that provide strong substrate adhesion[330,331]. The primary issue with silver is the requirement for high-temperature annealing of the printed film in order to achieve exceptional conductivity[332,333]. As a result, conductive inks that are also hybrids with silver are an excellent cost-cutting option. Due to the high cost of silver-based conductive fillers, hybrid fillers for thermally and/or electrically conductive inks have recently gained interest[90,334,335]. Silver flakes (σ = 6.107 S/m)[336] and carbon nanotubes (σ = 1.104 - 2.105 S/m)[337,338] have recently been used to create a new type of filler with extremely high electrical and thermal conductivities. Furthermore, because CNTs have a high aspect ratio[339,340], highly conductive hybrid CNTs/silver flakes inks can be developed with less silver than conventional silver-filled inks.

Table 8 summarizes previous research on inks made of CNTs, silver, and a combination of CNTs and silver. The majority of CNT and silver-based conductive inks were made with toxic solvents that are harmful to both humans and the

environment. Silver must also be annealed at a high temperature to improve its electrical conductivity. Furthermore, because of the sensitivity of plastic and paper substrates to degradation at high annealing temperatures, the use of silver-based inks in flexible electronics is limited[333,341,342]. As a consequence, developing a high-quality, long-lasting hybrid ink that retains its high conductivity even after being exposed to a low annealing temperature is critical.

Table 8. The previous studies on conductive inks based on CNTs, silver and its hybrid.

Inks	Solvent	Printing Method	Substrate	Annealing condition	Rs or σ
AgNPs/Graphene	Ethanol and Acetone	Inkjet	PET	-	4.74 Ω/sq
MWCNTs/ GelMA/DNA	Water	Screen printing	Paper, hydrogels, elastomers	-	24 ± 1.8 S.cm $^{-1}$
AgNPs/Graphene	DMF:EG:G	Inkjet	polyvinyl alcohol	80 °C- 10 to 30 min	0.3545 to 2.1517 S.m^{-1}
AgNPs/CNTs	Chloroform and DMF	free-standing composite	-	mild condition	1228 S.cm^{-1}
MWCNTs	lysozyme solution (acidic buffer)	Pen direct writing	Glass, PET, Silicon	mild condition	500-1500 Ω/sq
AgNPs/Graphene	DMF	Inkjet	PI	400°C, 30 min	20±1 Ω/sq
Ag Flakes/CNTs	Emulsion system	Spray coating	Paper/ cotton fabric/ Nitrile gloves	110°C-120 min	290 Ω/sq

As a result of the importance of environmentally friendly conductive ink for humans and the environment, the research trend is shifting toward minimizing the use of organic solvents and investigating the possibility of replacing them in conductive ink formulations with eco-friendly alternatives such as water. As a result, selecting appropriate, environmentally sustainable solvents is a critical focus of this work. In addition, polymeric biomaterials based on polylactic acid blends are promising candidates for use as biocompatible, bioresorbable carriers in regenerative medicine applications. PLA is very susceptible to hydrolytic and enzymatic degradation in the amorphous region due to the ease with which water can permeate it; however, when PLA is combined with other polymer matrices, phase separation occurs, thereby increasing water absorption. Using a bio-based binder composed of PLA and water-based polyurethane (PUDs) improves PLA degradation by creating a more hydrophilic composite. In addition, it increases PLA's fragility, making it suitable for tactile applications.

5.2 EXPERIMENTAL SECTION

5.2.1 Chemicals and Materials

Nature Works (USA) provided amorphous PLA pellets (IngeoTM Biopolymer 6060D) with a density of 1.24 g/cm^3 and a glass transition temperature (Tg) of 55–60 °C. Lamberti S.p.A. in Varese, Italy, delivered waterborne bio-based polyurethane (ROLFLEX® BiO 49) with a relative density of 0.907 g/cm^3 calculated from dried film. Merck Life Science S.r.l., Milan, Italy, purchased multi-walled carbon nanotubes (MWCNTs) with a relative density of 2.1 g/cm^3, an average diameter of 110–170 nm, a length of 5–9 microns, and a carbon content of 90% by weight. The Silver Flakes 99.9% trace metal basis was supplied by Merck Life Science S.r.l. in Milan, Italy, with an average particle size of 10 and a density of 10.49 g/cm^3. Ethyl acetate (EtOAc) was purchased from Merck Life Science S.r.l. in Milan, Italy, and was used as a solvent to create a 99.5% pure polymer solution. Merck Life Science S.r.l., Italy, supplied the polyethylene glycol sorbitan monooleate (Tween®80) and sorbitane monooleate (Span®80) used as non-ionic surfactants. Mili-Q ultrapure water is used in the production of emulsion-based ink. As substrates, 100% cotton plain-woven fabric that had been bleached and had a mass density of 180.5 g/m^2 and 24 threads/cm in both the warp and weft directions, commercial nitrile rubber (acrylonitrile butadiene), which is used to make gloves, and cellulose chromatography paper were chosen to study the adhesion properties. PDMS is prepared by Sylgard 184 silicon elastomer kit supplied by Sigma Aldrich, Germany.

5.2.2 Ink design

The following steps were involved in the formulation process of ink, which will be explained in detail in the subsequent paragraphs:

First, the polylactic acid was dissolved in ethyl acetate, a solvent that is environmentally friendly. At 100 °C, 1.54 g of PLA 6060D was dissolved in 15 mL of ethyl acetate with continuous stirring for 3 hours. Second, PLA/PUDs pre-emulsion was created using the oil-in-water (O/W, ethyl acetate/water) emulsion technique in the presence of non-ionic surfactants, approximately 50 µL from each one of the Tween®80 and Span®80. Using sonication (30 s; 35Amp), the prepared PLA solution was emulsified into a 15 mL diluted aqueous solution of water-borne polyurethane (including 7 mL of PUDs diluted with 8 mL of water to yield 1.54 g of dried PUDs).

CNTs were initially dispersed in Mili-Q water to create the filler dispersions. Briefly, 0.22 grams of CNTs powder was combined with 15 ml of Mili-Q water. After that, 1.1 g of silver flake dissolved in 15 ml of ethyl acetate was added to the CNTs dispersion in the presence of the same mixture of the non-ionic surfactants to create a silver flake and CNT hybrid filler. The final distribution consisted of silver flakes, and CNTs were sonicated for 120 minutes in a sonic bath with a vibration amplitude of 59%. The final silver-to-CNTs volume ratio was set at 50%vol.

Various CNTs/silver flakes/PLA/PUD conductive emulsion-based inks were formulated, sprayed on glass, and peeled off to determine the percolation threshold. The hybrid filler was evenly distributed throughout the emulsion during the spraying process up to 50%vol, while at a higher concentration of 50% vol, it was evident that the CNTs were aggregated together. Under such a perspective, 30% of the coating material's volume comprised fillers (Ag flakes and CNTs).

Finally, the ink was sprayed onto glass and peeled off after drying to exemplify its properties. The coated samples were sintered in a temperature and humidity-controlled chamber to improve compactness, adhesion, and conductivity.

5.2.3 Coating method

Coating processes come in a wide variety due to the wide range of applications and needs in various markets. Coating is a method of transferring an ink layer to a substrate by pouring, painting, spraying, casting, or smearing it over the surface[245,343]. Blade coating, spray coating, painting, slot-die coating, curtain coating, and slide coating are all coating methods. Spray coating techniques have a high potential for large-scale production because they are free of substrate size limitations and low polymer consumption, and they have the potential to replace existing spin coating methods[344]. To achieve a uniform coated layer, conductive ink was deposited onto substrates using spray coating. The conductive ink patterns can be seen to be sprayed across the substrate evenly and uniformly. The collected samples were allowed to dry before being sintered for 30 minutes at various temperatures to increase conductivity by enhancing the self-diffusion of surface atoms of conductive fillers, specifically metal particles, at the spray-coated layer.

5.3 SIGNIFICANT FINDINGS

5.3.1 Stability and characterization of nanoparticle-surfactant-polymer stabilized emulsions

The mean droplet size of the PLA emulsion (in yellow) was monitored during testing for six hours to evaluate its stability (see **Figure 19**a); the droplet size distribution slightly increased during the first 10 minutes after emulsion preparation and then reached a fixed plateau value. This could be attributed to particle reconnection inside the emulsion[226].

Furthermore, the addition of PUDs (in green colour) into the PLA emulsion increased the mean droplet size of the emulsions significantly. By switching from transparent PLA emulsion to white PLA emulsion and PUDs, the emulsions' consistency improved noticeably. This could be due to the fact that the permanent hydrophilic groups from the water-based polyurethane polymer chains in the PLA emulsion's continuous phase, such as the carboxyl group or ammonium salt, are physically linked together[345]. An optical microscope was used to investigate the microstructure of PLA emulsion and PUDs further (see **Figure 19**b). Optical images revealed the presence of oil droplets within the emulsion's continuous phase. This assumes that PUDs increase emulsion stability and viscosity by forming a protective layer around the oil particles within the emulsion.

The results also show that the PLA emulsion and PUDs have a lower viscosity than ink. This could be attributed to the presence of Pickering emulsion[288,346]. As previously reported, carbon nanotubes and silver flakes can form a bonding layer at the oil-water interface. Because of the grafting of hydrophobic groups onto the polymer chain, the ink had high interfacial stability[347–349].

Furthermore, **Figure 19**c and **Figure 19**d show the ink's storage stability under ambient conditions, which has excellent stability for three days without phase separation. However, after five days, silver flakes started to settle in the ink. According to these findings, the accumulation of silver flakes is primarily responsible for the low stability of silver-based conductive inks[350]. Although nanoparticles settle slowly and their Brownian motion can counteract gravity's effect, these nanoparticles still aggregate due to the attractive van der Waals forces between them. Because sedimentation velocity is proportional to the square of particle diameter when particles

collide and aggregate, larger agglomerates settle much faster and reduce the printability of silver-based conductive inks[351]. The attractive van der Waals forces between materials can be calculated using Hamaker constants. Metals have relatively high Hamaker constants when compared to common solvents. As a result of the robust and attractive force between them, silver suspension cannot maintain a well-dispersed state for a lengthy period of time (see **Figure 19**e). Similarly, increasing the sonication time resulted in a noticeable increase in emulsion consistency. This could be attributed to the physical entanglements of the polymers, which resulted in an increase in ink consistency[352,353]. All solutions, aqueous dispersions, and emulsions were diluted to 0.1 mg/mL for the measurement, and each sample was measured three times.

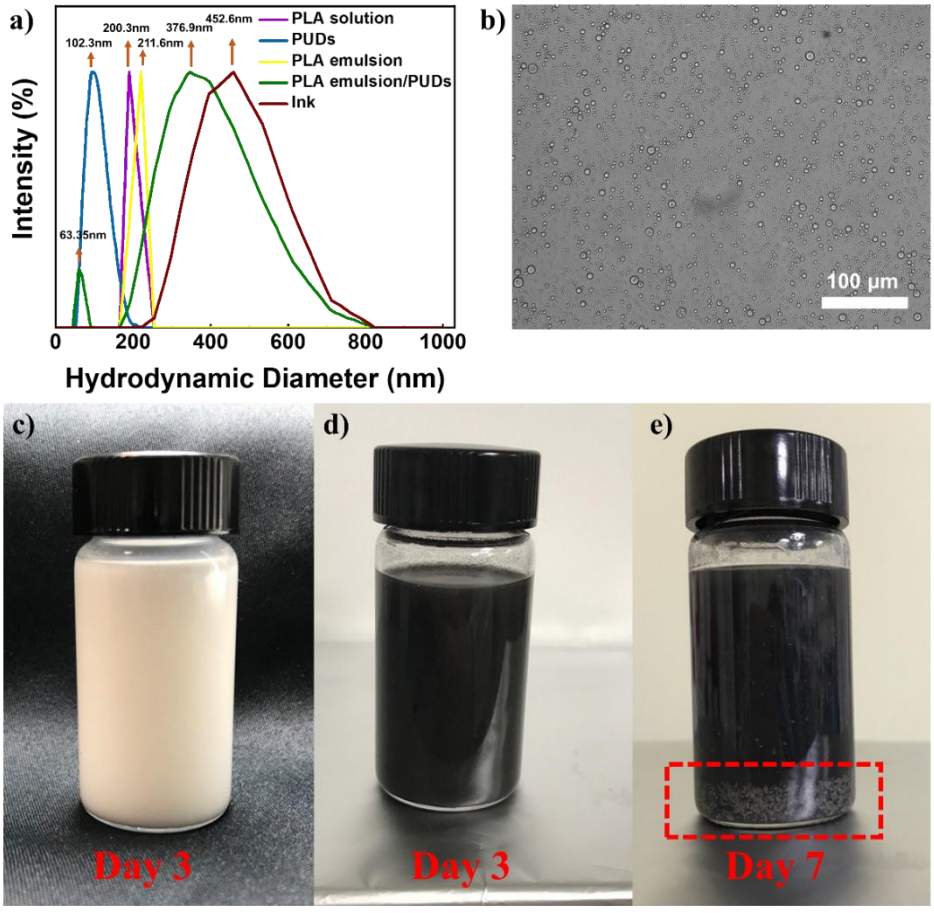

Figure 19. a) DLS analysis specifies the droplet size distribution of solution, emulsions, and conductive ink. b) Image of PLA emulsion/PUDs using an optical microscope. Photographs of c) PLA emulsion/PUDs after 3 days, d) ink after 3 days, and e) Ag flakes agglomerates within the ink after 7 days.

5.3.2 Ink surface morphology pre- and post-thermal treatment and substrate compatibility

Metallic nanofillers with high electrical conductivities and the ability to sinter at temperatures significantly lower than their melting points are usually the first choice when high electrical conductivity is required. While maintaining the ink's high electrical conductivity is important, using a small amount of metallic fillers is preferable[354]. To increase the electrical conductivity of ink at a given concentration, an optimal distribution of nanofillers is required. It has been demonstrated that a heterogeneous distribution (i.e., the fillers are not uniformly distributed across the matrix) is preferable to a homogeneous distribution for achieving higher conductivities at similar nanofiller loadings[355,356]. It was demonstrated that approaches including double percolation in hybrid systems with two different fillers, confining nanofillers in any one of the phases of a biphasic polymer, and generating repulsive forces with both nanofillers and the host polymer (e.g., polar or non-polar) were all efficient ways to boost the ink's conductivity[357].

Figure 20 shows the surface and cross-section view of ink coatings before (see **Figure 20**a and **Figure 20**b) and after isothermal annealing at temperatures of 55 (see **Figure 20**d and **Figure 20**e), 80 (see **Figure 20**g and **Figure 20**h), and 110 °C (see **Figure 20**j and **Figure 20**k) for 30 minutes. The morphology of the coatings changed slightly during the annealing steps at different conditions, as shown in **Figure 20**. With increasing annealing temperature, a microstructural evolution of the coating materials is observed, resulting in coatings with a connecting feature (top view and cross-section). After annealing at higher temperatures, a relatively rough surface with granular features became smoother. The material may have become denser by increasing the annealing temperature from 55 to 110 °C, as evidenced by a minor change in thickness (seen via cross-sectional observation). This hypothesis, however, was validated by measuring the thickness. According to TGA tests (**Figure 22**b), a portion of the insulating impurities that remained in the inks gradually evaporated off during annealing, causing the silver flakes to shrink, come into closer contact, and possibly sinter. EDS is used to examine the distribution of silver flakes within the ink before (see **Figure 20**c) and after (see **Figure 20**f, **Figure 20**i and **Figure 20**l) annealing. As previously stated, a heterogeneous distribution is preferable when increasing

conductivity. This is supported by the presence of densely packed silver flakes as well as sparsely filled silver flakes (highlighted with a red circle).

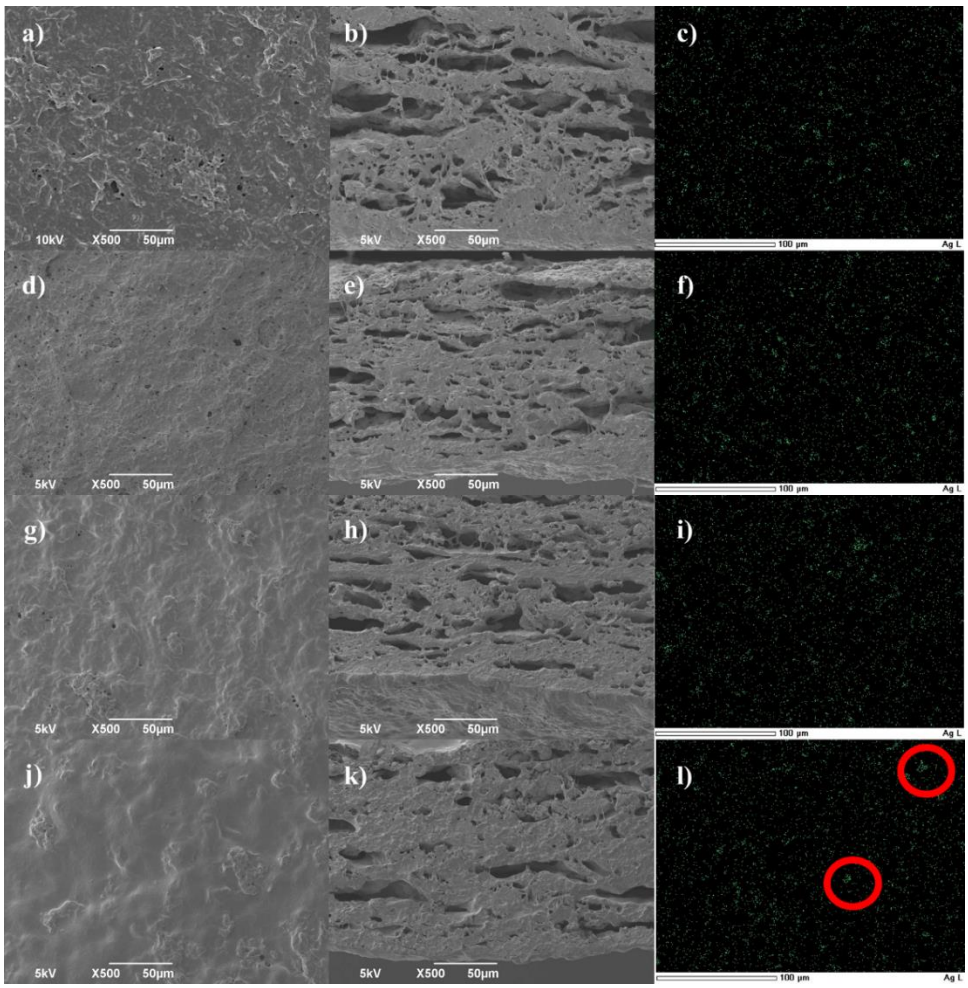

Figure 20. SEM images and EDS analyses of the coatings' microstructural evolution: a, b, and c) before annealing. SEM images and EDS analyses of the coatings' microstructural evolution after annealing at different temperatures: d, e, and f) 55°C. g, h, and I 80°C. j, k, and l) 110°C.(all first columns belongs to top views and middle columns are cross-section views).

The adhesion strength of a coating layer to the substrate is critical for its effective functioning, and it can be evaluated through a simple scotch tape test. The adhesion quality of any coating is critical because it determines whether the coating will remain on a specific substrate and perform its intended function during use. The tape peel test is the only quick and easy way to determine the adherence strength of a coating to the substrate. A quantitative "peel test" with adhesive tape provides valuable information about thin coating layers and their adhesion strength when applied to various substrates[358,359]. The adhesive tape peel test was used to assess the quality of each manufactured coating. The results showed that the printed layers on the paper substrate

were more resistant to the scotch tape test than the nitrile gloves and textile-based substrate, which can be attributed to the surface roughness of the paper and its ability to quickly absorb the solvent after coating[334,360] (see **Figure 21**a). Aside from that, the electrical performance of the paper substrates with the highest conductivity for the printed patterns was comparable to that of nitrile gloves and textile-based substrates. The paper substrate with the best electrical performance after thermally treated at 110°C of the printed layers was used to make sensors with a low operating voltage (see **Figure 21**b). Furthermore, the motivation stems from the fact that paper is a visually appealing and environmentally friendly option for printed electronics. It is a biodegradable material that is widely available, environmentally friendly, low in cost, light in weight, and extremely versatile.

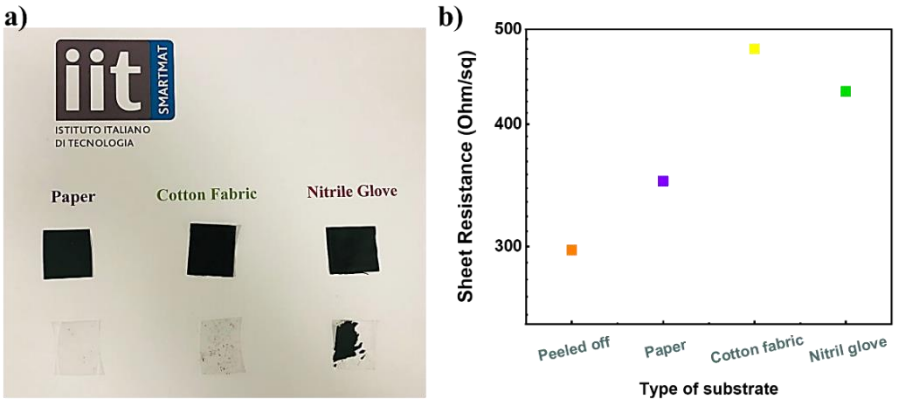

Figure 21. a) Scotch test to evaluate coating's adhesion strength on the different substrates. b) Sheet resistance values of the peeled-off ink and ink sprayed on the different substrate and have been thermally treated at 110 ºC during 2h by the error value ~ ±2 ohm/sq.

5.4 THERMAL TREATMENT CHARACTERIZATION

5.4.1 Thermal treatment temperature

Thermal treatment aims to improve the conductivity of the samples. A DSC measurement of the ink has been realized to select several temperatures for thermal treatment. Indeed, to induce microstructural changes, the temperatures chosen must be close to the glass transition temperature of the ink to allow the polymer chains to have global and cooperative motions[361].

Figure 22 depicts the DSC runs of the ink. Two runs have been performed: the first heating run (violet curve) is made on the pristine sprayed ink, then a fast-

quenching step has been realized (not shown), and finally, a second heating run (cyan curve) has been performed. The first part of the protocol aims at erasing the thermal history of the material, while the second heating run is the proper measurement[361–363].

According to the shape of the first run signal, it can be proposed that the sprayed ink is arranged in a complex network. Indeed, the baseline is hard to determine, and the glass transition is followed by thermal dilatation. The typical enthalpy release of PLA during the glass transition crossing is well visible[364]. Then, in a will of clarity, it has been decided to conclude only from the second heating run. From this measurement and with a heating rate of 5 ºC/min, the glass temperature read seems to be around 49 ºC for the ink. According to this measurement, three temperatures close to the glass transition temperature have been chosen to perform the thermal treatment: 55 ºC, 80 ºC, and 110 ºC as it is assuming that they belong in a temperature range where chains have mobility[364] and can trigger microstructural changes that will improve the conductivity of the material, as it has been done for PEDOT: PSS films[365,366]. Thermogravimetric Analysis (TGA) revealed no degradation characteristics in the temperature range of interest (see **Figure 22**b) (e.g. thermal decomposition).

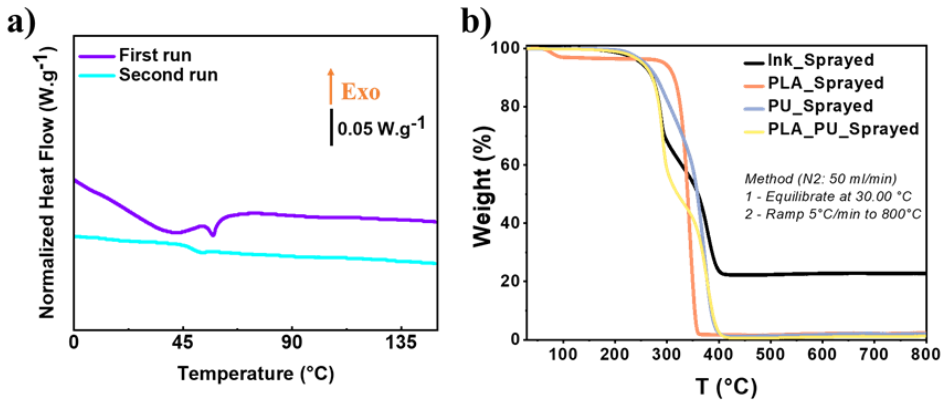

Figure 22. a) Differential Scanning Calorimetry (DSC) measurement at 5 °C/min with heating runs ranging from 0 to 150 °C. b) Thermogravimetric Analysis (TGA) graph of Ink and its ingredient.

5.4.2 Thermal treatments effect on ink conductivity

The peeled-off ink was sintered for two hours at the selected temperatures. Sheet resistance measurements were used to determine the efficiency of the thermal treatment at each temperature. **Figure 23**a shows the sheet resistance after thermal treatment at 55 °C (ATT-55-120min), 80 °C (ATT-80-120min), and 110 °C (ATT-

110-120min). The pristine sample's sheet resistance is also included (BTT). Other groups working with PMMA filled with carbon nanotubes, polymer blends filled with carbon black, ladder polymers (BLL), PEDOT: PSS, or PP filled with carbon nanotubes have also reported the influence of thermal treatment on sheet resistance[367–372]. A slight decrease in the sheet resistance value is visible after the 55 °C treatment compared to the pristine sample, but this difference is minor. After 2 hours at 80 °C, the sheet resistance has roughly quadrupled. A decrease in sheet resistance was also observed after thermal treatment at 110 °C for 2 hours. Heat treatment directly affects filler distribution, and this temperature allowed for some efficient microstructural changes in the ink, which improved the connections between the conductive particulates[372]. The best result was obtained at the highest temperature (110 °C), where the sheet resistance decreased over several decades and remains at 290 ± 2.23 Ω/sq. It has been determined that thermal treatment for 2 hours at 110 °C is the most efficient way to cause microstructural rearrangements that reduce ink sheet resistance. Still, it is possible that increasing the time spent at this temperature can decrease sheet resistance even more. **Figure 23**b depicts the evolution of sheet resistance at various annealing times ranging from 5 minutes to 5 hours at 110 °C. **Figure 23**b shows that even after only 5 minutes at 110 °C, the sheet resistance has decreased and reached a value comparable to the one measured after 2 hours at 80 °C (as visible in **Figure 23**a). The sheet resistance at 110 °C remains relatively constant from 15 minutes to 2 hours. The sheet resistance increases slightly at 60 and 90 min, but this may be an artifact because the sheet resistance reaches close to those reported for lower temperatures.

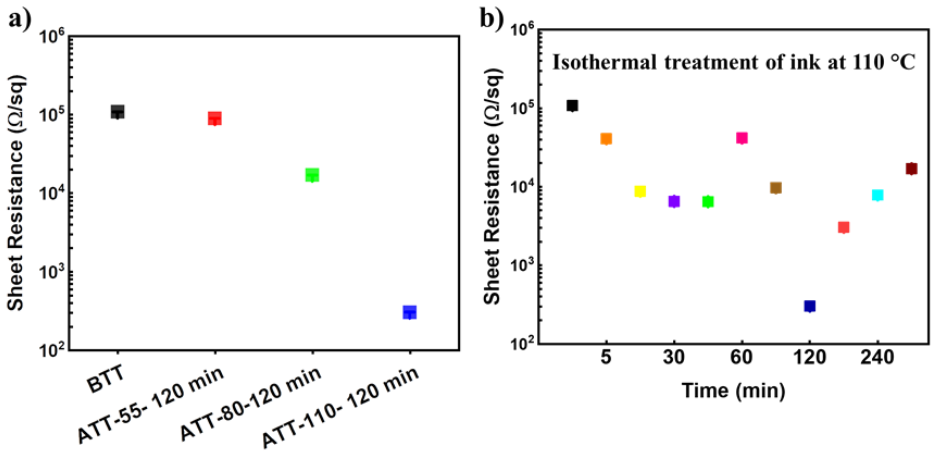

Figure 23. a) Sheet resistance values of the pristine sample (BTT) and samples thermally treated for two hours at 55, 80, and 110 °C. b) Sheet resistance for the isothermal treated sample at 110 °C for 5 minutes to 5 hours.

The sheet resistance slowly increases from 3h to 5h at 110 °C, which can be explained by SEM images taken after the isothermal treatment at 110 °C from 2h to 5h (see **Figure 24**). After 2h at 110 °C, there are no cracks in ink, and good connections appear between the various compounds. Some cracks are visible on the ink after 3h at 110 °C where as these cracks are not visible in the photograph taken after 2h at 110 °C. It is noticeable that cracks become more numerous and deeper between three hours and five hours. This effect appears to be time-dependent, as the crack's depth, length, and width increased over 2h of exposure. The increase in crack characteristics causes defects in the electrical network, increasing the sample sheet resistance[226,299].

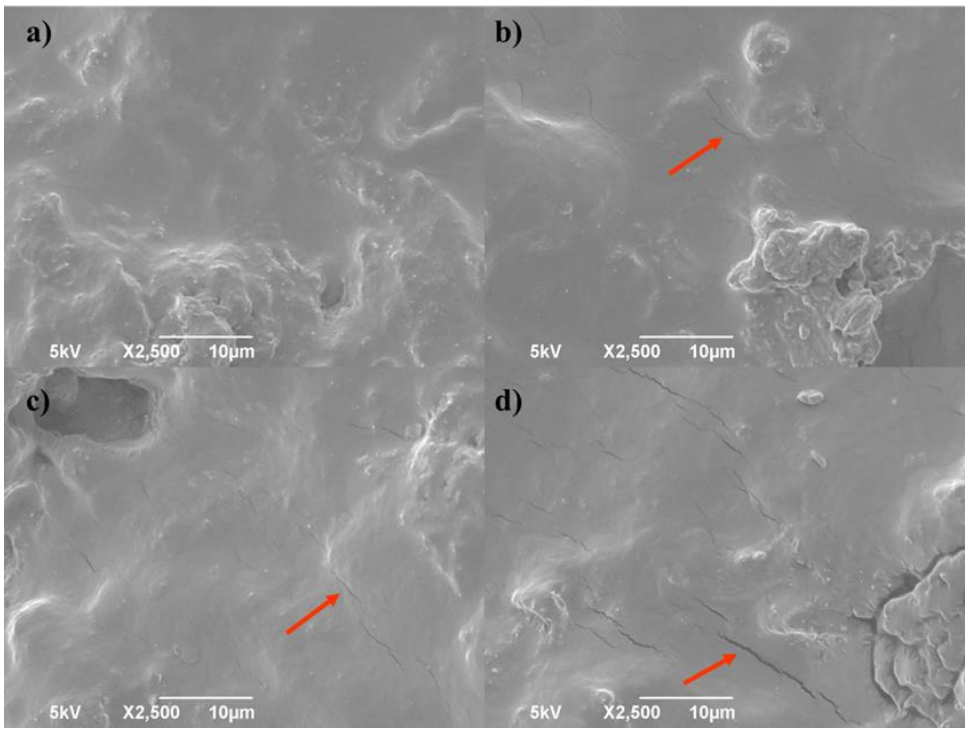

Figure 24. SEM images were taken after the isothermal treatment at 110°C during a) 2h. b) 3h. c) 4h and d) 5h.

5.4.3 Impact of thermal treatment on the microstructure of ink

DSC isotherms were performed for 2 hours at each temperature (55, 80, and 110 °C) to see if there is a change in the heat flow measured that could be due to ink crystallization and to better understand the origin of the sheet resistance decrease after thermal treatment from a microstructural perspective. Indeed, the presence of a crystal can increase polymer conductivity[299,372,373]. Following the isothermal treatment, the samples were quenched at -200 °C/min and a fast heating run (5 °C/min) from 0 to 150

°C was performed. **Figure 25**a shows the isotherms, while **Figure 25**c shows the second heating run of the pristine and treated samples.

The heat flow remains constant throughout all measurements, as shown by the isothermal graphs (**Figure 25**a). It indicates that no crystallization occurred during this step; XRD measurements support these findings (see **Figure 25**b). Furthermore, as shown in **Figure 25**c, the thermal treatment had no effect on the glass transition temperature when compared to the pristine sample. The only microstructural changes responsible for the decrease in sheet resistance are caused by the removal of some microstructural constraints that exist after spraying (as seen in the first run of the pristine sample, **Figure 22**a), resulting in reorganization of the polymer chains as a result of the thermal energy provided by this treatment and the formation of new interactions that aid in electron displacement, thus improving electrical conductivity. However, because there are no differences in the glass transition temperature for all temperatures tested when compared to the pristine sample, the electrical conductivity increase can be attributed to enhanced filler connections and structural reordering[371,372].

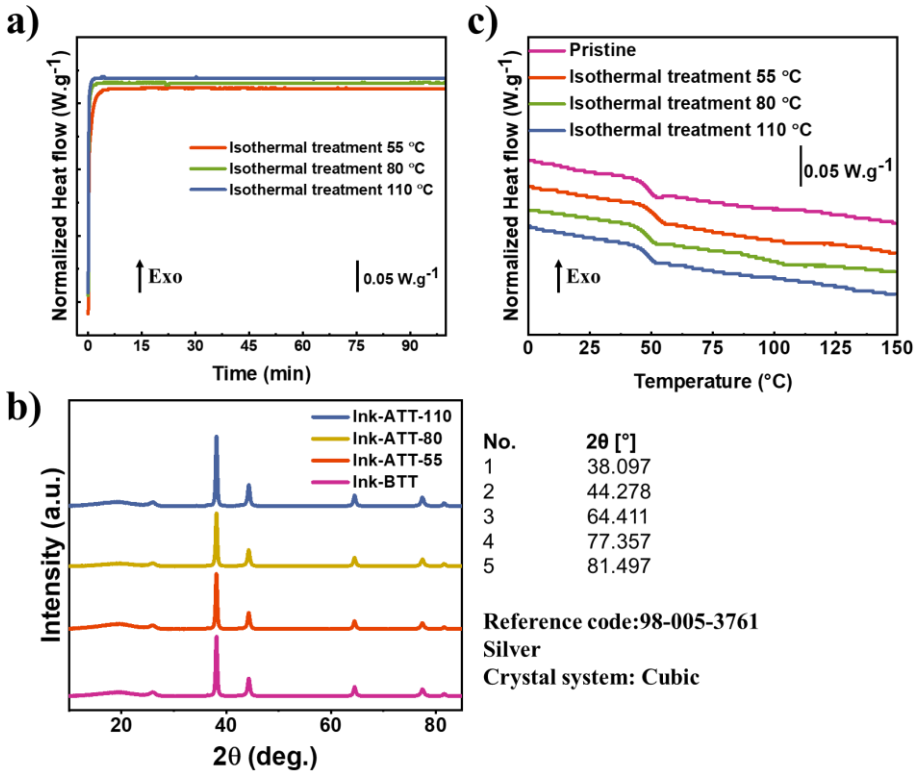

Figure 25. a) Isothermal treatment at 55 ºC, 80 ºC and 110 ºC. b) XRD measurements of Ink annealed at different temperature. c) Second heating run at 5 ºC/min from 0 to 150 °C.

DSC measurements revealed that the decrease in sheet resistance is due to filler reorganization rather than crystallization at all temperatures tested. It is now interesting to learn why 110 °C is the best temperature because it has significantly reduced sheet resistance over several decades. As a result, a DMA measurement was performed to better understand how rigidity changes with temperature (**Figure 26**). The black crosses on the storage modulus of the pristine sample (pink curve) represent the three thermal treatment temperatures (55 °C, 80 °C, and 110 °C).

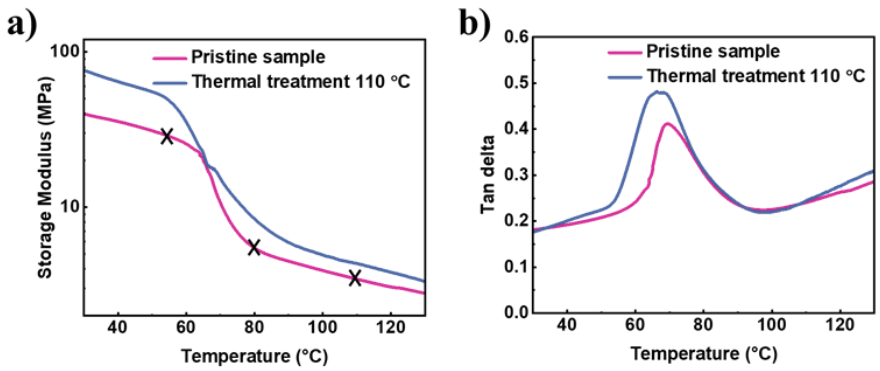

Figure 26. a) DMTA measurement of the pristine samples and the sample treated at 110 ºC. The black crosses on the pristine curve represent the three selected temperatures for the thermal treatment. b) The measurements have been performed from 30 ºC to 130 ºC performed at a 10 Hz frequency of and with a heating rate of 5 ºC/min.

Figure 26a shows three typical zones of polymer viscoelastic behaviour: the glassy plateau, up to around 60 ºC, where chains have low mobility, followed by α-relaxation, which is visible by a drastic decrease in rigidity. Because the chains possess low mobility, this relaxation results in a rubbery plateau with low rigidity. The three temperatures chosen for the thermal treatment (55, 80, and 110 °C) fall roughly into these three zones. In addition, a thermal treatment performed at 110 °C allows the polymer chains to have greater mobility (middle of the rubbery plateau) when compared to treatments performed at 55 °C (beginning of the α-relaxation) and 80 °C (end of the α-relaxation). At 110 °C, the chains move quickly, allowing the ink to rearrange itself while improving the connections between the various conductive particles (carbon nanotubes and silver nanoparticles)[373]. This DMA curve explains the good results of the sheet resistance reduction observed with the 110 °C treatment. The pristine sample (pink curve) and the thermally treated sample (blue curve) can also be compared in this graph. The rigidity of the treated samples has nearly doubled (as seen in the storage modulus curve) as a result of reorganization in this microstructure. Even

after α-relaxation and on the rubbery plateau, the rigidity of the treated sample remains higher than that of the pristine sample until the end of the measurement. It means that the microstructural rearrangements made during the thermal treatment are stable enough to remain even after the α-relaxation temperature has been reached. The α-relaxation temperatures of the pristine and treated samples are similar (a little lower for the treated samples, 67 °C vs. 68 °C for the pristine) and also agree with what is commonly reported for PLA depending on the measurement methods. Because the presence of fillers reduces the mobility of the polymer chains, the α-relaxation temperature is higher than that of a PLA[374,375]. The magnitude of the Tan delta peak of the treated sample is greater during the transition, as shown in **Figure 26**b. It reveals that the treated sample has the greatest increase in chain mobility when compared to the pristine one[375]. Indeed, one of the pristine samples is slightly more constrained as a result of the spraying (as seen in **Figure 22**, DSC curve with the first and second heating), whereas the treated samples' chains have received more thermal energy to reorganize the constrained areas. Sheet resistance measurements confirm the DMA results, which showed that chain mobility was higher at 110°C than at 80 °C.

5.5 BIOCHEMICAL OXYGEN DEMAND (BOD) IN SEAWATER

Polylactic acid (PLA) has been the subject of a lot of research lately. This is not only because it has great mechanical properties, but also because it can be made from lactic acid by fermentation and biodegrades in industrial compost[376]. However, the increased use of PLA has resulted in an increase in the contamination of the environment with PLA-containing products. This is due to the fact that PLA does not degrade even after three years of immersion in water or burial in soil[376].

The degradation rates of the coating and its ingredients, namely PLA/PUDs and PLA and PUDs, were studied separately in seawater under laboratory conditions for one month (see **Figure 27**a). The blend of waterborne polyurethane with polylactic acid can improve the biodegradability of PLA due to several reasons:

Increase in Surface Area: When PUDs is blended with PLA, it can form a stable, immiscible blend with a larger surface area. This increased surface area provides more space for microorganisms to attach to and break down the PLA, leading to faster biodegradation (see **Figure 27**b).

Increased Hydrophilicity: PLA is hydrophobic in nature, which means it resists water absorption. However, when PUDs is blended with PLA, it increases the hydrophilicity of the blend, making it more susceptible to water absorption. Water absorption can provide an ideal environment for microorganisms to colonize and break down the PLA. The wettability of peeled-off ink before and after the BOD test is shown in **Figure 27**c. As can be seen, blending PLA/PUDs/fillers produces a more hydrophilic structure (water contact angle 32.8°± 0.3°), which increases water diffusion and, as a result, the ink's degradation rate. The hydrophobicity of the ink (water contact angle 94.9° ±1.1°) after BOD can then be explained by increasing the ink's surface roughness.

Synergistic Effects: The combination of PUDs and PLA can also have a synergistic effect, meaning the properties of the blend are greater than the sum of its parts. This synergistic effect can result in a combination that is more easily biodegradable than either component alone.

Overall, the blend of PUs with PLA can improve the biodegradability of PLA by increasing surface area, hydrophilicity and exhibiting synergistic effects[59,377–380].

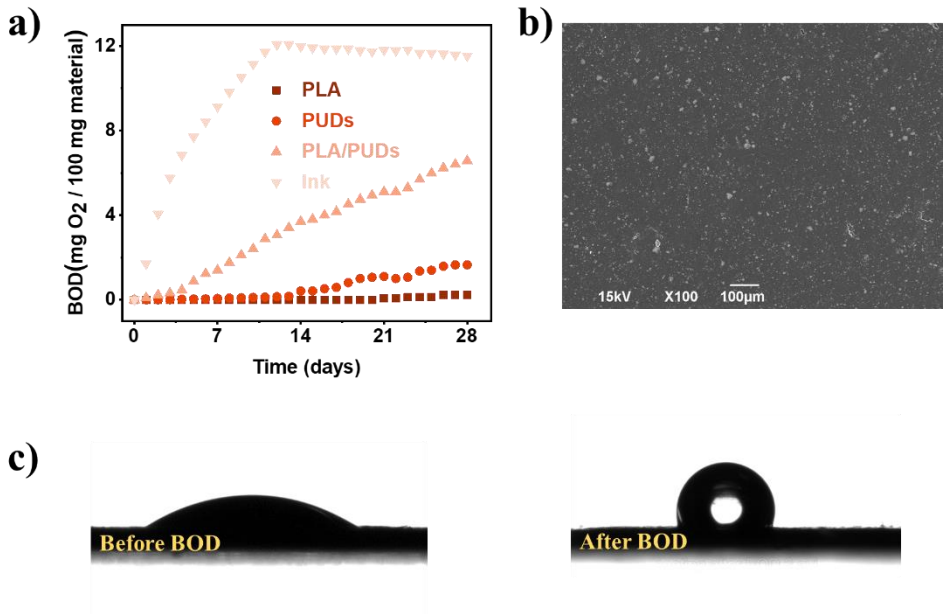

Figure 27. a) Biochemical oxygen demand (BOD) of peeled-off ink treated at 110 °C and its component in seawater. b) SEM image of PLA/PUDs film. c) Surface wettability measurement before and after BOD.

Figure 28a and **Figure 28**b, imaged by the Zeta profilometer, show that penetrating sea salt increases the surface roughness of ink after it has been exposed inside the sea water, with the presence of the sea salt later confirmed by SEM analyses (**Figure 28**c and **Figure 28**d).

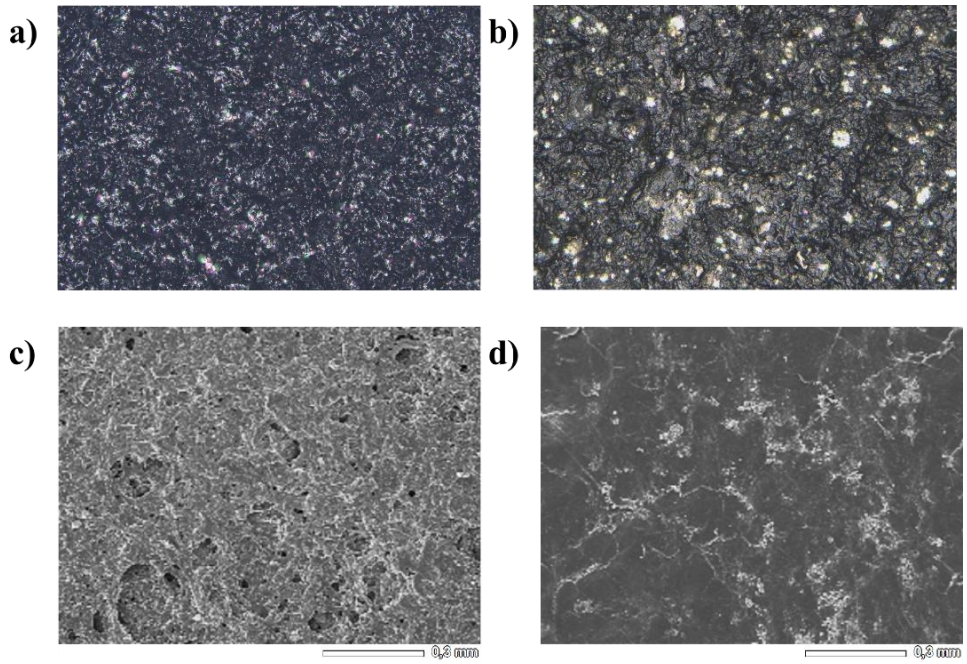

Figure 28. Images of the surface roughness of peel-off ink taken with the Zeta profilometer. a) Prior to BOD, b) Following BOD. SEM analysis of the surface components of the coating c) Prior to BOD, d) Following the BOD test.

5.6 FABRICATION AND SENSING MECHANISM OF THE SENSOR

There are several methods for producing interdigitated electrodes, including wet etching, photolithography, inkjet printing and subsequent metal Au or Ag deposition, and screen-printing silver paste[56]. **Figure 29** depicts a schematic representation of the sensor manufacturing process, which consists of two simple steps: first, ink was applied to the paper, which was then thermally treated at 110°C for two hours to obtain the desired electrical properties.

In a vacuum desiccator, liquid PDMS and curing agent (Sylgard 184) were mixed at a weight ratio of 10:1. The degassed PDMS was poured on top of the FR4 substrate, which was then degassed and baked for 1 hour at 80 °C. Commercially available conductive silver ink was printed on the FR4 substrate coated with PDMS film using the Voltera V-One PCB printer to increase the sensitivity of pressure sensors. The polymerized PDMS detached from the FR4 substrate after the printing

layout was completely dried. The printed layout has an eight-finger interdigitate with total dimensions of X= 21.0 mm Y= 13.0 mm, a distance of approximately 500 µm between two adjacent electrode fingers. To ensure good conduction, copper wire was attached on both sides of the sensor and the sensor was sealed with adhesive tape.

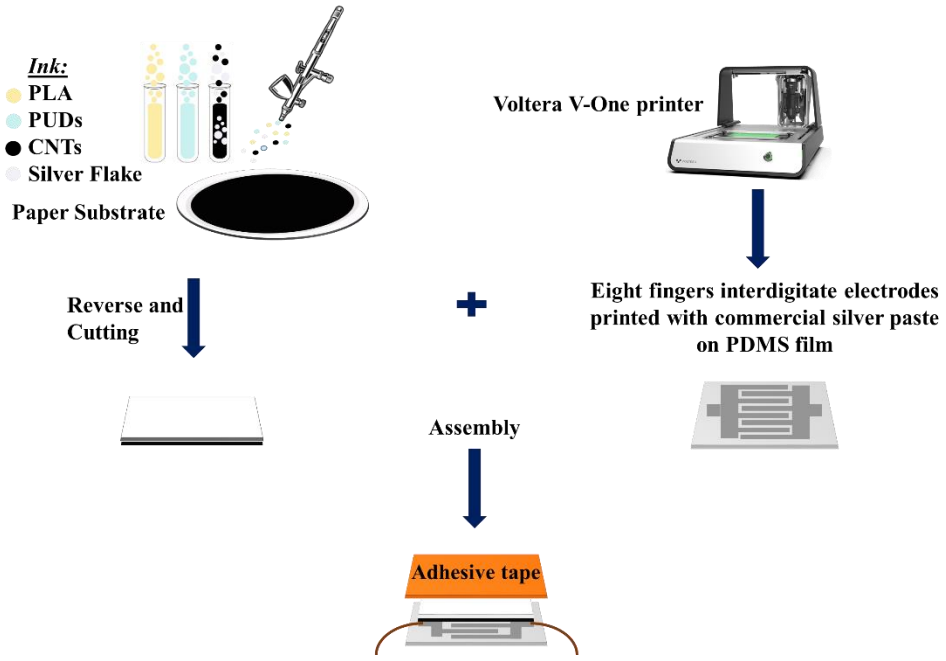

Figure 29. Graphical representation of the pressure sensor production procedure.

5.7 PROGRESSIVE COMPRESSION TEST

Since the sensor is designed to monitor repetitive pressure sensing, therefore it was subjected to a cyclic progressive compression test, and the effect of cyclic deformation on the resistance was investigated through Instron-Keithley coupled measurements. Since these cycles frequently use either constant pressure or variable force, sensor performance was assessed in both scenarios. Given the applied electric voltage V and the measured current I, the resistance was calculated at each instant for each graph using the standard Ohm's law and is plotted for independent sensors in **Figure 30** normalized to the initial resistance value R_0.

In the first scenario (**Figure 30**a), the constructed sensor was positioned between Instron clamping plates. A low-power load cell (10N) was used to apply precise pressure, which was gradually increased from 0.2 kPa to 10 kPa (pressure values with more in details; 0.2-0.3-0.4-0.5-1-2-5-10 kPa) with a 30-second relaxation period in between two different loading pressures. Continually in all unloading modes, the

pressure dropped back to 0.1 kPa, and each cycle was repeated five times. To avoid a short circuit, the clamping plates were taped off. The sensor output is unchanged in the pressure range of less than 0.3 kPa, as highlighted by the red circle in the inset magnification of **Figure 30**a. The current detection performance was found to be stable and continuous, with no apparent signal loss when loading and unloading, despite the increase in applied pressure at each cycle.

Looking at **Figure 30**b, the second scenario involves putting the sensor through a pressure range that goes from 0.5 kPa all the way up to 10 kPa using a low-power load cell. Each cycle consists of 30 seconds of applying pressure, followed by 30 seconds of releasing it. After each cycle, the sensor demonstrated an excellent recovery from pressure when left to relax the stress, going back to almost the same resistance value in comparison to the initial R0. This was particularly noticeable at a higher pressure range, which ranged from 10 to 500 kPa (**Figure 30**c), where the same behaviour was observed. This drop in the sensor's relative resistance after being loaded with pressure is most likely caused by a better arrangement of the fillers contained within the coating[381]. The cone-shaped structure of the graph changed when the applied force was greater than 5 kPa. This may be because, when the sensor is subjected to pressure, the coating rearranges itself while the PDMS film slightly contrasts the applied force. The sensor was subjected to a constant pressure of 2 kPa in the final scenario (**Figure 30**d) to test further the sensor' sensitivity to the applied constant pressure and capability to recover the initial resistance. Increasing the time of applied stress from 1 second to 10 seconds clearly resulted in a gradual decrease in resistance under constant pressure. In contrast, for the time greater than 15 seconds, the change in resistance value will be stabilized on a straight line, highlighted with a dashed red line.

In general, when the sensor is subjected to pressure, two phenomena occur in the system. The first is the formation of conductive networks as a result of conducting particle rearrangements, and the second is the destruction of some conductive networks as the inter-particle gap increases. The changes in electrical properties will be determined by the dominance of one of these two phenomena. According to the above analysis, adding external pressure reduces the distance between two neighbouring conductive fillers, i.e., the average inter-particle gap is smaller, resulting in a lower sensor total resistance[382–384].

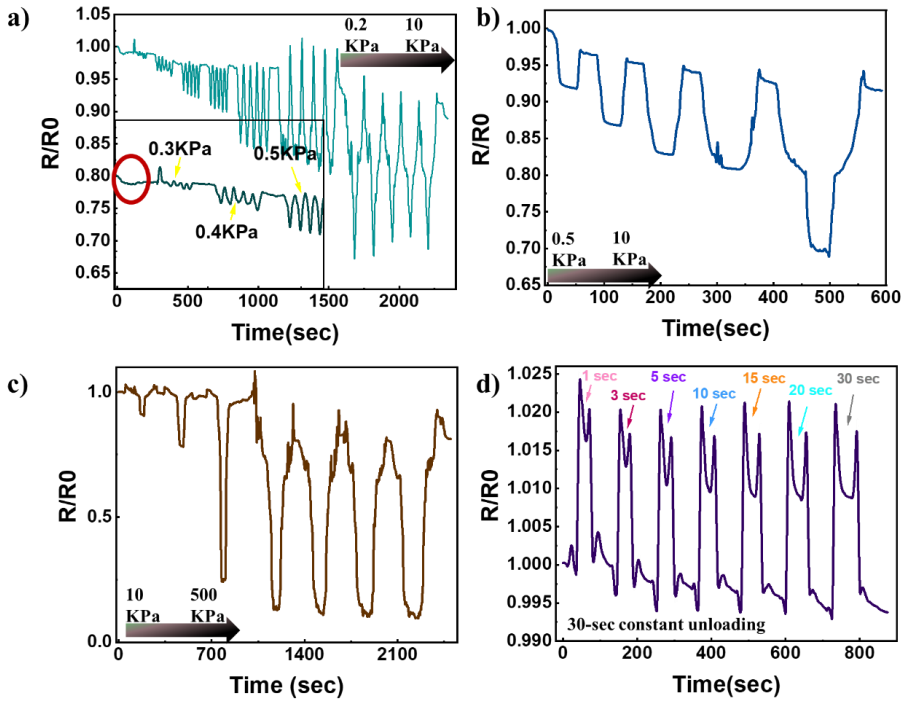

Figure 30. Sensor response during loading and unloading a) Cyclic low power pressure ranging from 0.2 kPa to 10kPa, b) Step low power pressure ranging from 0.5 kPa to 10 kPa, c) Step high power pressure ranging from 10 kPa to 500 kPa, d) Constant pressure of 2 kPa with varying relaxation time.

5.8 CONCLUSION

In conclusion, conductive ink is developed in this chapter using silver flakes, multi-walled carbon nanotubes, and PLA-based aqueous emulsions. One of the primary objectives of this chapter followed by previous chapter, is to discourage the use of chloroform and other non-renewable solvents in PLA-based inks and suspensions. Emulsifying replaces a significant portion of the solvent with water. If the solvent is not biodegradable, the costs and emissions are reduced. Dynamic light scattering and optical microscopy analysis of the emulsion and ink revealed a highly distributed oil in water emulsion containing PLA and hybrid fillers that can remain stable for several days. To investigate the effects of annealing for varying amounts of time and temperatures, various techniques are used. The results show that subsequent treatment at 110°C for 2 hours improves the electrical properties of the coated sample for several decades. Moreover, a paper-based sensor yields high-pressure sensitivity (0.3 kPa) along with an operational range (0.1- 500 kPa). During the cyclic pressure test, there is a decrease in the relative resistance, which may be explained by the fact that the distance between two adjacent conductive fillers is decreased as a result of the

external pressure. In addition, ink is capable of biodegradation in marine environments, which results in a gradual reduction in the accumulation of the substance within the ecosystem. This leads to an increase in the overall health of the ecosystem.

Chapter 6: Recyclable electrically conductive vitrimer-based inks for strain sensor

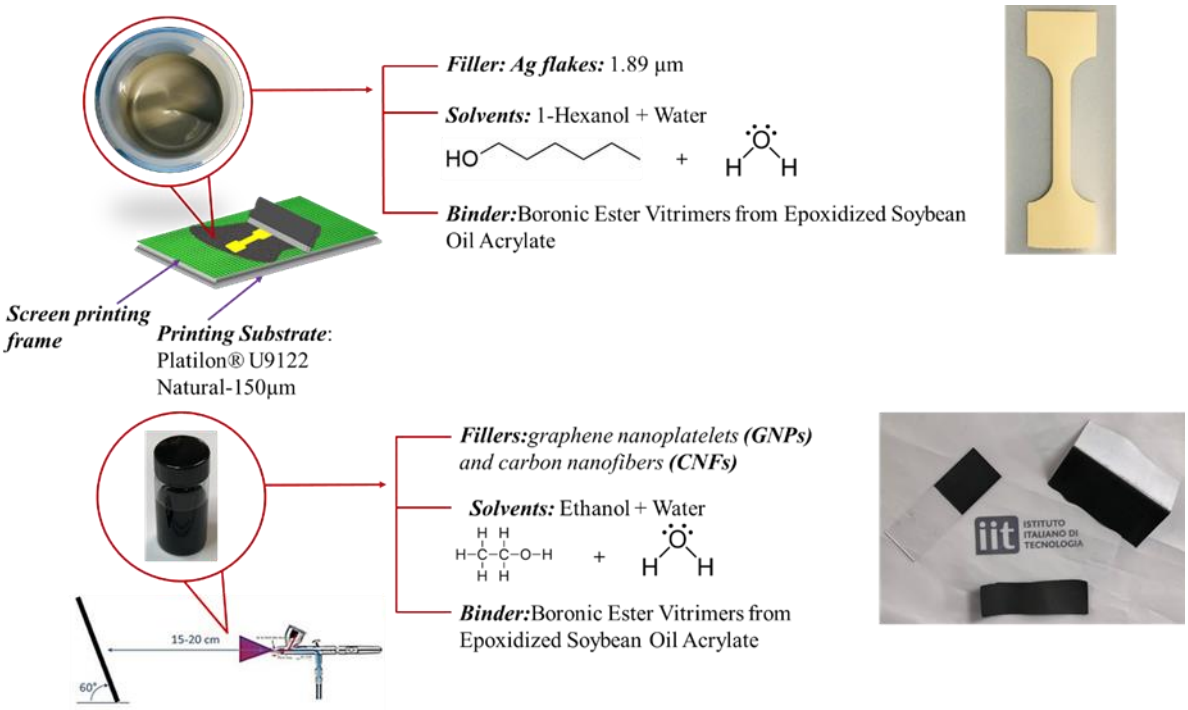

Sensors and transducers are well-known devices that are seeing an increase in research and development due to their numerous applications in electronics and robotics[385]. They are found in measuring instruments, but they are also widely used in medicine, industry, and control systems. Furthermore, every smart object requires sensors to perform its functions, and it is thanks to sensors that smart is becoming so prevalent in everyday life. Sensor technology is especially important in robotics and artificial intelligence, two new fields that are rapidly expanding[386]. Furthermore, sensors, like electronics in general, are undergoing an actual transformation toward greener and more sustainable manufacturing, with the goal of producing fully recyclable devices and limiting the creation of e-waste. This chapter describes the fabrication of novel inks taking advantage of carbon-based conductive fillers, such as graphene nanoplatelets (GNPs) and carbon nanofibers (CNFs) or metallic conductive fillers, such as silver flake, with a dynamic thermoset (a so-called vitrimer) synthesized from a mixture of epoxidized soybean oil acrylate (ESOA) and diboronic easter dithiol

(DBEDT) dynamic cross linker. Due to its flexibility, recyclability, and capacity to self-heal damages like cuts or cracks at ambient conditions, the boronic ester vitrimer made from soybean oil was chosen as a binder.

Indeed, it will be demonstrated that the presented conductive inks have a lot of potential in flexible electronics, particularly in the field of sensors, due to their conductivity similar to that of conductive polymers and their self-healing characteristics inherited from the vitrimer matrix. Further to that, the material's recycling and reusing possibilities make it an appealing option available for advanced and innovative electronic devices, addressing a topic of critical importance in today's technologies, such as sustainability and circular economy.

6.1 BORONIC ESTER VITRIMER: A BIOBASED, BIODEGRADABLE, SELF-HEALING MATERIAL

The class of polymers known as thermosets is distinguished by a permanent, three-dimensional network created by covalent cross-links. Due to their cross-linked nature, which provides high mechanical strength, chemical resistance, as well as thermal and dimensional stability, they find a wide range of applications, including adhesives, coatings, and polymer matrices in composites for transportation, wind blades, aircrafts, sporting goods, and electrical materials[387,388].

Unfortunately, most epoxy resins are made from fossil feed stocks and toxic chemicals like BPA and epichlorohydrin. BPA, an endocrine disruptor, can negatively affect human health. Traditional thermosets also accelerate fossil-based feedstock consumption and create persistent plastic waste[389,390].

Thus, renewable, biodegradable thermosets are needed to be urgently developed. Due to their renewability, availability, and environmental friendliness, plant oils could be used to make thermosets. Oils from different origins contain functional groups like double bonds, esters, and hydroxyl groups for chemical reactions, making them versatile[391].

Soybean oil has several unsaturated double bonds within the fatty acids; nevertheless, they are not very reactive and must frequently be converted into more reactive functional groups. Epoxy groups can be implemented directly into the soybean oil by reacting it with hydrogen peroxide and either acetic or formic acid. This type of

epoxidized soybean oil (ESO) is commonly employed in the manufacturing of epoxy resins utilizing curing agents such diamines, dicarboxylic acids, or anhydrides. ESO is also used as a green plasticizer in polymers such as polyvinyl chloride and polylactic acid[392,393].

Traditional thermosets have a significant disadvantage in that they cannot be easily reprocessed or recycled after their use period, so they are either disposed of as waste in landfills or incinerated, which causes serious environmental concerns and significantly increases the overall material cost[394]. To address these concerns, dynamic cross-links capable of exchanging reactions can be incorporated into thermosets, allowing network rearrangements, malleability, and reprocess ability. Such created dynamic thermosets constitute a new class of materials known as vitrimers because they flow like vitreous silica (quartz glass) according to the Arrhenius law[395]. Because of this, vitrimers, like thermoplastic polymers, can be repaired, reshaped, and reprocessed using extrusion, injection or compression molding, and 3D printing, drastically lowering both the price and the effect to the environment[181,396,397].

Appendix A describes an eco-friendly synthesis of a diboronic ester dithiol (DBEDT) dynamic cross-linker used for the preparation of catalyst-free, bio-based vitrimers via thiol-acrylate coupling of ESOA and DBEDT.

ESOA-DBEDT, like thermoplastics, can be reprocessed numerous times without affecting its mechanical performance. Additionally, a recycling procedure was established in which the vitrimer can be regenerated by hydrolysis and dissolution in 90% v/v ethanol, followed by solution evaporation. The ESOA-DBEDT vitrimer had excellent potential as a self-healing coating and was biodegradable, removing issues regarding waste accumulation in the environment[181].

6.2 CONDUCTIVE INK PREPARATION

6.2.1 Carbon-based vitrimer ink

The binding vitrimer polymer ESOA-DBEDT was hydrolysed and dissolved in a solution of 1mL H_2O and 9mL ethanol at room temperature for 24 hours and then filtered to remove any possible solid residues (<1%). CNFs and GNPs were dispersed separately in 20 mL of ethanol using ~50 µL of the dispersing agent Tween®80 and sonicated for one hour. By combining the components mentioned earlier, three mixtures containing 10, 20, and 30% by weight of the fillers (GNPs and CNFs

combined, with the weight ratio of 1:1) concerning the total weight of the coating material were obtained. Each contains 49 mL of ethanol, 1 mL of water, and ~100 µL of Tween®80 as a solvent. The prepared carbon-based vitrimer inks were sonicated for an additional hour before spray coating onto the substrate.

6.2.2 Silver-based vitrimer ink

There is a range of acceptable viscosity for different printing methods; ink viscosity is very important due to its efficiency when spread on the substrate and is affected by various parameters, the most important of which is the solvent evaporation rate[398]. The lower the boiling point of the solvent, the faster it evaporates, influencing the actual composition of the wet ink, increasing its viscosity, and causing differences in the printed mass. The faster-evaporating solvent also has an effect on the internal structure after deposition because faster-drying films have much higher internal tension, which should result in lower resistivity values. When ink does not successfully transfer to the substrate but remains in the screen meshes, a clear solvent spot on the substrate appears as evidence of contact between the solvent front and the substrate. The ink flows through the mesh as a core of particulates protected by a vehicle-rich layer. The effective viscosity of the ink is reduced during printing as a result of the ink structure. Furthermore, the presence of a solvent with a lower boiling point results in an increase in surface roughness[399,400]. In this light, 1-hexanol was chosen as an ethanol substitute to achieve a good performance-sustainability balance. Several kinds of ink were formulated, following the quantities reported in **Table 9**, by mixing the hydrolysed vitrimer in 1-hexanol and water with silver flakes.

Table 9. Different silver-based ink formulation.

Ink	Filler (g)	Binder (g)	Filler vol.% Density: 10.490 g/cm³	Binder vol.% Density: 1.09±0.05 g/cm³
1	0.29	0.3	9	91
2	0.48	0.3	14	86
3	0.75	0.3	20	80
4	1.125	0.3	28	72
5	1.63	0.3	36	64
6	2.56	0.3	47	53

6.3 SIGNIFICANT FINDINGS

6.3.1 Carbon-based vitrimer ink characterization

The adhesion of the conductive pattern to the substrate and its conductivity are critical for the practical applications of flexible electronic devices. **Figure 31** depicts SEM images of vitrimer ink coated on natural rubber (**Figure 31**a and b), glass (**Figure 31**c and d), and paper (**Figure 31**e and f) substrates with varying nature and mechanical properties and then compress moulded to increase the coating's compactness. Vitrimer in formulated ink may vastly improve the adhesion property of the conductive pattern. If the ink's adhesion properties to the substrate are poor, the formed conductive pattern will be easily cracked and detached from the substrate. As a result, it is critical for ink solutions to select a suitable solvent to improve adhesion with appropriate surface tension gradients[401,402].

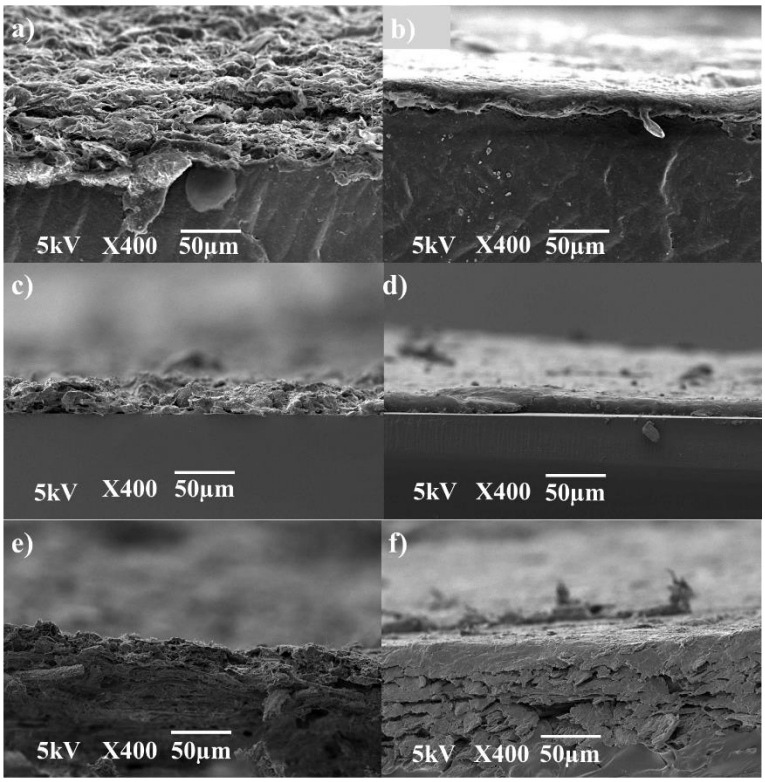

Figure 31. SEM images of cross-section view for the carbon-based vitrimer ink. The right column images belong to samples before the hot-press, coated on a) natural rubber, c) glass, and e) paper. The left column images belong to samples after compression molding, coated on b) natural rubber, d) glass, and f) paper.

For the recyclability test, carbon-based ink was sprayed onto a glass substrate. This idea is based on the fact that hydrolysis and the subsequent regeneration of boronic esters vitrimer after solvent evaporation and drying can be used to recycle and reuse

the ink and can be performed multiple times. The electrical characteristics of the ink sample were measured, along with an analysis of the sheet resistance of the dried printed layers. The goal of this test was to environmentally friendly recover the sensor's components to support the thesis's goal of developing a sensor with a circular economy perspective. The coated glass was immersed for three hours in a solution of 90% volume ethanol and 10% volume water to remove the coating by hydrolysis and dissolution of the vitrimer binder. The glass substrate was then removed and washed with a small amount of water and ethanol. The obtained recycled ink was sprayed again on the same glass substrate to recreate the original material. Emphasis was put on the investigation of changes induced by recycling on the electrical properties. **Figure 32**a and **Figure 32**b present SEM images of the sensor on the glass substrate both before recycling and after recycling and further spraying, respectively. **Figure 32**c, in fact, shows that the relative resistance of the ink did not change significantly following recycling and additional spraying. **Figure 32**d depicts the recyclability test's methodology.

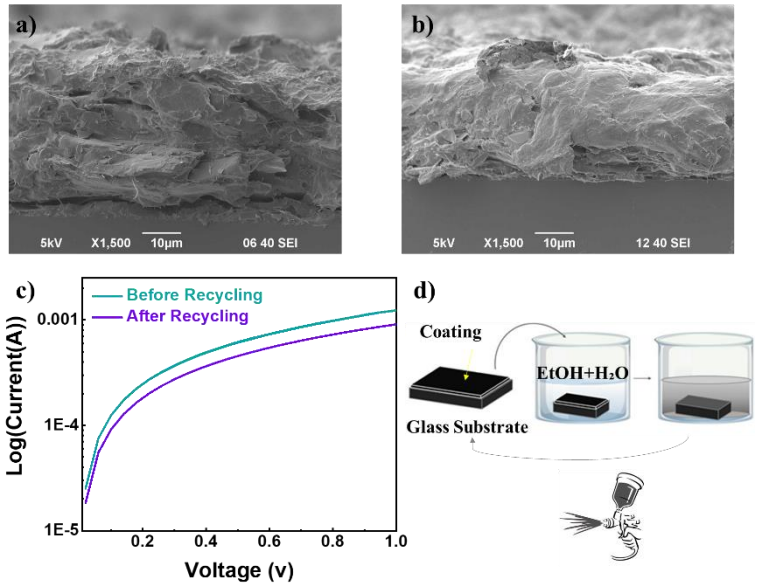

Figure 32. Cross-section view of coating state on the glass a) before recycling, b) after recycling. c) Relative value of the resistance for the initial sensor and after recycling. d) Schematic illustration of the recyclability test.

6.3.2 Silver-based vitrimer ink characterization

Figure 33a depicts the relationship between sheet resistance and silver flake loading. The studies were carried out on screen-printed samples on a TPU substrate before and after 30 minutes of sintering at 160 degrees. The sheet resistance decreased

significantly as the loading of silver flakes (AgF) increased, and a severe decrease after sintering is visible in the sample with a higher content of conductive filler. Clearly, sintering causes conductive filler densification through the conductive network. When the conductive filler loading is raised from 20 vol% to 28 vol%, there is a six-order-of-magnitude decrease in the sheet resistance value. As a result, the electrical percolation threshold is within this range of nanofiller concentration. As shown in **Figure 33**a, the sheet resistance, measured with four point probe, decreased to around 7.96 Ohm/sq before sintering at 36 vol% AgF and $0.18 \pm 5.5 \times 10^{-6}$ Ohm/sq after sintering, maintaining a similar value at higher loading. After monitoring the sheet resistance for a month, it was evident that there had been no change in the values for the high conductive filler content; consequently, the silver flake would not oxidize after sintering. At the same time, the sample containing 28 vol% conductive filler started to lose its properties after two hours. Such an effect can be explained by analyzing the electrical conductivity behavior as a function of filler content.

Adding electrically conductive particulate fillers, such as metal nanoparticles, to electrically insulating polymeric matrices is generally a fascinating alternative method of giving the material long-lasting good electrical properties[403]. When polymeric matrices are given a specific quantity of conductive particulate (referred to as the electrical percolation threshold content). Physical contact between the electrically conductive particles creates electron-conductive paths within the polymer networks, enabling electronic flow and an increase in the polymer's electrical conductivity of many orders of magnitude (**Figure 33**b). Tunnelling between conductive particles that are sufficiently close to one another (less than 10 nm) can also cause the charge flow inside polymer networks. When a power law current-voltage (I-V) relationship is seen for the material, the tunnelling effect may be taken into account as the dominant electron-conduction mechanism. On the other hand, when a linear I-V relationship is confirmed, the electronic conductivity is significantly influenced by the direct contact between the filler particles[404].

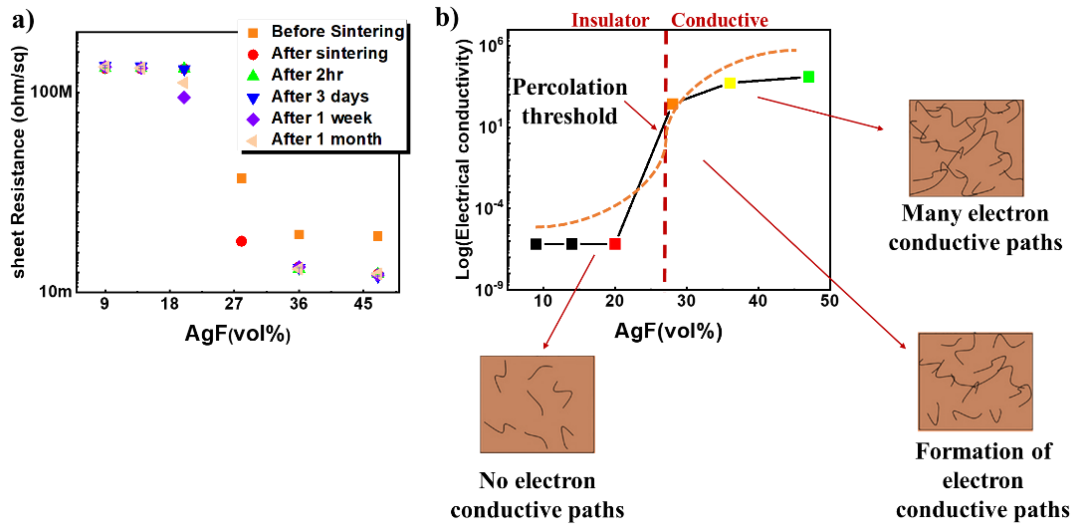

Figure 33. a) Measuring the sheet resistance versus different silver flakes loading for screen printed samples on TPU substrate before and after sintering up to one month. b) Characteristic graph of electrical conductivity as a function of filler content for conductive networks.

The percolation mechanism in polymeric matrix with conductive fillers has been studied extensively. The nature of the percolating state and the zone of percolation, however, remain uncertain, and they are dependent on the aspect ratio and the nature of the conductive fillers. Understanding the relaxation and conductivity behaviour in the composite clarifies the role of fillers and the percolation mechanism[405–407]. Indeed, three relaxation processes induced by the filler, polymer matrix, and interfaces between the filler and the polymeric matrix govern conductive channels[408]. The conductivity behaviour with different silver flakes loadings suggested that charge tunnelling between AgF-AgF and AgF-vitrimer matrix should induce the transition from an insulating to a conducting state. By forming conductive channels near the percolation threshold, this unique physical mechanism for the sample containing 28 vol% silver flakes was realized, as it is clear in **Figure 33**b. To gain a better understanding of our hypothesis that relaxation in the polymeric matrix could influence the unstable electrical properties of the sample containing 28 vol% silver flakes, DMTA for the relaxation dependence of vitrimer at various temperatures and frequencies must be performed.

Through morphological properties, as-printed Ag-filled patterns using two types of inks strike a clear stance, where the microstructures varied in dispensation and degree of contact. **Figure 34**a and **Figure 34**b conduct images from the surface of the sample with 28 vol% silver flakes. As can be seen, an irregular spread of silver flakes

on the surface, consisting of small and large areas of silver flake aggregation (highlighted with orange circles), exhibited an uneven surface morphology that consequently made a disturbance in the pathway for the transportation of electrons. In contrast, as seen in **Figure 34**c and **Figure 34**d, coating layers containing 36 vol% conductive particulates before and after sintering were relatively smooth and uniform on the TPU substrate, and adjacent particles connected to network structures. Indeed, the slight trace of the screen mesh on the surface is noticeable in this sample which confirms the suitable viscosity of the ink for this method. Densely packed Ag flakes are evidenced in the high-magnification images in the cross-section view for the sample containing 36 vol% conductive filler before and after sintering, as shown in **Figure 34**e and **Figure 34**f, respectively. Furthermore, cracks are absent on the surface; confirming that thermal sintering did not cause any damage to the coating layer. Moreover, the appearance of voids in both Ag printed layers was caused primarily by the rapid evaporation of low boiling point solvents in Ag ink following the annealing process[409,410]. The cross-sectional thickness of Ag-printed on the TPU substrate was around 6.5-8 μm. The estimated thickness was later utilized to calculate the bulk resistivity[226].

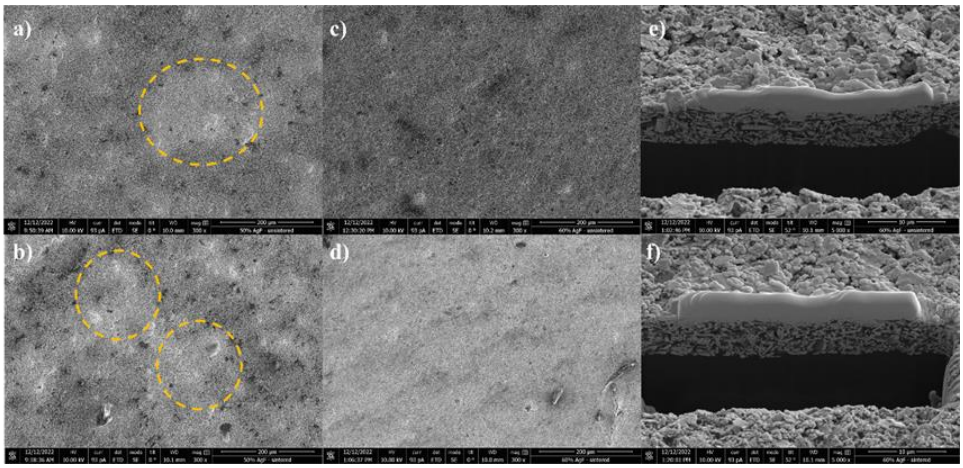

Figure 34. SEM images of Ag patterns printed on TPU substrate containing: 28 vol% silver flakes a) before sintering, b) after sintering, and 36 vol% silver flakes c) before sintering, d) after sintering. FIB cross-sectional images of Ag- patterns on TPU substrate containing 36 vol% silver flakes e) before sintering, f) after sintering.

The filler content, which must be as low as possible while still allowing it to fulfil its electrical requirements, is extremely crucial in the production of conductive inks[410]; otherwise, the mixing process would become challenging, the mechanical

properties also seem to be poor, and the final price is high. Under such a perspective, all measurements are based on a sample containing 36 vol% silver flakes.

To ensure both the sensor system's effectiveness and the screen-printed film's reliability, a quantitative assessment of the adhesion properties of thin films is necessary. Scratch tests were performed in this regard to identify the critical loads and damage mechanism of the screen-printed ink layer. The four-point probe technique is used to measure the difference in sheet resistance after scratch tests with various loading forces, as shown in **Figure 35**a. The critical load, 3000 mN, is nearly 150 times higher than that determined for the commercial ink, which is 20 mN[411]. For the loading higher than 3000mN, the sheet resistance started to rise dramatically. Therefore, as reported by Zych et al[180], differences in adhesion between commercial and prepared inks may also be related to the unique chemical nature of the vitrimer binder with dynamic crosslinks in these inks. However, a variety of other factors, such as surface energy, the polarity of the joined surfaces, solvent residues in the inks, or solvent absorption into substrate surfaces, may also have an impact on adhesion[412]. According to the optical images in **Figure 35**b and **Figure 35**c, a further increase in applied load eventually results in breaking the conductive layer through cracking along its thickness.

Since a sintered sample with a denser microstructure would increase the free path of electrons and produce a higher conductivity, the observed higher load-bearing capability in the sintered sample was expected. This indicates that enhanced densification in the sintering process is essential to achieving ideal electrical properties.

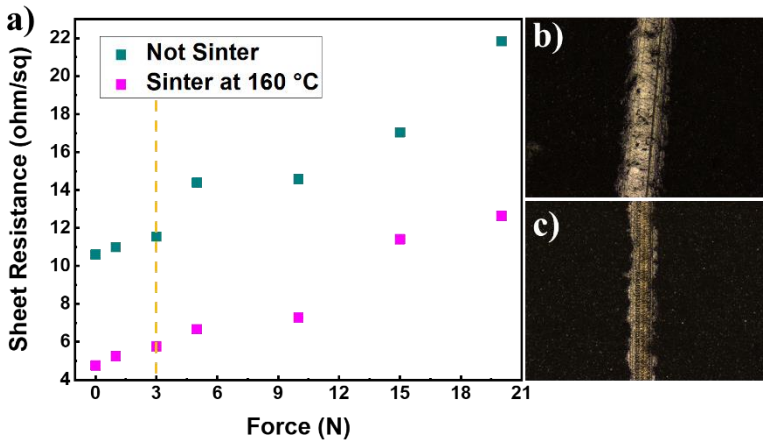

Figure 35. a) Assessment of sheet resistance after scratching under different loads. Optical images of scratch tracks for Ag patterns: b) before sintering at 20 N, c) after sintering at 20N.

Since strain sensors are intended to monitor repetitive motions, fabricated sensors with 36 vol% AgF screen-printed on TPU substrates were subjected to cyclic strains. The functionality of the strain sensors were tested with simultaneous electrical resistance measurements under applied cyclic strain. The effect of cyclic deformation on the resistance was studied through ZwickRoell coupled with the Keithley source meter. **Figure 36** illustrates the results of measuring the resistance by stretching the sensor 500 times up to 10% strain at various speeds ranging from 1 mm/sec to 10 mm/sec and then keeping it under constant 0% strain until the resistance values saturated. For the not sintered sensor, the normalized resistance as a function of time is shown in **Figure 36**a. It is anticipated that the delamination and breaking of the connections in the 3D network will be the main factors contributing to the increase in resistance for the non-sintered sensor. When the strain rate reaches a value of 10 mm/sec, in the case of the not sintered sensor, the resistance increases exponentially as a function of the strain rate. The increase in inter-particle distance and the breaking of the contacts between silver flakes in the case of the sintered sensor (**Figure 36**b) can be used to explain the increase in resistance with a high stretching rate. The breaking of the 3D network formed by the conductive fillers, loss of contact between different particles, an increase in the inter-filler distance, delamination of particles, reorientation of particles, and a decrease in the volume fraction of filler material as the material extends are just a few of the phenomena that can explain how tensile strain affects conductivity[413,414].

The results in **Figure 36**c show that resistance increases during cyclic stretch but also recovers, which is time-dependent. Resistance values were significantly lower than those initially measured in cyclic strain tests when sensors were allowed to relax after each cycle (**Figure 36**c, black curve), indicating that these test results are highly dependent on the timeframe in which resistances were measured. An enlarged 200 first seconds of the outcomes from **Figure 36**c with different relaxation times is presented in **Figure 36**d. As can be seen, bond exchange within the vitrimer, which enables the rearrangement of the network and causes a decrease in resistance concurrent with the tension of the sample, outweighs the resistance increase phenomenon, which is ruled by the detachment of the conductive nanoparticles due to strain.

The sensor's resistance was also more than recovered after being stretched back to its original length and given 90 seconds to relax, in contrast to the resistances of

sensors with a relaxation time of 0–30–60 seconds, which showed a residual increase compared to their initial values. The reorganization of the conductive networks within the coating is responsible for the decrease in (R-R0/R0), which can be explained by a stretched exponential for relaxation in disordered systems. In addition, the structural characteristics of TPU probably contributed to the time-dependent recovery[415].

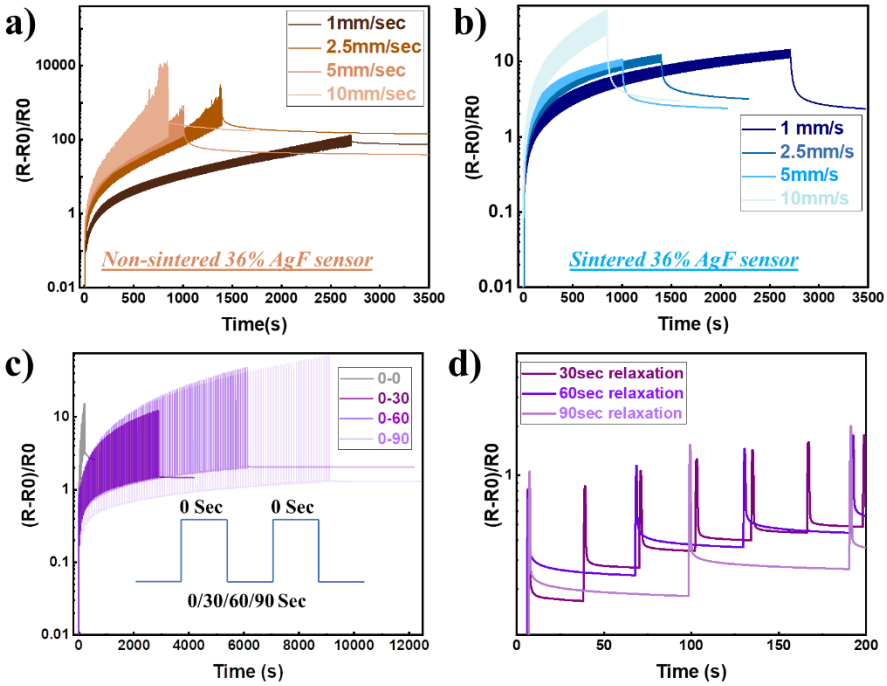

Figure 36. Evolution of the relative resistance over the 500 cycles up to 10% strain at various speeds a) Non-sinter 36 vol% AgF screen-printed ink, b) Sinter 36 vol% AgF screen-printed ink. c) Normalized resistances as a function of relaxation time. d) Magnified graph c from 0 second to 200 seconds.

The recyclability test procedure followed the same method used for recycling the carbon-based vitrimer ink (**Figure 32**d). 1-Hexanol was replaced instead of ethanol since the ink was formulated with this solvent. The remaining solution is then filtered using three cellulose filter papers of grade 2.5 stacked on top of each other in the following day after the sensor has been immersed in the solvents and all of the coating has separated from its substrate. As shown in **Figure 37**a, the solution required several consecutive filtration cycles to achieve an acceptable transparent-like colour. The recycled elements of the sensor after the complete solvent evaporation, were then analysed with the scanning electron microscope obtaining the images in **Figure 37**b and **Figure 37**c after and before recycling, respectively. To examine if there is any residue from the vitrimer inside the recycled silver flakes, EDS analyses were performed on

the recycled element; the results confirm the recycling process was successfully done, and the peaks are the same for the silver flakes after and before recycling as shown in **Figure 37**d. Interestingly, despite the fact that the silver flakes are sintered at 160°C, we can counter the hypothesis that silver flakes oxidize.

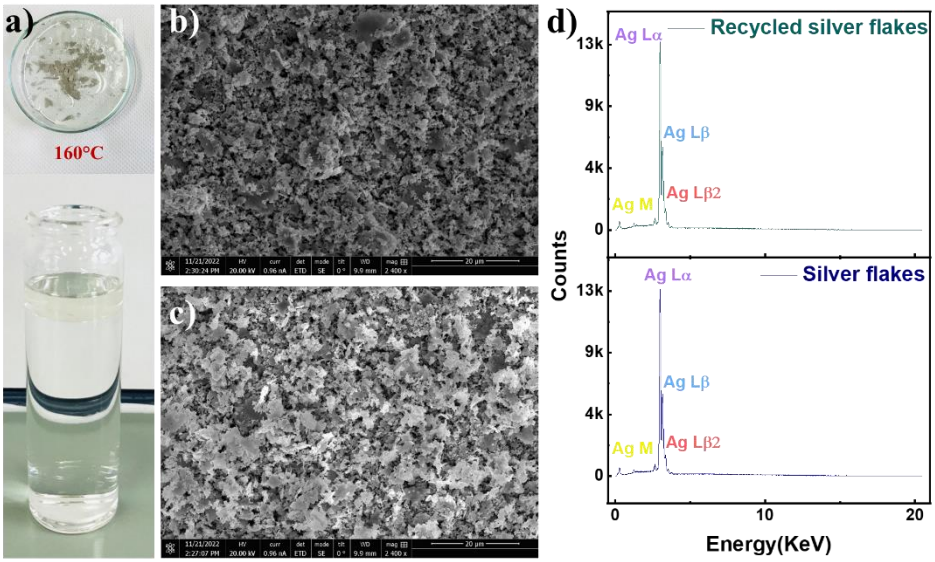

Figure 37. a) Separated silver flakes and filtered solvents after recyclability test. SEM images of the silver flakes powder b) after the recyclability test, c) before the recyclability test. d) Energy dispersive spectroscopy (EDS) spectra of recycled and original silver flakes.

This chapter describes the development of environmentally friendly strain sensors based on a novel class of biopolymer called vitrimer that is filled with various conductive particulates. From the selection of materials to the manufacturing procedure, the conductive coating was created by combining the electrical insulation vitrimer ESOA-DBEDT with green solvents diluted with water. Ink's variable viscosity made it possible to create strain sensors by using various coating techniques. Regarding repeatability and stability, all of the sensors demonstrated excellent recovery abilities following the relaxation of the strain and displayed good stability throughout the entire cyclic strain test. The sensor's recyclability has also been investigated and tested, with outstanding outcomes in both formulation techniques.

Chapter 7: Conclusions

In the twenty-first century, there has been an exponential increase in the production and usage of electrical and electronic equipment (EEE), which has occurred concurrently with an increase in environmental warnings about the negative effects of anthropogenic activities. This prompted the need to relate these two phenomena better, and it is now understood that EEE are both parts of the environmental cure and the environmental disease: while the increasing consumption and disposal of EEE have serious repercussions for the planet[416], the use of EEE can aid in saving energy and natural resources[152]. The functional classification of environmentally friendly electronics has increased significantly over the past few decades as a result of environmental legislation becoming increasingly stringent and an increase in environmentally friendly devices, which required business models to adjust in order to participate in this new market share[417,418].

In the electronics industry, printed, flexible, and wearable electronics and large area conductive coatings play a crucial role. Recently, the demand for innovative materials in such sectors has increased. This necessitates the development of novel materials utilizing a straightforward method to facilitate the fabrication of wearable devices with superior electronic properties. In printed electronics, conductive inks play a significant role. Even though there are numerous types of conductive inks on the market, certain obstacles persist and must be overcome. Toxic chemicals, low throughput, and complicated fabrication processes are a few of the limitations that make broader applications of conductive inks less economically viable.

Green flexible electronics are a promising technology that can enable sustainable future electronics. Sustainability and green electronics are at the centre of the investigation presented in this thesis, which tries to develop materials with the satisfying performance needed in flexible and wearable electronics which at the same time are bio-based and recyclable.

Under such a perspective, for the fabrication of flexible, stretchable, and wearable printed electronic devices, several conductive inks comprised of carbon and

metallic conductive filler mixed with bio-based polymers were found to be suitable options.

Our material selection is motivated by the desire to address environment-related aspects and the circular economy. Emulsion-based conductive ink made with PLA as a binder and GNPs as a conductive filler has also shown promising results for flexible strain sensors, providing good mechanical properties and electrical conductivity. Making ink with GNPs offers many advantages that make it a desirable material for use in electronic applications, particularly in the development of green and sustainable electronics. The high electrical and mechanical properties of GNPs, combined with their low toxicity and environmental sustainability, make them an attractive alternative to traditional electronic materials. Furthermore, using PLA as a binder reduces the amount of non-renewable resources needed for sensor production and reduces the amount of waste generated at the end of the sensor's life. Additionally, the use of green solvents, which are derived from renewable resources, can further reduce the environmental impact of the manufacturing process. Nevertheless, emulsions are much more eco-friendly, and emulsifying ensures that a significant portion of the solvent is replaced with water. This means less solvent cost and fewer toxic solvent emissions if the solvent is not biodegradable.

The immiscible blend of PUDs with PLA has emerged as a promising approach to improving the mechanical properties and biodegradability of PLA. The incorporation of PUDs into PLA can create a composite material that exhibits enhanced toughness and ductility. The WPU phase acts as a toughening agent by absorbing and dissipating energy during deformation, reducing stress concentrations in the PLA matrix, and resulting in improved mechanical properties. Moreover, the blend of PUDs with PLA can improve the biodegradability of PLA by increasing its surface area and hydrophilicity and exhibiting synergistic effects.

To provide economical and environmental benefits, two strategies are followed for making conductive inks with silver flakes:

1. Combination of silver flakes with carbon nanotubes (CNTs): By combining silver flakes with CNTs in the conductive ink, the amount of silver required can be reduced, which can help reduce the cost of the ink. Additionally, CNTs can improve the conductivity of the ink, which can lead to better performance in electronic devices. When CNTs are added to ink made with silver flakes, they can accelerate electron

transfer by acting as a bridge between the silver flakes. Silver flakes have a larger particle size compared to CNTs, which can result in poor electrical conductivity in the ink matrix. The addition of CNTs to the ink can provide a more efficient pathway for electron transfer between the silver flakes, resulting in a more conductive ink. The CNTs also provide additional benefits such as improved mechanical strength and flexibility, as well as increased thermal stability. This makes the ink suitable for use in flexible and stretchable electronic applications.

2. Recyclable vitrimer and silver flakes ink: To tackle environmental issues and follow green chemistry principles, vitrimer, as dynamic material with low glass transition, is used as a binder in conductive ink formulation. Such inks can be recycled by hydrolysis in water and green solvents, which allows the silver flakes to be recovered and reused. This approach can provide both economic benefits through the reuse of silver flakes and environmental benefits through waste reduction.

These inks are designed can be fabricated using printing and deposition techniques such as screen printing, spray coating, and rod coating. These methods provide advantages such as high throughput, precise thickness control, and wide material compatibility, making them suitable for low-cost and sustainable manufacturing processes. The suitability of each of the three inks for different printing and coating methods depends on various features of the ink, including its viscosity, solvents, and mechanical properties. For screen printing, an ink with higher viscosity and good adhesion and mechanical properties is preferred, while for spray coating, an ink with lower viscosity and good surface tension and wetting properties is required. For rod coating, an ink with medium viscosity and good mechanical properties is typically preferred. These factors play a crucial role in the printability and final quality of the ink, and it is essential to carefully consider these features when selecting an ink for a specific printing or coating application.

Furthermore, various post-printing techniques for enhancing performance were investigated extensively. In addition, different stretchable and flexible substrates were used to analyse the adhesion properties of inks for wearable electronic applications.

Green flexible electronics have the potential to revolutionize the electronics industry, enabling the development of sustainable and eco-friendly devices. By continuing to innovate and optimize the fabrication process, these technologies can contribute to a more sustainable future. It is worth noting that while neither of these

strategies for making conductive inks is currently in widespread use, ongoing research in this area suggests that they may have the potential for use in the future. By developing more sustainable and resource-efficient approaches to producing conductive inks, we can help create a more sustainable future for the electronics industry.

Bibliography

(1) European Parliament; European Council. Directive 2002/96/EC of the European Parliament and of the Council of 27 January 2003 on Waste Electrical and Electronic Equipment (WEEE) - Joint Declaration of the European Parliament, the Council and the Commission Relating to Article 9. *Off. J. Eur. Union* **2003**, *L 37*, 24–38.

(2) Schaller, R. R. Moore's Law: Past, Present, and Future. *IEEE Spectr.* **1997**, *34* (6), 52–55, 57. https://doi.org/10.1109/6.591665.

(3) Li, W.; Liu, Q.; Zhang, Y.; Li, C.; He, Z.; Choy, W. C. H.; Low, P. J.; Sonar, P.; Kyaw, A. K. K. Biodegradable Materials and Green Processing for Green Electronics. *Adv. Mater.* **2020**, *32* (33), 2001591. https://doi.org/10.1002/adma.202001591.

(4) Boutry, C. M.; Kaizawa, Y.; Schroeder, B. C.; Chortos, A.; Legrand, A.; Wang, Z.; Chang, J.; Fox, P.; Bao, Z. A Stretchable and Biodegradable Strain and Pressure Sensor for Orthopaedic Application. *Nat. Electron.* **2018**, *1* (5), 314–321. https://doi.org/10.1038/s41928-018-0071-7.

(5) Zidan, M. A.; Strachan, J. P.; Lu, W. D. The Future of Electronics Based on Memristive Systems. *Nat. Electron. 2017 11* **2018**, *1* (1), 22–29. https://doi.org/10.1038/s41928-017-0006-8.

(6) *E-Waste in Transition - From Pollution to Resource*. E-Waste in Transition - From Pollution to Resource. https://doi.org/10.5772/60487.

(7) Dias, P.; Bernardes, A. M.; Huda, N. Ensuring Best E-Waste Recycling Practices in Developed Countries: An Australian Example. *J. Clean. Prod.* **2019**, *209*, 846–854. https://doi.org/10.1016/j.jclepro.2018.10.306.

(8) Thakur, P.; Kumar, S. Evaluation of E-Waste Status, Management Strategies, and Legislations. *Int. J. Environ. Sci. Technol.* **2022**, *19* (7), 6957–6966. https://doi.org/10.1007/s13762-021-03383-2.

(9) Dias, P.; Bernardes, A. M.; Huda, N. Waste Electrical and Electronic Equipment (WEEE) Management: An Analysis on the Australian e-Waste Recycling Scheme. *J. Clean. Prod.* **2018**, *197*, 750–764. https://doi.org/10.1016/j.jclepro.2018.06.161.

(10) Wu, X.; Steiner, P.; Raine, T.; Pinter, G.; Kretinin, A.; Kocabas, C.; Bissett, M.; Cataldi, P. Hybrid Graphene/Carbon Nanofiber Wax Emulsion for Paper-Based Electronics and Thermal Management. *Adv. Electron. Mater.* **2020**, *6* (7), 2000232. https://doi.org/10.1002/aelm.202000232.

(11) Andeobu, L.; Wibowo, S.; Grandhi, S. A Systematic Review of E-Waste Generation and Environmental Management of Asia Pacific Countries. *Int. J. Environ. Res. Public Health* **2021**, *18* (17), 9051. https://doi.org/10.3390/ijerph18179051.

(12) Baldé, C. P.; Blumenthal, K.; Gill, S. F.; Kern, M.; Micheli, P.; Magpantay, E.; Huisman, J. E-Waste Statistics: Guidelines on Classifications, Reporting and Indicators. **2015**.

(13) *G7: "Mount Recyclemore" of leaders made from electronic waste in Cornwall - BBC News*. https://www.bbc.com/news/uk-england-cornwall-57406136 (accessed 2023-02-01).

(14) Liao, C. S.; Chuang, H. K. Determinants of Innovative Green Electronics: An Experimental Study of Eco-Friendly Laptop Computers. *Technovation* **2022**, *113*, 102424. https://doi.org/10.1016/j.technovation.2021.102424.

(15) Liu, H.; Jian, R.; Chen, H.; Tian, X.; Sun, C.; Zhu, J.; Yang, Z.; Sun, J.; Wang, C. Application of Biodegradable and Biocompatible Nanocomposites in Electronics: Current Status and Future Directions. **2019**. https://doi.org/10.3390/nano9070950.

(16) *Global Electronics Council | Home*. https://globalelectronicscouncil.org/ (accessed 2023-01-11).

(17) Adrian, S.; Drisse, M. B.; Cheng, Y.; Devia, L.; Deubzer, O.; Goldizen, F.; Gorman, J.; Herat, S.; Honda, S.; Lattoni, G.; Jingwei, W.; Jinhui, L.; Khetriwal, D. S.; Linnell, J.; Magalini, F.; Nnorom, I. C.; Onianwa, P.; Ott, D.; Ramola, A.; Silva, U.; Stillhart, R.; Tillekeratne, D.; Van Straalen, V.; Wagner, M.; Yamamoto, T.; Zeng, X. Quantities, Flows, and the Circular Economy Potential The Global E-Waste Monitor 2020. **2017**, No. July, 120.

(18) Feig, V. R.; Tran, H.; Bao, Z. Biodegradable Polymeric Materials in Degradable Electronic Devices. *ACS Cent. Sci.* **2018**, *4* (3), 337–348. https://doi.org/10.1021/acscentsci.7b00595.

(19) Misra, N. R.; Kumar, S.; Jain, A. A Review on E-Waste: Fostering the Need for Green Electronics. *Proc. - IEEE 2021 Int. Conf. Comput. Commun. Intell. Syst. ICCCIS 2021* **2021**, 1032–1036. https://doi.org/10.1109/ICCCIS51004.2021.9397191.

(20) Babu, B. R.; Parande, A. K.; Basha, C. A. Electrical and Electronic Waste: A Global Environmental Problem. *Waste Manag. Res.* **2007**, *25* (4), 307–318. https://doi.org/10.1177/0734242X07076941.

(21) Pokhrel, P.; Lin, S. L.; Tsai, C. T. Environmental and Economic Performance Analysis of Recycling Waste Printed Circuit Boards Using Life Cycle Assessment. *J. Environ. Manage.* **2020**, *276*, 111276. https://doi.org/10.1016/j.jenvman.2020.111276.

(22) Kumar, V.; Bee, D. J.; Shirodkar, P. S.; Tumkor, S.; Bettig, B. P.; Sutherland, J. W. Towards Sustainable "Product and Material Flow" Cycles: Identifying Barriers to Achieving Product Multi-Use and Zero Waste. *Energy Convers. Resour. 2005* **2005**, *2005*, 433–442. https://doi.org/10.1115/IMECE2005-81347.

(23) Tan, M. J.; Owh, C.; Chee, P. L.; Kyaw, A. K. K.; Kai, D.; Loh, X. J. Biodegradable Electronics: Cornerstone for Sustainable Electronics and Transient Applications. *J. Mater. Chem. C* **2016**, *4* (24), 5531–5558. https://doi.org/10.1039/c6tc00678g.

(24) Irimia-Vladu, M. "Green" Electronics: Biodegradable and Biocompatible Materials and

Devices for Sustainable Future. *Chem. Soc. Rev.* **2014**, *43* (2), 588–610. https://doi.org/10.1039/c3cs60235d.

(25) Liao, X.; Zhang, Z.; Liao, Q.; Liang, Q.; Ou, Y.; Xu, M.; Li, M.; Zhang, G.; Zhang, Y. Flexible and Printable Paper-Based Strain Sensors for Wearable and Large-Area Green Electronics. *Nanoscale* **2016**, *8* (26), 13025–13032. https://doi.org/10.1039/c6nr02172g.

(26) Liu, J.; Yang, C.; Wu, H.; Lin, Z.; Zhang, Z.; Wang, R.; Li, B.; Kang, F.; Shi, L.; Wong, C. P. Future Paper Based Printed Circuit Boards for Green Electronics: Fabrication and Life Cycle Assessment. *Energy Environ. Sci.* **2014**, *7* (11), 3674–3682. https://doi.org/10.1039/c4ee01995d.

(27) Lu, Y.; Ozcan, S. Green Nanomaterials: On Track for a Sustainable Future. *Nano Today* **2015**, *10* (4), 417–420. https://doi.org/10.1016/j.nantod.2015.04.010.

(28) Kang, J.; Cao, W.; Xie, X.; Sarkar, D.; Liu, W.; Banerjee, K. Graphene and Beyond-Graphene 2D Crystals for next-Generation Green Electronics. *Micro- Nanotechnol. Sensors, Syst. Appl. VI* **2014**, *9083*, 908305. https://doi.org/10.1117/12.2051198.

(29) Shirodkar, N.; Terkar, R. Stepped Recycling: The Solution for E-Waste Management and Sustainable Manufacturing in India. *Mater. Today Proc.* **2017**, *4* (8), 8911–8917. https://doi.org/10.1016/j.matpr.2017.07.242.

(30) Kumar, A.; Holuszko, M.; Espinosa, D. C. R. E-Waste: An Overview on Generation, Collection, Legislation and Recycling Practices. *Resour. Conserv. Recycl.* **2017**, *122*, 32–42. https://doi.org/10.1016/j.resconrec.2017.01.018.

(31) Wang, P.; Hu, M.; Wang, H.; Chen, Z.; Feng, Y.; Wang, J.; Ling, W.; Huang, Y. The Evolution of Flexible Electronics: From Nature, Beyond Nature, and To Nature. *Adv. Sci.* **2020**, *7* (20), 2001116. https://doi.org/10.1002/advs.202001116.

(32) Kim, Y. J.; Wu, W.; Chun, S. E.; Whitacre, J. F.; Bettinger, C. J. Biologically Derived Melanin Electrodes in Aqueous Sodium-Ion Energy Storage Devices. *Proc. Natl. Acad. Sci. U. S. A.* **2013**, *110* (52), 20912–20917. https://doi.org/10.1073/pnas.1314345110.

(33) Irimia-Vladu, M.; Troshin, P. A.; Reisinger, M.; Shmygleva, L.; Kanbur, Y.; Schwabegger, G.; Bodea, M.; Schwödiauer, R.; Mumyatov, A.; Fergus, J. W.; Razumov, V. F.; Sitter, H.; Sariciftci, N. S.; Bauer, S. Biocompatible and Biodegradable Materials for Organic Field-Effect Transistors. *Adv. Funct. Mater.* **2010**, *20* (23), 4069–4076. https://doi.org/10.1002/adfm.201001031.

(34) Hwang, S. W.; Park, G.; Edwards, C.; Corbin, E. A.; Kang, S. K.; Cheng, H.; Song, J. K.; Kim, J. H.; Yu, S.; Ng, J.; Lee, J. E.; Kim, J.; Yee, C.; Bhaduri, B.; Omennetto, F. G.; Huang, Y.; Bashir, R.; Goddard, L.; Popescu, G.; Lee, K. M.; Rogers, J. A. Dissolution Chemistry and Biocompatibility of Single-Crystalline Silicon Nanomembranes and Associated Materials for Transient Electronics. *ACS Nano* **2014**, *8* (6), 5843–5851. https://doi.org/10.1021/nn500847g.

(35) Luo, M.; Martinez, A. W.; Song, C.; Herrault, F.; Allen, M. G. A Microfabricated Wireless RF

Pressure Sensor Made Completely of Biodegradable Materials. *J. Microelectromechanical Syst.* **2014**, *23* (1), 4–13. https://doi.org/10.1109/JMEMS.2013.2290111.

(36) Zhu, B.; Wang, H.; Leow, W. R.; Cai, Y.; Loh, X. J.; Han, M. Y.; Chen, X. Silk Fibroin for Flexible Electronic Devices. *Adv. Mater.* **2016**, *28* (22), 4250–4265. https://doi.org/10.1002/ADMA.201504276.

(37) Irimia-Vladu, M.; Głowacki, E. D.; Voss, G.; Bauer, S.; Sariciftci, N. S. Green and Biodegradable Electronics. *Mater. Today* **2012**, *15* (7–8), 340–346. https://doi.org/10.1016/S1369-7021(12)70139-6.

(38) Htwe, Y. Z. N.; Mariatti, M. Surfactant-Assisted Water-Based Graphene Conductive Inks for Flexible Electronic Applications. *J. Taiwan Inst. Chem. Eng.* **2021**, *125*, 402–412. https://doi.org/10.1016/j.jtice.2021.06.022.

(39) Wang, Z.; Ma, Z.; Sun, J.; Yan, Y.; Bu, M.; Huo, Y.; Li, Y. F.; Hu, N. Recent Advances in Natural Functional Biopolymers and Their Applications of Electronic Skins and Flexible Strain Sensors. *Polymers (Basel).* **2021**, *13* (5), 1–18. https://doi.org/10.3390/polym13050813.

(40) Yin, Y.; Guo, C.; Li, H.; Yang, H.; Xiong, F.; Chen, D. The Progress of Research into Flexible Sensors in the Field of Smart Wearables. *Sensors 2022, Vol. 22, Page 5089* **2022**, *22* (14), 5089. https://doi.org/10.3390/S22145089.

(41) Yan, T.; Wang, Z.; Pan, Z. J. Flexible Strain Sensors Fabricated Using Carbon-Based Nanomaterials: A Review. *Curr. Opin. Solid State Mater. Sci.* **2018**, *22* (6), 213–228. https://doi.org/10.1016/j.cossms.2018.11.001.

(42) Zarei, M.; Lee, G.; Lee, S. G.; Cho, K. Advances in Biodegradable Electronic Skin: Material Progress and Recent Applications in Sensing, Robotics, and Human–Machine Interfaces. *Adv. Mater.* **2022**, 2203193. https://doi.org/10.1002/ADMA.202203193.

(43) Hartmann, F.; Baumgartner, M.; Kaltenbrunner, M. Becoming Sustainable, The New Frontier in Soft Robotics. *Adv. Mater.* **2021**, *33* (19), 2004413. https://doi.org/10.1002/adma.202004413.

(44) Wang, M.; Luo, Y.; Wang, T.; Wan, C.; Pan, L.; Pan, S.; He, K.; Neo, A.; Chen, X. Artificial Skin Perception. *Adv. Mater.* **2021**, *33* (19), 2003014. https://doi.org/10.1002/adma.202003014.

(45) Mazzolai, B.; Mondini, A.; Del Dottore, E.; Margheri, L.; Carpi, F.; Suzumori, K.; Cianchetti, M.; Speck, T.; Smoukov, S. K.; Burgert, I.; Keplinger, T.; Siqueira, G. D. F.; Vanneste, F.; Goury, O.; Duriez, C.; Nanayakkara, T.; Vanderborght, B.; Brancart, J.; Terryn, S.; Rich, S. I.; Liu, R.; Fukuda, K.; Someya, T.; Calisti, M.; Laschi, C.; Sun, W.; Wang, G.; Wen, L.; Baines, R.; Patiballa, S. K.; Kramer-Bottiglio, R.; Rus, D.; Fischer, P.; Simmel, F. C.; Lendlein, A. Roadmap on Soft Robotics: Multifunctionality, Adaptability and Growth without Borders. *Multifunct. Mater.* **2022**, *5* (3), 032001. https://doi.org/10.1088/2399-7532/ac4c95.

(46) Tan, Y. J.; Susanto, G. J.; Anwar Ali, H. P.; Tee, B. C. K. Progress and Roadmap for Intelligent Self-Healing Materials in Autonomous Robotics. *Adv. Mater.* **2021**, *33* (19), 2002800.

https://doi.org/10.1002/adma.202002800.

(47) Ilami, M.; Bagheri, H.; Ahmed, R.; Skowronek, E. O.; Marvi, H. Materials, Actuators, and Sensors for Soft Bioinspired Robots. *Adv. Mater.* **2021**, *33* (19), 2003139. https://doi.org/10.1002/adma.202003139.

(48) Kim, S.; Amjadi, M.; Lee, T. I.; Jeong, Y.; Kwon, D.; Kim, M. S.; Kim, K.; Kim, T. S.; Oh, Y. S.; Park, I. Wearable, Ultrawide-Range, and Bending-Insensitive Pressure Sensor Based on Carbon Nanotube Network-Coated Porous Elastomer Sponges for Human Interface and Healthcare Devices. *ACS Appl. Mater. Interfaces* **2019**, *11* (26), 23639–23648. https://doi.org/10.1021/acsami.9b07636.

(49) Lou, Z.; Li, L.; Wang, L.; Shen, G. Recent Progress of Self-Powered Sensing Systems for Wearable Electronics. *Small* **2017**, *13* (45), 1701791. https://doi.org/10.1002/smll.201701791.

(50) Islam, R.; Khair, N.; Ahmed, D. M.; Shahariar, H. Fabrication of Low Cost and Scalable Carbon-Based Conductive Ink for E-Textile Applications. *Mater. Today Commun.* **2019**, *19*, 32–38. https://doi.org/10.1016/j.mtcomm.2018.12.009.

(51) Aeby, X.; Bourely, J.; Poulin, A.; Siqueira, G.; Nyström, G.; Briand, D. Printed Humidity Sensors from Renewable and Biodegradable Materials. *Adv. Mater. Technol.* **2022**, 2201302. https://doi.org/10.1002/admt.202201302.

(52) Pal, R. K.; Farghaly, A. A.; Wang, C.; Collinson, M. M.; Kundu, S. C.; Yadavalli, V. K. Conducting Polymer-Silk Biocomposites for Flexible and Biodegradable Electrochemical Sensors. *Biosens. Bioelectron.* **2016**, *81*, 294–302. https://doi.org/10.1016/j.bios.2016.03.010.

(53) Kazemzadeh Farizhandi, A. A.; Khalajabadi, S. Z.; Krishnadoss, V.; Noshadi, I. Synthesized Biocompatible and Conductive Ink for 3D Printing of Flexible Electronics. *J. Mech. Behav. Biomed. Mater.* **2020**, *110*, 103960. https://doi.org/10.1016/j.jmbbm.2020.103960.

(54) Stephen, M.; Nawaz, A.; Lee, S. Y.; Sonar, P.; Leong, W. L. Biodegradable Materials for Transient Organic Transistors. *Adv. Funct. Mater.* **2022**, 2208521. https://doi.org/10.1002/adfm.202208521.

(55) Wei, Y.; Jiang, S.; Li, X.; Li, J.; Dong, Y.; Shi, S. Q.; Li, J.; Fang, Z. "green" Flexible Electronics: Biodegradable and Mechanically Strong Soy Protein-Based Nanocomposite Films for Human Motion Monitoring. *ACS Appl. Mater. Interfaces* **2021**, *13* (31), 37617–37627. https://doi.org/10.1021/acsami.1c09209.

(56) Wilfred, O.; Tai, H.; Marriott, R.; Liu, Q.; Tverezovskiy, V.; Curling, S.; Fan, Z.; Wang, W. Biodegradation of Polyactic Acid and Starch Composites in Compost and Soil. *Int. J. Nano Res.* **2018**, *1* (2), 1–11.

(57) Rim, Y. S.; Bae, S. H.; Chen, H.; De Marco, N.; Yang, Y. Recent Progress in Materials and Devices toward Printable and Flexible Sensors. *Adv. Mater.* **2016**, *28* (22), 4415–4440. https://doi.org/10.1002/adma.201505118.

(58) Ma, L. Y.; Soin, N. Recent Progress in Printed Physical Sensing Electronics for Wearable Health-Monitoring Devices: A Review. *IEEE Sens. J.* **2022**, *22* (5), 3844–3859. https://doi.org/10.1109/JSEN.2022.3142328.

(59) Samir, A.; Ashour, F. H.; Hakim, A. A. A.; Bassyouni, M. Recent Advances in Biodegradable Polymers for Sustainable Applications. *npj Mater. Degrad.* **2022**, *6* (1), 1–28. https://doi.org/10.1038/s41529-022-00277-7.

(60) Lochab, A.; Sharma, R.; Kumar, S.; Saxena, R. Recent Advances in Carbon Based Nanomaterials as Electrochemical Sensor for Toxic Metal Ions in Environmental Applications. *Mater. Today Proc.* **2021**.

(61) Choi, S.; Lee, H.; Ghaffari, R.; Hyeon, T.; Kim, D. H. Recent Advances in Flexible and Stretchable Bio-Electronic Devices Integrated with Nanomaterials. *Adv. Mater.* **2016**, *28* (22), 4203–4218. https://doi.org/10.1002/adma.201504150.

(62) Liu, L.; Shen, Z.; Zhang, X.; Ma, H. Highly Conductive Graphene/Carbon Black Screen Printing Inks for Flexible Electronics. *J. Colloid Interface Sci.* **2021**, *582*, 12–21. https://doi.org/10.1016/j.jcis.2020.07.106.

(63) Dimitriou, E.; Michailidis, N. Printable Conductive Inks Used for the Fabrication of Electronics: An Overview. *Nanotechnology* **2021**, *32* (50), 502009. https://doi.org/10.1088/1361-6528/abefff.

(64) Kwon, J.; DelRe, C.; Kang, P.; Hall, A.; Arnold, D.; Jayapurna, I.; Ma, L.; Michalek, M.; Ritchie, R. O.; Xu, T. Conductive Ink with Circular Life Cycle for Printed Electronics. *Adv. Mater.* **2022**, *34* (30), 2202177. https://doi.org/10.1002/adma.202202177.

(65) Yang, W.; Wang, C. Graphene and the Related Conductive Inks for Flexible Electronics. *J. Mater. Chem. C* **2016**, *4* (30), 7193–7207. https://doi.org/10.1039/c6tc01625a.

(66) Camargo, J. R.; Orzari, L. O.; Araújo, D. A. G.; de Oliveira, P. R.; Kalinke, C.; Rocha, D. P.; Luiz dos Santos, A.; Takeuchi, R. M.; Munoz, R. A. A.; Bonacin, J. A.; Janegitz, B. C. Development of Conductive Inks for Electrochemical Sensors and Biosensors. *Microchem. J.* **2021**, *164*, 105998. https://doi.org/10.1016/j.microc.2021.105998.

(67) Saidina, D. S.; Eawwiboonthanakit, N.; Mariatti, M.; Fontana, S.; Hérold, C. Recent Development of Graphene-Based Ink and Other Conductive Material-Based Inks for Flexible Electronics. *J. Electron. Mater.* **2019**, *48* (6), 3428–3450. https://doi.org/10.1007/s11664-019-07183-w.

(68) Zhu, J.; Wang, X.; Xing, Y.; Li, J. Highly Stretchable All-Rubber-Based Thread-Shaped Wearable Electronics for Human Motion Energy-Harvesting and Self-Powered Biomechanical Tracking. *Nanoscale Res. Lett.* **2019**, *14* (1), 1–9. https://doi.org/10.1186/S11671-019-3085-9/FIGURES/5.

(69) Fiori, G.; Bonaccorso, F.; Iannaccone, G.; Palacios, T.; Neumaier, D.; Seabaugh, A.; Banerjee, S. K.; Colombo, L. Electronics Based on Two-Dimensional Materials. *Nat. Nanotechnol.* **2014**,

9 (10), 768–779. https://doi.org/10.1038/nnano.2014.207.

(70) Tran, T. S.; Dutta, N. K.; Choudhury, N. R. Graphene Inks for Printed Flexible Electronics: Graphene Dispersions, Ink Formulations, Printing Techniques and Applications. *Adv. Colloid Interface Sci.* **2018**, *261*, 41–61. https://doi.org/10.1016/j.cis.2018.09.003.

(71) Cano-Raya, C.; Denchev, Z. Z.; Cruz, S. F.; Viana, J. C. Chemistry of Solid Metal-Based Inks and Pastes for Printed Electronics – A Review. *Appl. Mater. Today* **2019**, *15*, 416–430. https://doi.org/10.1016/j.apmt.2019.02.012.

(72) Huang, L.; Huang, Y.; Liang, J.; Wan, X.; Chen, Y. Graphene-Based Conducting Inks for Direct Inkjet Printing of Flexible Conductive Patterns and Their Applications in Electric Circuits and Chemical Sensors. *Nano Res.* **2011**, *4* (7), 675–684. https://doi.org/10.1007/s12274-011-0123-z.

(73) Majee, S.; Liu, C.; Wu, B.; Zhang, S. L.; Zhang, Z. B. Ink-Jet Printed Highly Conductive Pristine Graphene Patterns Achieved with Water-Based Ink and Aqueous Doping Processing. *Carbon N. Y.* **2017**, *114*, 77–83. https://doi.org/10.1016/j.carbon.2016.12.003.

(74) Sharma, S.; Mondal, T. Polymeric Materials for Printed Electronics Application. *Prog. Polym. Res. Biomed. Energy Spec. Appl.* **2022**, 251–273. https://doi.org/10.1201/9781003200710-13.

(75) Rani, E.; Mohshim, S. A.; Ahmad, M. Z.; Goodacre, R.; Ahmad, S. A. A.; Wong, L. S. Polymer Pen Lithography-Fabricated DNA Arrays for Highly Sensitive and Selective Detection of Unamplified Ganoderma Boninense DNA. *Polymers (Basel).* **2019**, *11* (3), 561. https://doi.org/10.3390/polym11030561.

(76) Talukder, S.; Kumar, P.; Pratap, R. Electrolithography- A New and Versatile Process for Nano Patterning. *Sci. Rep.* **2015**, *5* (1), 1–11. https://doi.org/10.1038/srep17753.

(77) Perelaer, J.; Hendriks, C. E.; De Laat, A. W. M.; Schubert, U. S. One-Step Inkjet Printing of Conductive Silver Tracks on Polymer Substrates. *Nanotechnology* **2009**, *20* (16), 165303. https://doi.org/10.1088/0957-4484/20/16/165303.

(78) Kahn, B. E. Patterning Processes for Flexible Electronics. *Proc. IEEE* **2015**, *103* (4), 497–517. https://doi.org/10.1109/JPROC.2015.2401553.

(79) Wong, W. S.; Chabinyc, M. L.; Ng, T.-N.; Salleo, A. Materials and Novel Patterning Methods for Flexible Electronics. **2009**, 143–181. https://doi.org/10.1007/978-0-387-74363-9_6.

(80) Ko, S. H.; Pan, H.; Grigoropoulos, C. P.; Luscombe, C. K.; Fréchet, J. M. J.; Poulikakos, D. All-Inkjet-Printed Flexible Electronics Fabrication on a Polymer Substrate by Low-Temperature High-Resolution Selective Laser Sintering of Metal Nanoparticles. *Nanotechnology* **2007**, *18* (34), 345202. https://doi.org/10.1088/0957-4484/18/34/345202.

(81) Schwartz, E.; Ober, P. C. Roll to Roll Processing for Flexible Electronics MSE 542 : Flexible Electronics. *Flex. Electron.* **2006**, 1–24.

(82) Bagheri, A.; Bellani, S.; Beydaghi, H.; Eredia, M.; Najafi, L.; Bianca, G.; Zappia, M. I.;

Safarpour, M.; Najafi, M.; Mantero, E.; Sofer, Z.; Hou, G.; Pellegrini, V.; Feng, X.; Bonaccorso, F. Functionalized Metallic 2D Transition Metal Dichalcogenide-Based Solid-State Electrolyte for Flexible All-Solid-State Supercapacitors. *ACS Nano* **2022**, *16* (10), 16426–16442. https://doi.org/10.1021/acsnano.2c05640.

(83) Magdassi, S.; Grouchko, M.; Kamyshny, A. Copper Nanoparticles for Printed Electronics: Routes towards Achieving Oxidation Stability. *Materials (Basel).* **2010**, *3* (9), 4626–4638. https://doi.org/10.3390/ma3094626.

(84) Lin, C. H.; Fu, H. C.; Cheng, B.; Tsai, M. L.; Luo, W.; Zhou, L.; Jang, S. H.; Hu, L.; He, J. H. A Flexible Solar-Blind 2D Boron Nitride Nanopaper-Based Photodetector with High Thermal Resistance. *npj 2D Mater. Appl.* **2018**, *2* (1), 1–6. https://doi.org/10.1038/s41699-018-0070-6.

(85) Scidà, A.; Haque, S.; Treossi, E.; Robinson, A.; Smerzi, S.; Ravesi, S.; Borini, S.; Palermo, V. Application of Graphene-Based Flexible Antennas in Consumer Electronic Devices. *Mater. Today* **2018**, *21* (3), 223–230. https://doi.org/10.1016/j.mattod.2018.01.007.

(86) Manjakkal, L.; Núñez, C. G.; Dang, W.; Dahiya, R. Flexible Self-Charging Supercapacitor Based on Graphene-Ag-3D Graphene Foam Electrodes. *Nano Energy* **2018**, *51*, 604–612. https://doi.org/10.1016/j.nanoen.2018.06.072.

(87) Huang, Q.; Zhu, Y. Printing Conductive Nanomaterials for Flexible and Stretchable Electronics: A Review of Materials, Processes, and Applications. *Adv. Mater. Technol.* **2019**, *4* (5), 1800546. https://doi.org/10.1002/admt.201800546.

(88) Sekitani, T.; Nakajima, H.; Maeda, H.; Fukushima, T.; Aida, T.; Hata, K.; Someya, T. Stretchable Active-Matrix Organic Light-Emitting Diode Display Using Printable Elastic Conductors. *Nat. Mater. 2009 86* **2009**, *8* (6), 494–499. https://doi.org/10.1038/nmat2459.

(89) Guo, B.; Zhong, Y.; Chen, X.; Yu, S.; Bai, J. 3D Printing of Electrically Conductive and Degradable Hydrogel for Epidermal Strain Sensor. *Compos. Commun.* **2023**, *37*, 101454. https://doi.org/10.1016/j.coco.2022.101454.

(90) Htwe, Y. Z. N.; Mariatti, M. Printed Graphene and Hybrid Conductive Inks for Flexible, Stretchable, and Wearable Electronics: Progress, Opportunities, and Challenges. *J. Sci. Adv. Mater. Devices* **2022**, *7* (2), 100435. https://doi.org/10.1016/j.jsamd.2022.100435.

(91) Wang, X.; Guo, W.; Zhu, Y.; Liang, X.; Wang, F.; Peng, P. Electrical and Mechanical Properties of Ink Printed Composite Electrodes on Plastic Substrates. *Appl. Sci.* **2018**, *8* (11), 2101. https://doi.org/10.3390/app8112101.

(92) Kamyshny, A.; Magdassi, S. Conductive Nanomaterials for 2D and 3D Printed Flexible Electronics. *Chem. Soc. Rev.* **2019**, *48* (6), 1712–1740. https://doi.org/10.1039/c8cs00738a.

(93) Cheng, I.-C.; Wagner, S. Overview of Flexible Electronics Technology. **2009**, 1–28. https://doi.org/10.1007/978-0-387-74363-9_1.

(94) Corzo, D.; Tostado-Blázquez, G.; Baran, D. Flexible Electronics: Status, Challenges and

Opportunities. *Front. Electron.* **2020**, *1*, 2. https://doi.org/10.3389/felec.2020.594003.

(95) Khanna, V. K. Flexible Electronics. *Flex. Electron.* **2019**, *3*, 1–417. https://doi.org/10.1126/science.1171230.

(96) Wang, Z.; Sun, L.; Ni, Y.; Liu, L.; Xu, W. Flexible Electronics and Healthcare Applications. *Front. Nanotechnol.* **2021**, *3*, 1. https://doi.org/10.3389/fnano.2021.625989.

(97) Mineart, K. P.; Lin, Y.; Desai, S. C.; Krishnan, A. S.; Spontak, R. J.; Dickey, M. D. Ultrastretchable, Cyclable and Recyclable 1- and 2-Dimensional Conductors Based on Physically Cross-Linked Thermoplastic Elastomer Gels. *Soft Matter* **2013**, *9* (32), 7695–7700. https://doi.org/10.1039/c3sm51136g.

(98) Ahn, J. H.; Je, J. H. Stretchable Electronics: Materials, Architectures and Integrations. *J. Phys. D. Appl. Phys.* **2012**, *45* (10). https://doi.org/10.1088/0022-3727/45/10/103001.

(99) Yoon, J.; Zhang, Z.; Lu, N.; Suo, Z. The Effect of Coating in Increasing the Critical Size of Islands on a Compliant Substrate. *Appl. Phys. Lett.* **2007**, *90* (21), 211912. https://doi.org/10.1063/1.2742911.

(100) Wagner, S.; Bauer, S. Materials for Stretchable Electronics. *MRS Bull.* **2012**, *37* (3), 207–213. https://doi.org/10.1557/mrs.2012.37.

(101) Li, T.; Li, Y.; Zhang, T. Materials, Structures, and Functions for Flexible and Stretchable Biomimetic Sensors. *Acc. Chem. Res.* **2019**, *52* (2), 288–296. https://doi.org/10.1021/acs.accounts.8b00497.

(102) Almuslem, A. S.; Shaikh, S. F.; Hussain, M. M. Flexible and Stretchable Electronics for Harsh-Environmental Applications. *Adv. Mater. Technol.* **2019**, *4* (9), 1900145. https://doi.org/10.1002/admt.201900145.

(103) Sun, B.; Long, Y. Z.; Chen, Z. J.; Liu, S. L.; Zhang, H. Di; Zhang, J. C.; Han, W. P. Recent Advances in Flexible and Stretchable Electronic Devices via Electrospinning. *J. Mater. Chem. C* **2014**, *2* (7), 1209–1219. https://doi.org/10.1039/c3tc31680g.

(104) Chen, X.; Rogers, J. A.; Lacour, S. P.; Hu, W.; Kim, D. H. Materials Chemistry in Flexible Electronics. *Chem. Soc. Rev.* **2019**, *48* (6), 1431–1433. https://doi.org/10.1039/c9cs90019e.

(105) Choi, S.; Han, S. I.; Kim, D.; Hyeon, T.; Kim, D. H. High-Performance Stretchable Conductive Nanocomposites: Materials, Processes, and Device Applications. *Chem. Soc. Rev.* **2019**, *48* (6), 1566–1595. https://doi.org/10.1039/c8cs00706c.

(106) Kagan, C. R. Flexible Colloidal Nanocrystal Electronics. *Chem. Soc. Rev.* **2019**, *48* (6), 1626–1641. https://doi.org/10.1039/c8cs00629f.

(107) Son, D.; Bao, Z. Correction: Nanomaterials in Skin-Inspired Electronics: Toward Soft and Robust Skin-like Electronic Nanosystems (ACS Nano (2018) DOI: 10.1021/Acsnano.8b07738). *ACS Nano* **2018**, *12* (12), 12943. https://doi.org/10.1021/acsnano.8b09074.

(108) Wang, L.; Chen, D.; Jiang, K.; Shen, G. New Insights and Perspectives into Biological Materials for Flexible Electronics. *Chem. Soc. Rev.* **2017**, *46* (22), 6764–6815. https://doi.org/10.1039/c7cs00278e.

(109) Wang, L.; Wang, K.; Lou, Z.; Jiang, K.; Shen, G. Plant-Based Modular Building Blocks for "Green" Electronic Skins. *Adv. Funct. Mater.* **2018**, *28* (51), 1804510. https://doi.org/10.1002/adfm.201804510.

(110) Chun, S.; Kim, D. W.; Baik, S.; Lee, H. J.; Lee, J. H.; Bhang, S. H.; Pang, C. Conductive and Stretchable Adhesive Electronics with Miniaturized Octopus-Like Suckers against Dry/Wet Skin for Biosignal Monitoring. *Adv. Funct. Mater.* **2018**, *28* (52), 1805224. https://doi.org/10.1002/adfm.201805224.

(111) Min, S. Y.; Kim, T. S.; Kim, B. J.; Cho, H.; Noh, Y. Y.; Yang, H.; Cho, J. H.; Lee, T. W. Large-Scale Organic Nanowire Lithography and Electronics. *Nat. Commun.* **2013**, *4*. https://doi.org/10.1038/ncomms2785.

(112) De Rossi, F.; Renno, G.; Taheri, B.; Yaghoobi Nia, N.; Ilieva, V.; Fin, A.; Di Carlo, A.; Bonomo, M.; Barolo, C.; Brunetti, F. Modified P3HT Materials as Hole Transport Layers for Flexible Perovskite Solar Cells. *J. Power Sources* **2021**, *494*, 229735. https://doi.org/10.1016/j.jpowsour.2021.229735.

(113) Liu, Y.; Wang, L.; Zhao, L.; Yao, K.; Xie, Z.; Zi, Y.; Yu, X. Thin, Skin-Integrated, Stretchable Triboelectric Nanogenerators for Tactile Sensing. *Adv. Electron. Mater.* **2020**, *6* (1), 1901174. https://doi.org/10.1002/aelm.201901174.

(114) Tao, J.; Wang, R.; Yu, H.; Chen, L.; Fang, D.; Tian, Y.; Xie, J.; Jia, D.; Liu, H.; Wang, J.; Tang, F.; Song, L.; Li, H. Highly Transparent, Highly Thermally Stable Nanocellulose/Polymer Hybrid Substrates for Flexible OLED Devices. *ACS Appl. Mater. Interfaces* **2020**, *12* (8), 9701–9709. https://doi.org/10.1021/acsami.0c01048.

(115) Sahoo, R.; Mishra, S.; Ramadoss, A.; Mohanty, S.; Mahapatra, S.; Nayak, S. K. An Approach towards the Fabrication of Energy Harvesting Device Using Ca-Doped ZnO/ PVDF-TrFE Composite Film. *Polymer (Guildf).* **2020**, *205*, 122869. https://doi.org/10.1016/J.POLYMER.2020.122869.

(116) Koo, D.; Jung, S.; Seo, J.; Jeong, G.; Choi, Y.; Lee, J.; Lee, S. M.; Cho, Y.; Jeong, M.; Lee, J.; Oh, J.; Yang, C.; Park, H. Flexible Organic Solar Cells Over 15% Efficiency with Polyimide-Integrated Graphene Electrodes. *Joule* **2020**, *4* (5), 1021–1034. https://doi.org/10.1016/j.joule.2020.02.012.

(117) Li, L.; Han, L.; Hu, H.; Zhang, R. A Review on Polymers and Their Composites for Flexible Electronics. *Mater. Adv.* **2022**. https://doi.org/10.1039/d2ma00940d.

(118) Tucker, M. B.; Li, T. SOME MECHANICS CHALLENGES AND SOLUTIONS IN FLEXIBLE ELECTRONICS. **2009**.

(119) Mao, Y.; Ji, B.; Chen, G.; Hao, C.; Zhou, B.; Tian, Y. Robust and Wearable Pressure Sensor

Assembled from AgNW-Coated PDMS Micropillar Sheets with High Sensitivity and Wide Detection Range. *ACS Appl. Nano Mater.* **2019**, *2* (5), 3196–3205. https://doi.org/10.1021/acsanm.9b00503.

(120) Boutry, C. M.; Nguyen, A.; Lawal, Q. O.; Chortos, A.; Rondeau-Gagné, S.; Bao, Z. A Sensitive and Biodegradable Pressure Sensor Array for Cardiovascular Monitoring. *Adv. Mater.* **2015**, *27* (43), 6954–6961. https://doi.org/10.1002/adma.201502535.

(121) Fan, G.; Shen, Y.; Hao, X.; Yuan, Z.; Zhou, Z. Large-Scale Wireless Temperature Monitoring System for Liquefied Petroleum Gas Storage Tanks. *Sensors* **2015**, *15* (9), 23745–23762. https://doi.org/10.3390/S150923745.

(122) Amoli, V.; Kim, J. S.; Jee, E.; Chung, Y. S.; Kim, S. Y.; Koo, J.; Choi, H.; Kim, Y.; Kim, D. H. A Bioinspired Hydrogen Bond-Triggered Ultrasensitive Ionic Mechanoreceptor Skin. *Nat. Commun.* **2019**, *10* (1), 1–13. https://doi.org/10.1038/s41467-019-11973-5.

(123) Ha, M.; Lim, S.; Park, J.; Um, D. S.; Lee, Y.; Ko, H. Bioinspired Interlocked and Hierarchical Design of Zno Nanowire Arrays for Static and Dynamic Pressure-Sensitive Electronic Skins. *Adv. Funct. Mater.* **2015**, *25* (19), 2841–2849. https://doi.org/10.1002/adfm.201500453.

(124) Liu, J.; Bao, S.; Wang, X. Applications of Graphene-Based Materials in Sensors: A Review. *Micromachines* **2022**, *13* (2), 184. https://doi.org/10.3390/mi13020184.

(125) Souri, H.; Banerjee, H.; Jusufi, A.; Radacsi, N.; Stokes, A. A.; Park, I.; Sitti, M.; Amjadi, M. Wearable and Stretchable Strain Sensors: Materials, Sensing Mechanisms, and Applications. *Adv. Intell. Syst.* **2020**, *2* (8), 2000039. https://doi.org/10.1002/aisy.202000039.

(126) Yang, T.; Xie, D.; Li, Z.; Zhu, H. Recent Advances in Wearable Tactile Sensors: Materials, Sensing Mechanisms, and Device Performance. *Mater. Sci. Eng. R Reports* **2017**, *115*, 1–37. https://doi.org/10.1016/j.mser.2017.02.001.

(127) Lee, H. K.; Chang, S. Il; Yoon, E. A Flexible Polymer Tactile Sensor: Fabrication and Modular Expandability for Large Area Deployment. *J. Microelectromechanical Syst.* **2006**, *15* (6), 1681–1686. https://doi.org/10.1109/JMEMS.2006.886021.

(128) Laskarakis, A.; Logothetidis, S.; Kassavetis, S.; Papaioannou, E. Surface Modification of Poly(Ethylene Terephthalate) Polymeric Films for Flexible Electronics Applications. *Thin Solid Films* **2008**, *516* (7), 1443–1448. https://doi.org/10.1016/j.tsf.2007.03.170.

(129) Lee, H. K.; Chang, S. Il; Kim, K. H.; Kim, S. J.; Yun, K. S.; Yoon, E. A Modular Expandable Tactile Sensor Using Flexible Polymer. *Proc. IEEE Int. Conf. Micro Electro Mech. Syst.* **2005**, 642–645. https://doi.org/10.1109/memsys.2005.1454011.

(130) Jayathilaka, W. A. D. M.; Qi, K.; Qin, Y.; Chinnappan, A.; Serrano-García, W.; Baskar, C.; Wang, H.; He, J.; Cui, S.; Thomas, S. W.; Ramakrishna, S. Significance of Nanomaterials in Wearables: A Review on Wearable Actuators and Sensors. *Adv. Mater.* **2019**, *31* (7), 1805921. https://doi.org/10.1002/adma.201805921.

(131) Liu, M. Y.; Hang, C. Z.; Zhao, X. F.; Zhu, L. Y.; Ma, R. G.; Wang, J. C.; Lu, H. L.; Zhang, D. W. Advance on Flexible Pressure Sensors Based on Metal and Carbonaceous Nanomaterial. *Nano Energy* **2021**, *87*, 106181. https://doi.org/10.1016/j.nanoen.2021.106181.

(132) Jang, H.; Park, Y. J.; Chen, X.; Das, T.; Kim, M. S.; Ahn, J. H. Graphene-Based Flexible and Stretchable Electronics. *Adv. Mater.* **2016**, *28* (22), 4184–4202. https://doi.org/10.1002/adma.201504245.

(133) Lee, J.; Kim, S.; Lee, J.; Yang, D.; Park, B. C.; Ryu, S.; Park, I. A Stretchable Strain Sensor Based on a Metal Nanoparticle Thin Film for Human Motion Detection. *Nanoscale* **2014**, *6* (20), 11932–11939. https://doi.org/10.1039/c4nr03295k.

(134) Duan, L.; D'hooge, D. R.; Cardon, L. Recent Progress on Flexible and Stretchable Piezoresistive Strain Sensors: From Design to Application. *Prog. Mater. Sci.* **2020**, *114*, 100617. https://doi.org/10.1016/j.pmatsci.2019.100617.

(135) Fu, M.; Zhang, J.; Jin, Y.; Zhao, Y.; Huang, S.; Guo, C. F. A Highly Sensitive, Reliable, and High-Temperature-Resistant Flexible Pressure Sensor Based on Ceramic Nanofibers. *Adv. Sci.* **2020**, *7* (17), 2000258. https://doi.org/10.1002/advs.202000258.

(136) Kwon, S. S.; Hong, W. K.; Jo, G.; Maeng, J.; Kim, T. W.; Song, S.; Lee, T. Piezoelectric Effect on the Electronic Transport Characteristics of ZnO Nanowire Field-Effect Transistors on Bent Flexible Substrates. *Adv. Mater.* **2008**, *20* (23), 4557–4562. https://doi.org/10.1002/adma.200800691.

(137) Kerpa, O.; Weiss, K.; Wörn, H. Development of a Flexible Tactile Sensor System for a Humanoid Robot. *IEEE Int. Conf. Intell. Robot. Syst.* **2003**, *1*, 1–6. https://doi.org/10.1109/iros.2003.1250596.

(138) Chen, C. K.; Lin, D. T. W.; Juang, Y. Der; Hu, Y. C.; Kuo, Y. T.; Chen, C. Y. The Innovated Flexible Surface Acoustic Wave Devices on Fully InkJet Printing Technology. *Smart Sci.* **2013**, *1* (1), 13–17. https://doi.org/10.1080/23080477.2013.11665581.

(139) Liu, Q.; Yang, X.; Song, R.; Su, J.; Luo, M.; Zhong, J.; Wang, L. An Infrared Touch System for Automatic Behavior Monitoring. *Neurosci. Bull.* **2021**, *37* (6), 815–830. https://doi.org/10.1007/s12264-021-00661-4.

(140) Dan, L.; Elias, A. L. Flexible and Stretchable Temperature Sensors Fabricated Using Solution-Processable Conductive Polymer Composites. *Adv. Healthc. Mater.* **2020**, *9* (16), 2000380. https://doi.org/10.1002/adhm.202000380.

(141) Liu, T.; Liu, H.; Li, Y. F.; Chen, Z.; Zhang, Z.; Liu, S. Flexible FTIR Spectral Imaging Enhancement for Industrial Robot Infrared Vision Sensing. *IEEE Trans. Ind. Informatics* **2020**, *16* (1), 544–554. https://doi.org/10.1109/TII.2019.2934728.

(142) Wu, C. C. Ultra-High Transparent Sandwich Structure with a Silicon Dioxide Passivation Layer Prepared on a Colorless Polyimide Substrate for a Flexible Capacitive Touch Screen Panel. *Sol. Energy Mater. Sol. Cells* **2020**, *207*, 110350. https://doi.org/10.1016/j.solmat.2019.110350.

(143) Yan, T.; Wu, Y.; Yi, W.; Pan, Z. Recent Progress on Fabrication of Carbon Nanotube-Based Flexible Conductive Networks for Resistive-Type Strain Sensors. *Sensors Actuators, A Phys.* **2021**, *327*, 112755. https://doi.org/10.1016/j.sna.2021.112755.

(144) Afsarimanesh, N.; Nag, A.; Sarkar, S.; Sabet, G. S.; Han, T.; Mukhopadhyay, S. C. A Review on Fabrication, Characterization and Implementation of Wearable Strain Sensors. *Sensors Actuators, A Phys.* **2020**, *315*, 112355. https://doi.org/10.1016/j.sna.2020.112355.

(145) Mishra, R. B.; El-Atab, N.; Hussain, A. M.; Hussain, M. M. Recent Progress on Flexible Capacitive Pressure Sensors: From Design and Materials to Applications. *Adv. Mater. Technol.* **2021**, *6* (4), 2001023. https://doi.org/10.1002/admt.202001023.

(146) Son, D.; Kang, J.; Vardoulis, O.; Kim, Y.; Matsuhisa, N.; Oh, J. Y.; To, J. W.; Mun, J.; Katsumata, T.; Liu, Y.; McGuire, A. F.; Krason, M.; Molina-Lopez, F.; Ham, J.; Kraft, U.; Lee, Y.; Yun, Y.; Tok, J. B. H.; Bao, Z. An Integrated Self-Healable Electronic Skin System Fabricated via Dynamic Reconstruction of a Nanostructured Conducting Network. *Nat. Nanotechnol.* **2018**, *13* (11), 1057–1065. https://doi.org/10.1038/s41565-018-0244-6.

(147) Yang, Y.; Gao, W. Wearable and Flexible Electronics for Continuous Molecular Monitoring. *Chem. Soc. Rev.* **2019**, *48* (6), 1465–1491. https://doi.org/10.1039/c7cs00730b.

(148) Wang, Y.; Xu, C.; Yu, X.; Zhang, H.; Han, M. Multilayer Flexible Electronics: Manufacturing Approaches and Applications. *Mater. Today Phys.* **2022**, *23*, 100647. https://doi.org/10.1016/j.mtphys.2022.100647.

(149) Boutry, C. M.; Beker, L.; Kaizawa, Y.; Vassos, C.; Tran, H.; Hinckley, A. C.; Pfattner, R.; Niu, S.; Li, J.; Claverie, J.; Wang, Z.; Chang, J.; Fox, P. M.; Bao, Z. Biodegradable and Flexible Arterial-Pulse Sensor for the Wireless Monitoring of Blood Flow. *Nat. Biomed. Eng.* **2019**, *3* (1), 47–57. https://doi.org/10.1038/s41551-018-0336-5.

(150) Shi, Z.; Meng, L.; Shi, X.; Li, H.; Zhang, J.; Sun, Q.; Liu, X.; Chen, J.; Liu, S. Morphological Engineering of Sensing Materials for Flexible Pressure Sensors and Artificial Intelligence Applications. *Nano-Micro Lett.* **2022**, *14* (1), 1–48. https://doi.org/10.1007/s40820-022-00874-w.

(151) Ma, S.; Tang, J.; Yan, T.; Pan, Z. Performance of Flexible Strain Sensors With Different Transition Mechanisms: A Review. *IEEE Sens. J.* **2022**, *22* (8), 7475–7498. https://doi.org/10.1109/JSEN.2022.3156286.

(152) Cenci, M. P.; Scarazzato, T.; Munchen, D. D.; Dartora, P. C.; Veit, H. M.; Bernardes, A. M.; Dias, P. R. Eco-Friendly Electronics—A Comprehensive Review. *Adv. Mater. Technol.* **2022**, *7* (2), 2001263. https://doi.org/10.1002/admt.202001263.

(153) Jaiswal, A. K.; Kumar, V.; Jansson, E.; Huttunen, O.; Yamamoto, A.; Vikman, M.; Khakalo, A.; Hiltunen, J.; Behfar, M. H. Biodegradable Cellulose Nanocomposite Substrate for Recyclable Flexible Printed Electronics. *Adv. Electron. Mater.* **2023**, 2201094. https://doi.org/10.1002/aelm.202201094.

(154) Shtein, M.; Peumans, P.; Benziger, J. B.; Forrest, S. R. Direct, Mask- and Solvent-Free Printing of Molecular Organic Semiconductors. *Adv. Mater.* **2004**, *16* (18), 1615–1620. https://doi.org/10.1002/adma.200400260.

(155) Zhao, L.; Zhang, T.; Li, W.; Li, T.; Zhang, L.; Zhang, X.; Wang, Z. Engineering of Sodium-Ion Batteries: Opportunities and Challenges. *Engineering* **2022**. https://doi.org/10.1016/J.ENG.2021.08.032.

(156) Cheng, H.; Vepachedu, V. Recent Development of Transient Electronics. *Theor. Appl. Mech. Lett.* **2016**, *6* (1), 21–31. https://doi.org/10.1016/j.taml.2015.11.012.

(157) Yin, L.; Cheng, H.; Mao, S.; Haasch, R.; Liu, Y.; Xie, X.; Hwang, S. W.; Jain, H.; Kang, S. K.; Su, Y.; Li, R.; Huang, Y.; Rogers, J. A. Dissolvable Metals for Transient Electronics. *Adv. Funct. Mater.* **2014**, *24* (5), 645–658. https://doi.org/10.1002/adfm.201301847.

(158) Han, W. B.; Lee, J. H.; Shin, J. W.; Hwang, S. W. Advanced Materials and Systems for Biodegradable, Transient Electronics. *Adv. Mater.* **2020**, *32* (51), 2002211. https://doi.org/10.1002/adma.202002211.

(159) Fu, K. K.; Wang, Z.; Dai, J.; Carter, M.; Hu, L. Transient Electronics: Materials and Devices. *Chem. Mater.* **2016**, *28* (11), 3527–3539. https://doi.org/10.1021/ACS.CHEMMATER.5B04931/ASSET/IMAGES/LARGE/CM-2015-04931S_0012.JPEG.

(160) Li, G.; Wang, L.; Lei, X.; Peng, Z.; Wan, T.; Maganti, S.; Huang, M.; Murugadoss, V.; Seok, I.; Jiang, Q.; Cui, D.; Alhadhrami, A.; Ibrahim, M. M.; Wei, H. Flexible, yet Robust Polyaniline Coated Foamed Polylactic Acid Composite Electrodes for High-Performance Supercapacitors. *Adv. Compos. Hybrid Mater.* **2022**, *5* (2), 853–863. https://doi.org/10.1007/s42114-022-00501-7.

(161) Fallahi, H.; Azizi, H.; Ghasemi, I.; Karrabi, M. Preparation and Properties of Electrically Conductive, Flexible and Transparent Silver Nanowire/Poly (Lactic Acid) Nanocomposites. *Org. Electron.* **2017**, *44*, 74–84. https://doi.org/10.1016/j.orgel.2017.01.043.

(162) Luoma, E.; Välimäki, M.; Rokkonen, T.; Sääskilahti, H.; Ollila, J.; Rekilä, J.; Immonen, K. Oriented and Annealed Poly(Lactic Acid) Films and Their Performance in Flexible Printed and Hybrid Electronics. *J. Plast. Film Sheeting* **2021**, *37* (4), 429–462. https://doi.org/10.1177/8756087920988569.

(163) Saeidlou, S.; Huneault, M. A.; Li, H.; Park, C. B. Poly(Lactic Acid) Crystallization. *Prog. Polym. Sci.* **2012**, *37* (12), 1657–1677. https://doi.org/10.1016/j.progpolymsci.2012.07.005.

(164) Hwang, S. W.; Song, J. K.; Huang, X.; Cheng, H.; Kang, S. K.; Kim, B. H.; Kim, J. H.; Yu, S.; Huang, Y.; Rogers, J. A. High-Performance Biodegradable/Transient Electronics on Biodegradable Polymers. *Adv. Mater.* **2014**, *26* (23), 3905–3911. https://doi.org/10.1002/adma.201306050.

(165) Uva, A.; Lin, A.; Babi, J.; Tran, H. Bioderived and Degradable Polymers for Transient

Electronics. *J. Chem. Technol. Biotechnol.* **2022**, *97* (4), 801–809. https://doi.org/10.1002/jctb.6790.

(166) Geczy, A.; Csiszar, A.; Rozs, E.; Hajdu, I.; Medgyes, B.; Krammer, O.; Straubinger, D.; Gal, L. Novel PLA/Flax Based Biodegradable Printed Circuit Boards. *Proc. Int. Spring Semin. Electron. Technol.* **2022**, *2022-May*. https://doi.org/10.1109/ISSE54558.2022.9812827.

(167) Silva, V. A. O. P.; Fernandes-Junior, W. S.; Rocha, D. P.; Stefano, J. S.; Munoz, R. A. A.; Bonacin, J. A.; Janegitz, B. C. 3D-Printed Reduced Graphene Oxide/Polylactic Acid Electrodes: A New Prototyped Platform for Sensing and Biosensing Applications. *Biosens. Bioelectron.* **2020**, *170*, 112684. https://doi.org/10.1016/j.bios.2020.112684.

(168) Ma, X.; Hu, Q.; Dai, Y.; He, P.; Zhang, X. Disposable Sensors Based on Biodegradable Polylactic Acid Piezoelectret Films and Their Application in Wearable Electronics. *Sensors Actuators A Phys.* **2022**, *346*, 113834. https://doi.org/10.1016/j.sna.2022.113834.

(169) Wu, N.; Shi, Y. R.; Jia, T.; Du, X. N.; Yin, Y. X.; Xin, S.; Guo, Y. G. Green in Situ Growth Solid Electrolyte Interphase Layer with High Rebound Resilience for Long-Life Lithium Metal Anodes. *ACS Appl. Mater. Interfaces* **2019**, *11* (46), 43200–43205. https://doi.org/10.1021/acsami.9b15228.

(170) Ando, M.; Kawamura, H.; Kitada, H.; Sekimoto, Y.; Inoue, T.; Tajitsu, Y. Pressure-Sensitive Touch Panel Based on Piezoelectric Poly(L-Lactic Acid) Film. *Jpn. J. Appl. Phys.* **2013**, *52* (9 PART2), 09KD17. https://doi.org/10.7567/JJAP.52.09KD17.

(171) Singhvi, M. S.; Zinjarde, S. S.; Gokhale, D. V. Polylactic Acid: Synthesis and Biomedical Applications. *J. Appl. Microbiol.* **2019**, *127* (6), 1612–1626. https://doi.org/10.1111/jam.14290.

(172) Prontera, C. T.; Villani, F.; Palamà, I. E.; Maglione, M. G.; Manini, P.; Maiorano, V.; Tammaro, L. Fabrication and Biocompatibility Analysis of Flexible Organic Light Emitting Diodes on Poly(Lactic Acid) Substrates: Toward the Development of Greener Bio-Electronic Devices. *Polym. Adv. Technol.* **2022**, *33* (5), 1523–1532. https://doi.org/10.1002/pat.5618.

(173) Aulin, C.; Karabulut, E.; Tran, A.; Waìšgberg, L.; Lindström, T. Transparent Nanocellulosic Multilayer Thin Films on Polylactic Acid with Tunable Gas Barrier Properties. *ACS Appl. Mater. Interfaces* **2013**, *5* (15), 7352–7359. https://doi.org/10.1021/am401700n.

(174) Honaker, K.; Vautard, F.; Drzal, L. T. Influence of Processing Methods on the Mechanical and Barrier Properties of HDPE-GNP Nanocomposites. *Adv. Compos. Hybrid Mater.* **2021**, *4* (3), 492–504.

(175) Atreya, M.; Dikshit, K.; Marinick, G.; Nielson, J.; Bruns, C.; Whiting, G. L. Poly(Lactic Acid)-Based Ink for Biodegradable Printed Electronics with Conductivity Enhanced through Solvent Aging. *ACS Appl. Mater. Interfaces* **2020**, *12* (20), 23494–23501. https://doi.org/10.1021/acsami.0c05196.

(176) Lebedev, S. M.; Gefle, O. S.; Amitov, E. T.; Berchuk, D. Y.; Zhuravlev, D. V. Poly(Lactic Acid)-Based Polymer Composites with High Electric and Thermal Conductivity and Their

Characterization. *Polym. Test.* **2017**, *58*, 241–248. https://doi.org/10.1016/j.polymertesting.2016.12.033.

(177) Ning, W.; Xingxiang, Z.; Jiugao, Y.; Jianming, F. Partially Miscible Poly(Lactic Acid)-Blend-Poly(Propylene Carbonate) Filled with Carbon Black as Conductive Polymer Composite. *Polym. Int.* **2008**, *57* (9), 1027–1035. https://doi.org/10.1002/pi.2442.

(178) Yu, J.; Wang, N.; Ma, X. Fabrication and Characterization of Poly(Lactic Acid)/Acetyl Tributyl Citrate/Carbon Black as Conductive Polymer Composites. *Biomacromolecules* **2008**, *9* (3), 1050–1057. https://doi.org/10.1021/BM7012857/ASSET/IMAGES/LARGE/BM-2007-012857_0012.JPEG.

(179) Li, G.; Zhao, M.; Xu, F.; Yang, B.; Li, X.; Meng, X.; Teng, L.; Sun, F.; Li, Y. Synthesis and Biological Application of Polylactic Acid. *Molecules* **2020**, *25* (21), 5023. https://doi.org/10.3390/molecules25215023.

(180) Zych, A.; Tellers, J.; Bertolacci, L.; Ceseracciu, L.; Marini, L.; Mancini, G.; Athanassiou, A. Biobased, Biodegradable, Self-Healing Boronic Ester Vitrimers from Epoxidized Soybean Oil Acrylate. *ACS Appl. Polym. Mater.* **2020**, *3* (2), 1135–1144.

(181) Zych, A.; Pinalli, R.; Soliman, M.; Vachon, J.; Dalcanale, E. Polyethylene Vitrimers via Silyl Ether Exchange Reaction. *Polymer (Guildf).* **2020**, *199*, 122567. https://doi.org/10.1016/J.POLYMER.2020.122567.

(182) Zheng, J.; Png, Z. M.; Ng, S. H.; Tham, G. X.; Ye, E.; Goh, S. S.; Loh, X. J.; Li, Z. Vitrimers: Current Research Trends and Their Emerging Applications. *Mater. Today* **2021**, *51*, 586–625. https://doi.org/10.1016/J.MATTOD.2021.07.003.

(183) Cruz, S. M. F.; Rocha, L. A.; Viana, J. C. Printing Technologies on Flexible Substrates for Printed Electronics. *Flex. Electron.* **2018**. https://doi.org/10.5772/intechopen.76161.

(184) Li, R.; Wang, L.; Kong, D.; Yin, L. Recent Progress on Biodegradable Materials and Transient Electronics. *Bioact. Mater.* **2018**, *3* (3), 322–333. https://doi.org/10.1016/j.bioactmat.2017.12.001.

(185) Yu, X.; Shou, W.; Mahajan, B. K.; Huang, X.; Pan, H. Materials, Processes, and Facile Manufacturing for Bioresorbable Electronics: A Review. *Adv. Mater.* **2018**, *30* (28), 1707624. https://doi.org/10.1002/ADMA.201707624.

(186) Cummins, G.; Desmulliez, M. P. Y. Inkjet Printing of Conductive Materials: A Review. *Circuit World* **2012**, *38* (4), 193–213. https://doi.org/10.1108/03056121211280413.

(187) Rajan, K.; Roppolo, I.; Chiappone, A.; Bocchini, S.; Perrone, D.; Chiolerio, A. Silver Nanoparticle Ink Technology: State of the Art. *Nanotechnol. Sci. Appl.* **2016**, *9*. https://doi.org/10.2147/NSA.S68080.

(188) Wiklund, J.; Karakoç, A.; Palko, T.; Yigitler, H.; Ruttik, K.; Jäntti, R.; Paltakari, J. A Review on Printed Electronics: Fabrication Methods, Inks, Substrates, Applications and Environmental

Impacts. *J. Manuf. Mater. Process.* **2021**, *5* (3), 89. https://doi.org/10.3390/jmmp5030089.

(189) Nan, M.; Wang, F.; Kim, S.; Li, H.; Jin, Z.; Bang, D.; Kim, C. S.; Park, J. O.; Choi, E. Ecofriendly High-Performance Ionic Soft Actuators Based on Graphene-Mediated Cellulose Acetate. *Sensors Actuators, B Chem.* **2019**, *301*, 127127. https://doi.org/10.1016/j.snb.2019.127127.

(190) Ba, H.; Giambastiani, G.; Pham-Huu, C.; Truong-Phuoc, L.; Papaefthimiou, V.; Sutter, C.; Pronkin, S.; Bahouka, A.; Lafue, Y.; Nguyen-Dinh, L. Cotton Fabrics Coated with Few-Layer Graphene as Highly Responsive Surface Heaters and Integrated Lightweight Electronic-Textile Circuits. *ACS Appl. Nano Mater.* **2020**, *3* (10), 9771–9783. https://doi.org/10.1021/acsanm.0c01861.

(191) Ge, X.; Lu, J.; Ma, L.; Ma, J. Life Cycle Assessment of Different Nitrogen-Doped Reduced Graphene Oxide Production Routes within Early Research. *Polish J. Environ. Stud.* **2021**, *30* (2), 1601–1609. https://doi.org/10.15244/pjoes/125561.

(192) Arvidsson, R.; Kushnir, D.; Sandén, B. A.; Molander, S. Prospective Life Cycle Assessment of Graphene Production by Ultrasonication and Chemical Reduction. *Environ. Sci. Technol.* **2014**, *48* (8), 4529–4536. https://doi.org/10.1021/es405338k.

(193) Gordon, S. E.; Dorfman, J. R.; Kirk, D.; Adams, K. Advances in Conductive Inks across Multiple Applications and Deposition Platforms. *Ipc Apex Expo 2012* **2012**, *3*, 2217–2241.

(194) Tomotoshi, D.; Kawasaki, H. Surface and Interface Designs in Copper-Based Conductive Inks for Printed/Flexible Electronics. *Nanomaterials* **2020**, *10* (9), 1–53. https://doi.org/10.3390/nano10091689.

(195) Venkata Krishna Rao, R.; Venkata Abhinav, K.; Karthik, P. S.; Singh, S. P. Conductive Silver Inks and Their Applications in Printed and Flexible Electronics. *RSC Adv.* **2015**, *5* (95), 77760–77790. https://doi.org/10.1039/c5ra12013f.

(196) Aleeva, Y.; Pignataro, B. Recent Advances in Upscalable Wet Methods and Ink Formulations for Printed Electronics. *J. Mater. Chem. C* **2014**, *2* (32), 6436–6453. https://doi.org/10.1039/c4tc00618f.

(197) Wu, W. Inorganic Nanomaterials for Printed Electronics: A Review. *Nanoscale* **2017**, *9* (22), 7342–7372. https://doi.org/10.1039/c7nr01604b.

(198) Kang, B.; Lee, W. H.; Cho, K. Recent Advances in Organic Transistor Printing Processes. *ACS Appl. Mater. Interfaces* **2013**, *5* (7), 2302–2315. https://doi.org/10.1021/am302796z.

(199) Kwak, D.; Lim, J. A.; Kang, B.; Lee, W. H.; Cho, K. Self-Organization of Inkjet-Printed Organic Semiconductor Films Prepared in Inkjet-Etched Microwells. *Adv. Funct. Mater.* **2013**, *23* (42), 5224–5231. https://doi.org/10.1002/adfm.201300936.

(200) Zheng, Y. Q.; Wang, J. Y.; Pei, J. One-Dimensional (1D) Micro/Nanostructures of Organic Semiconductors for Field-Effect Transistors. *Sci. China Chem.* **2015**, *58* (6), 937–946.

https://doi.org/10.1007/S11426-015-5410-1/METRICS.

(201) Han, X.; Chen, Y.; Zhu, H.; Preston, C.; Wan, J.; Fang, Z.; Hu, L. Scalable, Printable, Surfactant-Free Graphene Ink Directly from Graphite. *Nanotechnology* **2013**, *24* (20), 205304. https://doi.org/10.1088/0957-4484/24/20/205304.

(202) Xu, H.; Chen, R.; Sun, Q.; Lai, W.; Su, Q.; Huang, W.; Liu, X. Recent Progress in Metal-Organic Complexes for Optoelectronic Applications. *Chem. Soc. Rev.* **2014**, *43* (10), 3259–3302. https://doi.org/10.1039/c3cs60449g.

(203) Tang, X. F.; Yang, Z. G.; Wang, W. J. A Simple Way of Preparing High-Concentration and High-Purity Nano Copper Colloid for Conductive Ink in Inkjet Printing Technology. *Colloids Surfaces A Physicochem. Eng. Asp.* **2010**, *360* (1–3), 99–104. https://doi.org/10.1016/j.colsurfa.2010.02.011.

(204) Jeong, S.; Song, H. C.; Lee, W. W.; Choi, Y.; Ryu, B. H. Preparation of Aqueous Ag Ink with Long-Term Dispersion Stability and Its Inkjet Printing for Fabricating Conductive Tracks on a Polyimide Film. *J. Appl. Phys.* **2010**, *108* (10), 102805. https://doi.org/10.1063/1.3511686.

(205) Jo, Y. H.; Jung, I.; Choi, C. S.; Kim, I.; Lee, H. M. Synthesis and Characterization of Low Temperature Sn Nanoparticles for the Fabrication of Highly Conductive Ink. *Nanotechnology* **2011**, *22* (22), 225701. https://doi.org/10.1088/0957-4484/22/22/225701.

(206) Shankar, R.; Groven, L.; Amert, A.; Whites, K. W.; Kellar, J. J. Non-Aqueous Synthesis of Silver Nanoparticles Using Tin Acetate as a Reducing Agent for the Conductive Ink Formulation in Printed Electronics. *J. Mater. Chem.* **2011**, *21* (29), 10871–10877. https://doi.org/10.1039/c0jm04521g.

(207) Perelaer, J.; Smith, P. J.; Mager, D.; Soltman, D.; Volkman, S. K.; Subramanian, V.; Korvink, J. G.; Schubert, U. S. Printed Electronics: The Challenges Involved in Printing Devices, Interconnects, and Contacts Based on Inorganic Materials. *J. Mater. Chem.* **2010**, *20* (39), 8446–8453. https://doi.org/10.1039/c0jm00264j.

(208) Liao, Y.; Zhang, R.; Qian, J. Printed Electronics Based on Inorganic Conductive Nanomaterials and Their Applications in Intelligent Food Packaging. *RSC Adv.* **2019**, *9* (50), 29154–29172. https://doi.org/10.1039/c9ra05954g.

(209) Pawar, S. D.; Murugavel, P.; Lal, D. M. Effect of Relative Humidity and Sea Level Pressure on Electrical Conductivity of Air over Indian Ocean. *J. Geophys. Res. Atmos.* **2009**, *114* (2). https://doi.org/10.1029/2007JD009716.

(210) Anto, B. T.; Sivaramakrishnan, S.; Chua, L. L.; Ho, P. K. H. Hydrophilic Sparse Ionic Monolayer-Protected Metal Nanoparticles: Highly Concentrated Nano-Au and Nano-Ag "Inks" That Can Be Sintered to near-Bulk Conductivity at 150°C. *Adv. Funct. Mater.* **2010**, *20* (2), 296–303. https://doi.org/10.1002/adfm.200901336.

(211) Asghar, M. A.; Asghar, M. A. Green Synthesized and Characterized Copper Nanoparticles Using Various New Plants Extracts Aggravate Microbial Cell Membrane Damage after

Interaction with Lipopolysaccharide. *Int. J. Biol. Macromol.* **2020**, *160*, 1168–1176. https://doi.org/10.1016/j.ijbiomac.2020.05.198.

(212) Wang, B. Y.; Yoo, T. H.; Song, Y. W.; Lim, D. S.; Oh, Y. J. Cu Ion Ink for a Flexible Substrate and Highly Conductive Patterning by Intensive Pulsed Light Sintering. *ACS Appl. Mater. Interfaces* **2013**, *5* (10), 4113–4119. https://doi.org/10.1021/am303268k.

(213) Fukuda, K.; Sekine, T.; Kumaki, D.; Tokito, S. Profile Control of Inkjet Printed Silver Electrodes and Their Application to Organic Transistors. *ACS Appl. Mater. Interfaces* **2013**, *5* (9), 3916–3920. https://doi.org/10.1021/am400632s.

(214) Meng, X.; Xu, Y.; Wang, Q.; Yang, X.; Guo, J.; Hu, X.; Tan, L.; Chen, Y. Silver Mesh Electrodes via Electroless Deposition-Coupled Inkjet-Printing Mask Technology for Flexible Polymer Solar Cells. *Langmuir* **2019**, *35* (30), 9713–9720. https://doi.org/10.1021/acs.langmuir.9b00846.

(215) Raman, V.; Jo, J.; Kim, H. K. ITO and Graphene-Covered Ag Grids Embedded in PET Substrate by Thermal Roll Imprinting for Flexible Organic Solar Cells. *Mater. Sci. Semicond. Process.* **2020**, *120*, 105277. https://doi.org/10.1016/j.mssp.2020.105277.

(216) Yang, C.; Wong, C. P.; Yuen, M. M. F. Printed Electrically Conductive Composites: Conductive Filler Designs and Surface Engineering. *J. Mater. Chem. C* **2013**, *1* (26), 4052–4069. https://doi.org/10.1039/c3tc00572k.

(217) Nath, S.; Jana, S.; Pradhan, M.; Pal, T. Ligand-Stabilized Metal Nanoparticles in Organic Solvent. *J. Colloid Interface Sci.* **2010**, *341* (2), 333–352. https://doi.org/10.1016/j.jcis.2009.09.049.

(218) Li, J.; Lei, W.; Zhang, X.; Zhou, X.; Wang, Q.; Zhang, Y.; Wang, B. Field Emission Characteristic of Screen-Printed Carbon Nanotube Cathode. *Appl. Surf. Sci.* **2003**, *220* (1–4), 96–104. https://doi.org/10.1016/S0169-4332(03)00749-9.

(219) Wang, J.; Tian, B.; Nascimento, V. B.; Angnes, L. Performance of Screen-Printed Carbon Electrodes Fabricated from Different Carbon Inks. *Electrochim. Acta* **1998**, *43* (23), 3459–3465. https://doi.org/10.1016/S0013-4686(98)00092-9.

(220) Kordás, K.; Mustonen, T.; Tóth, G.; Jantunen, H.; Lajunen, M.; Soldano, C.; Talapatra, S.; Kar, S.; Vajtai, R.; Ajayan, P. M. Inkjet Printing of Electrically Conductive Patterns of Carbon Nanotubes. *Small* **2006**, *2* (8–9), 1021–1025. https://doi.org/10.1002/smll.200600061.

(221) Baechler, C.; Gardin, S.; Abuhimd, H.; Kovacs, G. Inkjet Printed Multiwall Carbon Nanotube Electrodes for Dielectric Elastomer Actuators. *Smart Mater. Struct.* **2016**, *25* (5), 055009. https://doi.org/10.1088/0964-1726/25/5/055009.

(222) Geim, A. K.; Novoselov, K. S. The Rise of Graphene. *Nat. Mater.* **2007**, *6* (3), 183–191. https://doi.org/10.1038/nmat1849.

(223) Chen, J. H.; Ishigami, M.; Jang, C.; Hines, D. R.; Fuhrer, M. S.; Williams, E. D. Printed

Graphene Circuits. *Adv. Mater.* **2007**, *19* (21), 3623–3627. https://doi.org/10.1002/adma.200701059.

(224) Secor, E. B.; Prabhumirashi, P. L.; Puntambekar, K.; Geier, M. L.; Hersam, M. C. Inkjet Printing of High Conductivity, Flexible Graphene Patterns. *J. Phys. Chem. Lett.* **2013**, *4* (8), 1347–1351. https://doi.org/10.1021/jz400644c.

(225) Zhang, W.; Bi, E.; Li, M.; Gao, L. Synthesis of Ag/RGO Composite as Effective Conductive Ink Filler for Flexible Inkjet Printing Electronics. *Colloids Surfaces A Physicochem. Eng. Asp.* **2016**, *490*, 232–240. https://doi.org/10.1016/J.COLSURFA.2015.11.014.

(226) Najafi, M.; Zahid, M.; Ceseracciu, L.; Safarpour, M.; Athanassiou, A.; Bayer, I. S. Polylactic Acid-Graphene Emulsion Ink Based Conductive Cotton Fabrics. *J. Mater. Res. Technol.* **2022**, *18*, 5197–5211. https://doi.org/10.1016/j.jmrt.2022.04.119.

(227) Lammens, N.; Kersemans, M.; Luyckx, G.; Van Paepegem, W.; Degrieck, J. Improved Accuracy in the Determination of Flexural Rigidity of Textile Fabrics by the Peirce Cantilever Test (ASTM D1388). *Text. Res. J.* **2014**, *84* (12), 1307–1314. https://doi.org/10.1177/0040517514523182.

(228) Huang, S.; Liu, Y.; Zhao, Y.; Ren, Z.; Guo, C. F. Flexible Electronics: Stretchable Electrodes and Their Future. *Adv. Funct. Mater.* **2019**, *29* (6), 1805924. https://doi.org/10.1002/adfm.201805924.

(229) Sukumaran, S.; Chatbouri, S.; Rouxel, D.; Tisserand, E.; Thiebaud, F.; Ben Zineb, T. Recent Advances in Flexible PVDF Based Piezoelectric Polymer Devices for Energy Harvesting Applications. *J. Intell. Mater. Syst. Struct.* **2021**, *32* (7), 746–780.

(230) Wang, C.; Xia, K.; Wang, H.; Liang, X.; Yin, Z.; Zhang, Y. Advanced Carbon for Flexible and Wearable Electronics. *Adv. Mater.* **2019**, *31* (9), 1801072.

(231) Chang, X.; Chen, L.; Chen, J.; Zhu, Y.; Guo, Z. Advances in Transparent and Stretchable Strain Sensors. *Adv. Compos. Hybrid Mater.* **2021**, *4* (3), 435–450.

(232) Liu, K.; Tran, H.; Feig, V. R.; Bao, Z. Biodegradable and Stretchable Polymeric Materials for Transient Electronic Devices. *MRS Bull.* **2020**, *45* (2), 96–102.

(233) Gao, W.; Ota, H.; Kiriya, D.; Takei, K.; Javey, A. Flexible Electronics toward Wearable Sensing. *Acc. Chem. Res.* **2019**, *52* (3), 523–533.

(234) Lim, H.-R.; Kim, H. S.; Qazi, R.; Kwon, Y.-T.; Jeong, J.-W.; Yeo, W.-H.; Lim, H.-R.; Kwon, Y.-T.; Woodruff, G. W.; Kim, S.; Qazi, R.; Jeong, J.-W.; Yeo, -H W. Advanced Soft Materials, Sensor Integrations, and Applications of Wearable Flexible Hybrid Electronics in Healthcare, Energy, and Environment. *Adv. Mater.* **2020**, *32* (15), 1901924. https://doi.org/10.1002/ADMA.201901924.

(235) Lee, S. H.; Jeong, C. K.; Hwang, G.-T.; Lee, K. J. Self-Powered Flexible Inorganic Electronic System. *Nano Energy* **2015**, *14*, 111–125.

(236) Zahid, M.; Zych, A.; Dussoni, S.; Spallanzani, G.; Donno, R.; Maggiali, M.; Athanassiou, A. Wearable and Self-Healable Textile-Based Strain Sensors to Monitor Human Muscular Activities. *Compos. Part B Eng.* **2021**, 108969.

(237) Zahid, M.; Papadopoulou, E. L.; Athanassiou, A.; Bayer, I. S. Strain-Responsive Mercerized Conductive Cotton Fabrics Based on PEDOT: PSS/Graphene. *Mater. Des.* **2017**, *135*, 213–222.

(238) Li, R.; Wang, L.; Yin, L. Materials and Devices for Biodegradable and Soft Biomedical Electronics. *Materials (Basel).* **2018**, *11* (11), 2108.

(239) Peng, X.; Dong, K.; Wu, Z.; Wang, J.; Wang, Z. L. A Review on Emerging Biodegradable Polymers for Environmentally Benign Transient Electronic Skins. *J. Mater. Sci.* **2021**, 1–25.

(240) Gonçalves, F. A. M. M.; Santos, M.; Cernadas, T.; Ferreira, P.; Alves, P. Advances in the Development of Biobased Epoxy Resins: Insight into More Sustainable Materials and Future Applications. *Int. Mater. Rev.* **2022**, 1–31.

(241) Zhang, J.; Wan, L.; Gao, Y.; Fang, X.; Lu, T.; Pan, L.; Xuan, F. Highly Stretchable and Self-healable MXene/Polyvinyl Alcohol Hydrogel Electrode for Wearable Capacitive Electronic Skin. *Adv. Electron. Mater.* **2019**, *5* (7), 1900285.

(242) Li, Y.; Xiong, X.; Yu, X.; Sun, X.; Yang, J.; Zhu, L.; Qin, G.; Dai, Y.; Chen, Q. Tough and Conductive Nanocomposite Hydrogels for Human Motion Monitoring. *Polym. Test.* **2019**, *75*, 38–47.

(243) Elmowafy, E. M.; Tiboni, M.; Soliman, M. E. Biocompatibility, Biodegradation and Biomedical Applications of Poly (Lactic Acid)/Poly (Lactic-Co-Glycolic Acid) Micro and Nanoparticles. *J. Pharm. Investig.* **2019**, *49* (4), 347–380.

(244) Garakani, M. A.; Bellani, S.; Pellegrini, V.; Oropesa-Nuñez, R.; Castillo, A. E. D. R.; Abouali, S.; Najafi, L.; Martín-García, B.; Ansaldo, A.; Bondavalli, P.; Demirci, C.; Romano, V.; Mantero, E.; Marasco, L.; Prato, M.; Bracciale, G.; Bonaccorso, F. Scalable Spray-Coated Graphene-Based Electrodes for High-Power Electrochemical Double-Layer Capacitors Operating over a Wide Range of Temperature. *Energy Storage Mater.* **2021**, *34*, 1–11. https://doi.org/10.1016/J.ENSM.2020.08.036.

(245) Saidina, D. S.; Zubir, S. A.; Fontana, S.; Hérold, C.; Mariatti, M. Synthesis and Characterization of Graphene-Based Inks for Spray-Coating Applications. *J. Electron. Mater.* **2019**, *48* (9), 5757–5770. https://doi.org/10.1007/S11664-019-07376-3.

(246) López Barreiro, D.; Martín-Moldes, Z.; Yeo, J.; Shen, S.; Hawker, M. J.; Martin-Martinez, F. J.; Kaplan, D. L.; Buehler, M. J. Conductive Silk-Based Composites Using Biobased Carbon Materials. *Adv. Mater.* **2019**, *31* (44), 1904720. https://doi.org/10.1002/ADMA.201904720.

(247) Petti, L.; Münzenrieder, N.; Vogt, C.; Faber, H.; Büthe, L.; Cantarella, G.; Bottacchi, F.; Anthopoulos, T. D.; Tröster, G. Metal Oxide Semiconductor Thin-Film Transistors for Flexible Electronics. *Appl. Phys. Rev.* **2016**, *3* (2), 21303.

(248) Luo, X.; Yang, G.; Schubert, D. W. Electrically Conductive Polymer Composite Containing Hybrid Graphene Nanoplatelets and Carbon Nanotubes: Synergistic Effect and Tunable Conductivity Anisotropy. *Adv. Compos. Hybrid Mater.* **2021**, 1–13.

(249) Oh, J. Y.; Kim, S.; Baik, H.; Jeong, U. Conducting Polymer Dough for Deformable Electronics. *Adv. Mater.* **2016**, *28* (22), 4455–4461.

(250) Lee, S.; Koo, J.; Kang, S.-K.; Park, G.; Lee, Y. J.; Chen, Y.-Y.; Lim, S. A.; Lee, K.-M.; Rogers, J. A. Metal Microparticle–Polymer Composites as Printable, Bio/Ecoresorbable Conductive Inks. *Mater. Today* **2018**, *21* (3), 207–215.

(251) Jarrell, W. M.; Page, A. L.; Elseewi, A. A. Molybdenum in the Environment. *Residue Rev.* **1980**, *VOL.74*, 1–43. https://doi.org/10.1007/978-1-4612-6096-7_1/COVER.

(252) Akhtar, M. J.; Ahamed, M.; Alhadlaq, H. A.; Alshamsan, A.; Majeed Khan, M. A.; Alrokayan, S. A. Antioxidative and Cytoprotective Response Elicited by Molybdenum Nanoparticles in Human Cells. *J. Colloid Interface Sci.* **2015**, *457*, 370–377. https://doi.org/10.1016/J.JCIS.2015.07.034.

(253) Kaynak, A.; Foitzik, R. Methods of Coating Textiles with Soluble Conducting Polymers. *Res. J. Text. Appar.* **2011**, *15* (2), 107–113.

(254) Htwe, Y. Z. N.; Abdullah, M. K.; Mariatti, M. Optimization of Graphene Conductive Ink Using Solvent Exchange Techniques for Flexible Electronics Applications. *Synth. Met.* **2021**, *274*, 116719. https://doi.org/10.1016/j.synthmet.2021.116719.

(255) Li, J.; Sollami Delekta, S.; Zhang, P.; Yang, S.; Lohe, M. R.; Zhuang, X.; Feng, X.; Östling, M. Scalable Fabrication and Integration of Graphene Microsupercapacitors through Full Inkjet Printing. *ACS Nano* **2017**, *11* (8), 8249–8256. https://doi.org/10.1021/acsnano.7b03354.

(256) Desimone, J. M. Practical Approaches to Green Solvents.

(257) Lotya, M.; King, P. J.; Khan, U.; De, S.; Coleman, J. N. High-Concentration, Surfactant-Stabilized Graphene Dispersions. *ACS Nano* **2010**, *4* (6), 3155–3162. https://doi.org/10.1021/nn1005304.

(258) *Emulsion Templating Using High Internal Phase Supercritical Fluid Emulsions - Butler - 2001 - Advanced Materials - Wiley Online Library*. https://onlinelibrary.wiley.com/doi/epdf/10.1002/1521-4095%28200110%2913%3A19%3C1459%3A%3AAID-ADMA1459%3E3.0.CO%3B2-K (accessed 2023-02-08).

(259) Palazzo, I.; Lamparelli, E. P.; Ciardulli, M. C.; Scala, P.; Reverchon, E.; Forsyth, N.; Maffulli, N.; Santoro, A.; Della Porta, G. Supercritical Emulsion Extraction Fabricated PLA/PLGA Micro/Nano Carriers for Growth Factor Delivery: Release Profiles and Cytotoxicity. *Int. J. Pharm.* **2021**, *592*, 120108. https://doi.org/10.1016/J.IJPHARM.2020.120108.

(260) McClements, D. J. Crystals and Crystallization in Oil-in-Water Emulsions: Implications for

Emulsion-Based Delivery Systems. *Adv. Colloid Interface Sci.* **2012**, *174*, 1–30.

(261) Gao, J.; Li, B.; Huang, X.; Wang, L.; Lin, L.; Wang, H.; Xue, H. Electrically Conductive and Fluorine Free Superhydrophobic Strain Sensors Based on SiO2/Graphene-Decorated Electrospun Nanofibers for Human Motion Monitoring. *Chem. Eng. J.* **2019**, *373*, 298–306. https://doi.org/10.1016/J.CEJ.2019.05.045.

(262) Lin, L.; Wang, L.; Li, B.; Luo, J.; Huang, X.; Gao, Q.; Xue, H.; Gao, J. Dual Conductive Network Enabled Superhydrophobic and High Performance Strain Sensors with Outstanding Electro-Thermal Performance and Extremely High Gauge Factors. *Chem. Eng. J.* **2020**, *385*, 123391. https://doi.org/10.1016/J.CEJ.2019.123391.

(263) Zhang, L.; Luo, J.; Zhang, S.; Yan, J.; Huang, X.; Wang, L.; Gao, J. Interface Sintering Engineered Superhydrophobic and Durable Nanofiber Composite for High-Performance Electromagnetic Interference Shielding. *J. Mater. Sci. Technol.* **2022**, *98*, 62–71. https://doi.org/10.1016/J.JMST.2021.05.014.

(264) Li, B.; Luo, J.; Huang, X.; Lin, L.; Wang, L.; Hu, M.; Tang, L.; Xue, H.; Gao, J.; Mai, Y. W. A Highly Stretchable, Super-Hydrophobic Strain Sensor Based on Polydopamine and Graphene Reinforced Nanofiber Composite for Human Motion Monitoring. *Compos. Part B Eng.* **2020**, *181*, 107580. https://doi.org/10.1016/J.COMPOSITESB.2019.107580.

(265) Jung, Y. H.; Chang, T. H.; Zhang, H.; Yao, C.; Zheng, Q.; Yang, V. W.; Mi, H.; Kim, M.; Cho, S. J.; Park, D. W.; Jiang, H.; Lee, J.; Qiu, Y.; Zhou, W.; Cai, Z.; Gong, S.; Ma, Z. High-Performance Green Flexible Electronics Based on Biodegradable Cellulose Nanofibril Paper. *Nat. Commun.* **2015**, *6* (1), 1–11. https://doi.org/10.1038/ncomms8170.

(266) Cataldi, P.; Bonaccorso, F.; Esau del Rio Castillo, A.; Pellegrini, V.; Jiang, Z.; Liu, L.; Boccardo, N.; Canepa, M.; Cingolani, R.; Athanassiou, A. Cellulosic Graphene Biocomposites for Versatile High-Performance Flexible Electronic Applications. *Adv. Electron. Mater.* **2016**, *2* (11), 1600245.

(267) Nambiar, S.; Yeow, J. T. W. Conductive Polymer-Based Sensors for Biomedical Applications. *Biosens. Bioelectron.* **2011**, *26* (5), 1825–1832.

(268) Komaiko, J.; McClements, D. J. Food-Grade Nanoemulsion Filled Hydrogels Formed by Spontaneous Emulsification and Gelation: Optical Properties, Rheology, and Stability. *Food Hydrocoll.* **2015**, *46*, 67–75. https://doi.org/10.1016/J.FOODHYD.2014.12.031.

(269) McClements, D. J.; Li, Y. Structured Emulsion-Based Delivery Systems: Controlling the Digestion and Release of Lipophilic Food Components. *Adv. Colloid Interface Sci.* **2010**, *159* (2), 213–228.

(270) Chen, G.; Tao, D. An Experimental Study of Stability of Oil–Water Emulsion. *Fuel Process. Technol.* **2005**, *86* (5), 499–508.

(271) Costa, C.; Medronho, B.; Filipe, A.; Mira, I.; Lindman, B.; Edlund, H.; Norgren, M. Emulsion Formation and Stabilization by Biomolecules: The Leading Role of Cellulose. *Polymers*

(Basel). **2019**, *11* (10), 1570.

(272) Knowlton, J. L. Emulsion Theory. In *Poucher's Perfumes, Cosmetics and Soaps*; Springer, 2000; pp 601–623.

(273) Gadhave, A. Determination of Hydrophilic-Lipophilic Balance Value. *Int. J. Sci. Res* **2014**, *3* (4), 573–575.

(274) Pasquali, R. C.; Taurozzi, M. P.; Bregni, C. Some Considerations about the Hydrophilic–Lipophilic Balance System. *Int. J. Pharm.* **2008**, *356* (1–2), 44–51.

(275) Schultz, S.; Wagner, G.; Urban, K.; Ulrich, J. High-pressure Homogenization as a Process for Emulsion Formation. *Chem. Eng. Technol. Ind. Chem. Equipment-Process Eng.* **2004**, *27* (4), 361–368.

(276) da Silva, M.; Sad, C. M. S.; Pereira, L. B.; Corona, R. R. B.; Bassane, J. F. P.; dos Santos, F. D.; Neto, D. M. C.; Silva, S. R. C.; Castro, E. V. R.; Filgueiras, P. R. Study of the Stability and Homogeneity of Water in Oil Emulsions of Heavy Oil. *Fuel* **2018**, *226*, 278–285.

(277) Dickinson, E.; Ritzoulis, C. Creaming and Rheology of Oil-in-Water Emulsions Containing Sodium Dodecyl Sulfate and Sodium Caseinate. *J. Colloid Interface Sci.* **2000**, *224* (1), 148–154. https://doi.org/10.1006/JCIS.1999.6682.

(278) Fatima, M.; Sheraz, M. A.; Ahmed, S.; Kazi, S. H.; Ahmad, I. Emulsion Separation, Classification and Stability Assessment. *RADS J. Pharm. Pharm. Sci.* **2014**, *2* (2), 56–62.

(279) Melle, S.; Lask, M.; Fuller, G. G. Pickering Emulsions with Controllable Stability. *Langmuir* **2005**, *21* (6), 2158–2162.

(280) He, Y.; Wu, F.; Sun, X.; Li, R.; Guo, Y.; Li, C.; Zhang, L.; Xing, F.; Wang, W.; Gao, J. Factors That Affect Pickering Emulsions Stabilized by Graphene Oxide. *ACS Appl. Mater. Interfaces* **2013**, *5* (11), 4843–4855.

(281) Sun, Z.; Yan, X.; Xiao, Y.; Hu, L.; Eggersdorfer, M.; Chen, D.; Yang, Z.; Weitz, D. A. Pickering Emulsions Stabilized by Colloidal Surfactants: Role of Solid Particles. *Particuology* **2022**, *64*, 153–163. https://doi.org/10.1016/J.PARTIC.2021.06.004.

(282) Tsabet, È.; Fradette, L. Effect of the Properties of Oil, Particles, and Water on the Production of Pickering Emulsions. *Chem. Eng. Res. Des.* **2015**, *97*, 9–17. https://doi.org/10.1016/J.CHERD.2015.02.016.

(283) Binks, B. P.; Lumsdon, S. O. Pickering Emulsions Stabilized by Monodisperse Latex Particles: Effects of Particle Size. *Langmuir* **2001**, *17* (15), 4540–4547. https://doi.org/10.1021/LA0103822/ASSET/IMAGES/LARGE/LA0103822F00013.JPEG.

(284) Wang, Z.; Yao, Z.; Zhou, J.; He, M.; Jiang, Q.; Li, A.; Li, S.; Liu, M.; Luo, S.; Zhang, D. Improvement of Polylactic Acid Film Properties through the Addition of Cellulose Nanocrystals Isolated from Waste Cotton Cloth. *Int. J. Biol. Macromol.* **2019**, *129*, 878–886. https://doi.org/10.1016/J.IJBIOMAC.2019.02.021.

(285) Zhou, L.; Ke, K.; Yang, M. B.; Yang, W. Recent Progress on Chemical Modification of Cellulose for High Mechanical-Performance Poly(Lactic Acid)/Cellulose Composite: A Review. *Compos. Commun.* **2021**, *23*, 100548. https://doi.org/10.1016/J.COCO.2020.100548.

(286) Qu, P.; Gao, Y.; Wu, G.-F.; Zhang, L.-P. PLA/Cellulose Nanocomposites. *BioResources* **2010**, *5* (3), 1811–1823.

(287) Kohler, G.; Getoff, N. Spectroscopic Properties of Anisole in Mixed Polar Solvents. *J. Mol. Struct.* **1984**, *115* (C), 331–334. https://doi.org/10.1016/0022-2860(84)80081-2.

(288) Low, L. E.; Siva, S. P.; Ho, Y. K.; Chan, E. S.; Tey, B. T. Recent Advances of Characterization Techniques for the Formation, Physical Properties and Stability of Pickering Emulsion. *Adv. Colloid Interface Sci.* **2020**, *277*, 102117. https://doi.org/10.1016/J.CIS.2020.102117.

(289) Zhang, X.; Chen, L.; Mulholland, T.; Osswald, T. A. Effects of Raster Angle on the Mechanical Properties of PLA and Al/PLA Composite Part Produced by Fused Deposition Modeling. *Polym. Adv. Technol.* **2019**, *30* (8), 2122–2135.

(290) Mazzon, G.; Contardi, M.; Quilez-Molina, A.; Zahid, M.; Zendri, E.; Athanassiou, A.; Bayer, I. S. Antioxidant and Hydrophobic Cotton Fabric Resisting Accelerated Ageing. *Colloids Surfaces A Physicochem. Eng. Asp.* **2021**, *613*, 126061.

(291) Mohan, V. B.; Bhattacharyya, D. Mechanical Characterization of Functional Graphene Nanoplatelets Coated Natural and Synthetic Fiber Yarns Using Polymeric Binders. *Int. J. Smart Nano Mater.* **2020**, *11* (1), 78–91.

(292) Chieng, B. W.; Azowa, I. N.; Wan Md Zin, W. Y.; Hussein, M. Z. Effects of Graphene Nanopletelets on Poly (Lactic Acid)/Poly (Ethylene Glycol) Polymer Nanocomposites. In *Advanced Materials Research*; Trans Tech Publ, 2014; Vol. 1024, pp 136–139.

(293) Dastjerdi, R.; Montazer, M.; Shahsavan, S. A New Method to Stabilize Nanoparticles on Textile Surfaces. *Colloids Surfaces A Physicochem. Eng. Asp.* **2009**, *345* (1–3), 202–210.

(294) Yoo, B. M.; Shin, H. J.; Yoon, H. W.; Park, H. B. Graphene and Graphene Oxide and Their Uses in Barrier Polymers. *J. Appl. Polym. Sci.* **2014**, *131* (1).

(295) Cui, Y.; Kundalwal, S. I.; Kumar, S. Gas Barrier Performance of Graphene/Polymer Nanocomposites. *Carbon N. Y.* **2016**, *98*, 313–333.

(296) Lei, L.; Xia, Z.; Ou, C.; Zhang, L.; Zhong, L. Effects of Crosslinking on Adhesion Behavior of Waterborne Polyurethane Ink Binder. *Prog. Org. Coatings* **2015**, *88*, 155–163.

(297) Yin, L.; Huang, X.; Xu, H.; Zhang, Y.; Lam, J.; Cheng, J.; Rogers, J. A. Materials, Designs, and Operational Characteristics for Fully Biodegradable Primary Batteries. *Adv. Mater.* **2014**, *26* (23), 3879–3884.

(298) Krupka, J. Contactless Methods of Conductivity and Sheet Resistance Measurement for Semiconductors, Conductors and Superconductors. *Meas. Sci. Technol.* **2013**, *24* (6), 62001.

(299) Huang, X.; Liu, Y.; Hwang, S. W.; Kang, S. K.; Patnaik, D.; Cortes, J. F.; Rogers, J. A.

Biodegradable Materials for Multilayer Transient Printed Circuit Boards. *Adv. Mater.* **2014**, *26* (43), 7371–7377. https://doi.org/10.1002/ADMA.201403164.

(300) Kang, S.-K.; Park, G.; Kim, K.; Hwang, S.-W.; Cheng, H.; Shin, J.; Chung, S.; Kim, M.; Yin, L.; Lee, J. C. Dissolution Chemistry and Biocompatibility of Silicon-and Germanium-Based Semiconductors for Transient Electronics. *ACS Appl. Mater. Interfaces* **2015**, *7* (17), 9297–9305.

(301) Kong, L.-W.; Bai, W.; Guo, A.-G. Effects of Cracks on the Electrical Conductivity of a Fissured Laterite: A Combined Experimental and Statistical Study. *Geotech. Test. J.* **2012**, *35* (6), 870–878.

(302) Hu, M.; Gao, Y.; Jiang, Y.; Zeng, H.; Zeng, S.; Zhu, M.; Xu, G.; Sun, L. High-Performance Strain Sensors Based on Bilayer Carbon Black/PDMS Hybrids. *Adv. Compos. Hybrid Mater.* **2021**, 1–7.

(303) Zhu, S.; Wang, M.; Qiang, Z.; Song, J.; Wang, Y.; Fan, Y.; You, Z.; Liao, Y.; Zhu, M.; Ye, C. Multi-Functional and Highly Conductive Textiles with Ultra-High Durability through 'Green'Fabrication Process. *Chem. Eng. J.* **2021**, *406*, 127140.

(304) Tan, Y.-J.; Li, J. J.; Gao, Y.; Li, J. J.; Guo, S.; Wang, M. A Facile Approach to Fabricating Silver-Coated Cotton Fiber Non-Woven Fabrics for Ultrahigh Electromagnetic Interference Shielding. *Appl. Surf. Sci.* **2018**, *458*, 236–244.

(305) Torres, R.; Cheng, Z.; Ramalingame, R.; Kanoun, O. Electrical Characterization of Elongation Sensors Based on Sbs-Ctpu Filaments. In *2018 15th International Multi-Conference on Systems, Signals & Devices (SSD)*; IEEE, 2018; pp 1212–1215.

(306) Lozano-Pérez, C.; Cauich-Rodríguez, J. V; Avilés, F. Influence of Rigid Segment and Carbon Nanotube Concentration on the Cyclic Piezoresistive and Hysteretic Behavior of Multiwall Carbon Nanotube/Segmented Polyurethane Composites. *Compos. Sci. Technol.* **2016**, *128*, 25–32.

(307) Hu, C.; Li, Z.; Wang, Y.; Gao, J.; Dai, K.; Zheng, G.; Liu, C.; Shen, C.; Song, H.; Guo, Z. Comparative Assessment of the Strain-Sensing Behaviors of Polylactic Acid Nanocomposites: Reduced Graphene Oxide or Carbon Nanotubes. *J. Mater. Chem. C* **2017**, *5* (9), 2318–2328.

(308) Jiang, T.; Huang, R.; Zhu, Y. Interfacial Sliding and Buckling of Monolayer Graphene on a Stretchable Substrate. *Adv. Funct. Mater.* **2014**, *24* (3), 396–402.

(309) Wu, J.; Ma, Z.; Hao, Z.; Zhang, J. T.; Sun, P.; Zhang, M.; Liu, Y.; Cheng, Y.; Li, Y.; Zhong, B. Sheath–Core Fiber Strain Sensors Driven by in-Situ Crack and Elastic Effects in Graphite Nanoplate Composites. *ACS Appl. Nano Mater.* **2019**, *2* (2), 750–759.

(310) Li, X.; Zhang, R.; Yu, W.; Wang, K.; Wei, J.; Wu, D.; Cao, A.; Li, Z.; Cheng, Y.; Zheng, Q. Stretchable and Highly Sensitive Graphene-on-Polymer Strain Sensors. *Sci. Rep.* **2012**, *2* (1), 1–6.

(311) Delolo, F. G.; Dos Santos, E. N.; Gusevskaya, E. V. Anisole: A Further Step to Sustainable Hydroformylation. *Green Chem.* **2019**, *21* (5), 1091–1098. https://doi.org/10.1039/C8GC03750G.

(312) Li, Q.; Zhang, J.; Li, Q.; Li, G.; Tian, X.; Luo, Z.; Qiao, F.; Wu, X.; Zhang, J. Review of Printed Electrodes for Flexible Devices. *Front. Mater.* **2019**, *5*, 77. https://doi.org/10.3389/FMATS.2018.00077/BIBTEX.

(313) *The Internet of Trash: IoT Has a Looming E-Waste Problem - IEEE Spectrum*. https://spectrum.ieee.org/the-internet-of-trash-iot-has-a-looming-ewaste-problem (accessed 2022-09-24).

(314) *The Chemistry Of Inkjet Inks - Google Books*. https://books.google.de/books?hl=en&lr=&id=awnGCgAAQBAJ&oi=fnd&pg=PA225&dq=wide+range+use+of+inks+products+in++&ots=KPN2twKEU2&sig=_zQRHg2O5mM6VCFoXddjKLlj9LI&redir_esc=y#v=onepage&q=wide range use of inks products in&f=false (accessed 2022-12-05).

(315) Voon, S. L.; An, J.; Wong, G.; Zhang, Y.; Chua, C. K. 3D Food Printing: A Categorised Review of Inks and Their Development. *https://doi.org/10.1080/17452759.2019.1603508* **2019**, *14* (3), 203–218. https://doi.org/10.1080/17452759.2019.1603508.

(316) Yi, P. ; Mo, J. ; Liu, R. ; Fan, B. ; Xiao, K. ; Gao, J. ; Zhou, H.; Yi, P.; Mo, J.; Liu, R.; Fan, B.; Xiao, K.; Gao, J.; Zhou, H. Study on Corrosion Behavior of Waterborne Polyurethane Coating with High Thermal Conductivity. *Appl. Sci. 2022, Vol. 12, Page 2021* **2022**, *12* (4), 2021. https://doi.org/10.3390/APP12042021.

(317) Barhoum, A.; Samyn, P.; Öhlund, T.; Dufresne, A. Review of Recent Research on Flexible Multifunctional Nanopapers. *Nanoscale* **2017**, *9* (40), 15181–15205. https://doi.org/10.1039/C7NR04656A.

(318) Lipomi, D. J.; Vosgueritchian, M.; Tee, B. C. K.; Hellstrom, S. L.; Lee, J. A.; Fox, C. H.; Bao, Z. Skin-like Pressure and Strain Sensors Based on Transparent Elastic Films of Carbon Nanotubes. *Nat. Nanotechnol. 2011 612* **2011**, *6* (12), 788–792. https://doi.org/10.1038/nnano.2011.184.

(319) Kim, Y.; Zhu, J.; Yeom, B.; Di Prima, M.; Su, X.; Kim, J. G.; Yoo, S. J.; Uher, C.; Kotov, N. A. Stretchable Nanoparticle Conductors with Self-Organized Conductive Pathways. *Nat. 2013 5007460* **2013**, *500* (7460), 59–63. https://doi.org/10.1038/nature12401.

(320) Segev-Bar, M.; Haick, H. Flexible Sensors Based on Nanoparticles. *ACS Nano* **2013**, *7* (10), 8366–8378. https://doi.org/10.1021/NN402728G/ASSET/IMAGES/LARGE/NN-2013-02728G_0005.JPEG.

(321) Coleman, J. N.; Khan, U.; Gun'ko, Y. K. Mechanical Reinforcement of Polymers Using Carbon Nanotubes. *Adv. Mater.* **2006**, *18* (6), 689–706. https://doi.org/10.1002/ADMA.200501851.

(322) Zhao, S.; Li, J.; Cao, D.; Gao, Y.; Huang, W.; Zhang, G.; Sun, R.; Wong, C. P. Percolation

Threshold-Inspired Design of Hierarchical Multiscale Hybrid Architectures Based on Carbon Nanotubes and Silver Nanoparticles for Stretchable and Printable Electronics. *J. Mater. Chem. C* **2016**, *4* (27), 6666–6674. https://doi.org/10.1039/C6TC01728B.

(323) Lynch, P. J.; Ogilvie, S. P.; Large, M. J.; Graf, A. A.; O'Mara, M. A.; Taylor, J.; Salvage, J. P.; Dalton, A. B. Graphene-Based Printable Conductors for Cyclable Strain Sensors on Elastomeric Substrates. *Carbon N. Y.* **2020**, *169*, 25–31.

(324) Cai, L.; Wang, C. Carbon Nanotube Flexible and Stretchable Electronics. *Nanoscale Res. Lett.* **2015**, *10* (1), 1–21. https://doi.org/10.1186/S11671-015-1013-1/FIGURES/2.

(325) Kharissova, O. V.; Kharisov, B. I.; De Casas Ortiz, E. G. Dispersion of Carbon Nanotubes in Water and Non-Aqueous Solvents. *RSC Adv.* **2013**, *3* (47), 24812–24852. https://doi.org/10.1039/C3RA43852J.

(326) Bagotia, N.; Choudhary, V.; Sharma, D. K. Synergistic Effect of Graphene/Multiwalled Carbon Nanotube Hybrid Fillers on Mechanical, Electrical and EMI Shielding Properties of Polycarbonate/Ethylene Methyl Acrylate Nanocomposites. *Compos. Part B Eng.* **2019**, *159*, 378–388. https://doi.org/10.1016/J.COMPOSITESB.2018.10.009.

(327) Peng, X.; Tan, F.; Wang, W.; Qiu, X.; Sun, F.; Qiao, X.; Chen, J. Conductivity Improvement of Silver Flakes Filled Electrical Conductive Adhesives via Introducing Silver-Graphene Nanocomposites. *J. Mater. Sci. Mater. Electron.* **2014**, *25* (3), 1149–1155. https://doi.org/10.1007/S10854-013-1671-7/FIGURES/7.

(328) Hsu, C. Te; Wu, C.; Chuang, C. N.; Chen, S. H.; Chiu, W. Y.; Hsieh, K. H. Synthesis and Characterization of Nano Silver-Modified Graphene/PEDOT:PSS for Highly Conductive and Transparent Nanocomposite Films. *J. Polym. Res.* **2015**, *22* (10), 1–8. https://doi.org/10.1007/S10965-015-0847-7/FIGURES/7.

(329) Zhang, S.; Zhang, H.; Yao, G.; Liao, F.; Gao, M.; Huang, Z.; Li, K.; Lin, Y. Highly Stretchable, Sensitive, and Flexible Strain Sensors Based on Silver Nanoparticles/Carbon Nanotubes Composites. *J. Alloys Compd.* **2015**, *652*, 48–54. https://doi.org/10.1016/J.JALLCOM.2015.08.187.

(330) Yu, T.; Tao, Y.; Wang, B.; Wang, L.; Tai, Y. A Facile Approach to a Silver Conductive Ink with High Performance for Macroelectronics. *Nanoscale Res. Lett.* **2013**, *8* (1), 1–6. https://doi.org/10.1186/1556-276X-8-296/FIGURES/5.

(331) Black, K.; Singh, J.; Mehta, D.; Sung, S.; Sutcliffe, C. J.; Chalker, P. R. Silver Ink Formulations for Sinter-Free Printing of Conductive Films. *Sci. Reports 2016 61* **2016**, *6* (1), 1–7. https://doi.org/10.1038/srep20814.

(332) Mo, L.; Guo, Z.; Wang, Z.; Yang, L.; Fang, Y.; Xin, Z.; Li, X.; Chen, Y.; Cao, M.; Zhang, Q.; Li, L. Nano-Silver Ink of High Conductivity and Low Sintering Temperature for Paper Electronics. *Nanoscale Res. Lett.* **2019**, *14* (1), 1–11. https://doi.org/10.1186/S11671-019-3011-1/FIGURES/11.

(333) Li, W. W.; Xu, X.; Li, W. W.; Liu, P.; Zhao, Y.; Cen, Q.; Chen, M. One-Step Synthesis of Ag Nanoparticles for Fabricating Highly Conductive Patterns Using Infrared Sintering. *J. Mater. Res. Technol.* **2020**, *9* (1), 142–151. https://doi.org/10.1016/J.JMRT.2019.10.039.

(334) Htwe, Y. Z. N.; Abdullah, M. K.; Mariatti, M. Water-Based Graphene/AgNPs Hybrid Conductive Inks for Flexible Electronic Applications. *J. Mater. Res. Technol.* **2022**, *16*, 59–73. https://doi.org/10.1016/J.JMRT.2021.11.159.

(335) Ghadimi, S.; Mazinani, S.; Bazargan, A. M.; Sharif, F. Effect of Formulation and Process on Morphology and Electrical Conductivity of Ag-Graphene Hybrid Inks. *Synth. Met.* **2021**, *281*, 116913. https://doi.org/10.1016/J.SYNTHMET.2021.116913.

(336) Marcq, F.; Demont, P.; Monfraix, P.; Peigney, A.; Laurent, C.; Falat, T.; Courtade, F.; Jamin, T. *Carbon Nanotubes and Silver Flakes Filled Epoxy Resin for New Hybrid Conductive Adhesives*; Pergamon, 2011; Vol. 51, pp 1230–1234.

(337) Pop, E.; Mann, D.; Wang, Q.; Goodson, K.; Dai, H. Thermal Conductance of an Individual Single-Wall Carbon Nanotube above Room Temperature. *Nano Lett.* **2006**, *6* (1), 96–100. https://doi.org/10.1021/NL052145F/ASSET/IMAGES/LARGE/NL052145FF00006.JPEG.

(338) Yang, D. J.; Wang, S. G.; Zhang, Q.; Sellin, P. J.; Chen, G. Thermal and Electrical Transport in Multi-Walled Carbon Nanotubes. *Phys. Lett. A* **2004**, *329* (3), 207–213. https://doi.org/10.1016/J.PHYSLETA.2004.05.070.

(339) Park, S.; Vosguerichian, M.; Bao, Z. A Review of Fabrication and Applications of Carbon Nanotube Film-Based Flexible Electronics. *Nanoscale* **2013**, *5* (5), 1727–1752. https://doi.org/10.1039/C3NR33560G.

(340) Wang, C.; Takei, K.; Takahashi, T.; Javey, A. Carbon Nanotube Electronics – Moving Forward. *Chem. Soc. Rev.* **2013**, *42* (7), 2592–2609. https://doi.org/10.1039/C2CS35325C.

(341) Lee, C. L.; Chen, C. H.; Chen, C. W. Graphene Nanosheets as Ink Particles for Inkjet Printing on Flexible Board. *Chem. Eng. J.* **2013**, *230*, 296–302. https://doi.org/10.1016/J.CEJ.2013.06.093.

(342) Gao, M.; Li, L.; Song, Y. Inkjet Printing Wearable Electronic Devices. *J. Mater. Chem. C* **2017**, *5* (12), 2971–2993. https://doi.org/10.1039/C7TC00038C.

(343) Kang, J. W.; Kang, Y. J.; Jung, S.; Song, M.; Kim, D. G.; Su Kim, C.; Kim, S. H. Fully Spray-Coated Inverted Organic Solar Cells. *Sol. Energy Mater. Sol. Cells* **2012**, *103*, 76–79. https://doi.org/10.1016/J.SOLMAT.2012.04.027.

(344) Krebs, F. C. Fabrication and Processing of Polymer Solar Cells: A Review of Printing and Coating Techniques. *Sol. Energy Mater. Sol. Cells* **2009**, *93* (4), 394–412. https://doi.org/10.1016/J.SOLMAT.2008.10.004.

(345) Lei, L.; Zhong, L.; Lin, X.; Li, Y.; Xia, Z. Synthesis and Characterization of Waterborne Polyurethane Dispersions with Different Chain Extenders for Potential Application in

Waterborne Ink. *Chem. Eng. J.* **2014**, *253*, 518–525. https://doi.org/10.1016/J.CEJ.2014.05.044.

(346) Hu, Y. Q.; Yin, S. W.; Zhu, J. H.; Qi, J. R.; Guo, J.; Wu, L. Y.; Tang, C. H.; Yang, X. Q. Fabrication and Characterization of Novel Pickering Emulsions and Pickering High Internal Emulsions Stabilized by Gliadin Colloidal Particles. *Food Hydrocoll.* **2016**, *61*, 300–310. https://doi.org/10.1016/J.FOODHYD.2016.05.028.

(347) Zhai, W.; Li, G.; Yu, P.; Yang, L.; Mao, L. Silver Phosphate/Carbon Nanotube-Stabilized Pickering Emulsion for Highly Efficient Photocatalysis. *J. Phys. Chem. C* **2013**, *117* (29), 15183–15191.

(348) Briggs, N. M.; Weston, J. S.; Li, B.; Venkataramani, D.; Aichele, C. P.; Harwell, J. H.; Crossley, S. P. Multiwalled Carbon Nanotubes at the Interface of Pickering Emulsions. *Langmuir* **2015**, *31* (48), 13077–13084. https://doi.org/10.1021/ACS.LANGMUIR.5B03189/ASSET/IMAGES/LARGE/LA-2015-03189S_0009.JPEG.

(349) Zhu, J. Y.; Tang, C. H.; Yin, S. W.; Yang, X. Q. Development and Characterization of Novel Antimicrobial Bilayer Films Based on Polylactic Acid (PLA)/Pickering Emulsions. *Carbohydr. Polym.* **2018**, *181*, 727–735. https://doi.org/10.1016/J.CARBPOL.2017.11.085.

(350) Chang, C. W.; Cheng, T. Y.; Liao, Y. C. Encapsulated Silver Nanoparticles in Water/Oil Emulsion for Conductive Inks. *J. Taiwan Inst. Chem. Eng.* **2018**, *92*, 8–14.

(351) Zhang, W. Nanoparticle Aggregation: Principles and Modeling. *Adv. Exp. Med. Biol.* **2014**, *811*, 20–43. https://doi.org/10.1007/978-94-017-8739-0_2/COVER.

(352) Pinchuk, A. O. Size-Dependent Hamaker Constant for Silver Nanoparticles. *J. Phys. Chem. C* **2012**, *116* (37), 20099–20120. https://doi.org/10.1021/JP3061784/ASSET/IMAGES/JP-2012-061784_M013.GIF.

(353) El Badawy, A. M.; Scheckel, K. G.; Suidan, M.; Tolaymat, T. The Impact of Stabilization Mechanism on the Aggregation Kinetics of Silver Nanoparticles. *Sci. Total Environ.* **2012**, *429*, 325–331. https://doi.org/10.1016/J.SCITOTENV.2012.03.041.

(354) Yuan, J. K.; Yao, S. H.; Sylvestre, A.; Bai, J. Biphasic Polymer Blends Containing Carbon Nanotubes: Heterogeneous Nanotube Distribution and Its Influence on the Dielectric Properties. *J. Phys. Chem. C* **2012**, *116* (2), 2051–2058. https://doi.org/10.1021/JP210872W/SUPPL_FILE/JP210872W_SI_001.PDF.

(355) Al-Saleh, M. H.; Gelves, G. A.; Sundararaj, U. Copper Nanowire/Polystyrene Nanocomposites: Lower Percolation Threshold and Higher EMI Shielding. *Compos. Part A Appl. Sci. Manuf.* **2011**, *42* (1), 92–97. https://doi.org/10.1016/J.COMPOSITESA.2010.10.003.

(356) Dermanaki Farahani, R.; Gagne, M.; Klemberg-Sapieha, J. E.; Therriault, D. Electrically Conductive Silver Nanoparticles-Filled Nanocomposite Materials as Surface Coatings of Composite Structures. *Adv. Eng. Mater.* **2016**, *18* (7), 1189–1199.

https://doi.org/10.1002/ADEM.201500544.

(357) Farahani, R. D.; Klemberg-Sapieha, J. E.; Therriault, D. Enhanced Conductivity of Nanocomposite Films through Heterogeneous Distribution of Nanofillers during Processing. *Mater. Des.* **2015**, *88*, 1175–1182. https://doi.org/10.1016/J.MATDES.2015.09.088.

(358) Rezaee, M.; Tsai, L. C.; Haider, M. I.; Yazdi, A.; Sanatizadeh, E.; Salowitz, N. P. Quantitative Peel Test for Thin Films/Layers Based on a Coupled Parametric and Statistical Study. *Sci. Reports 2019 91* **2019**, *9* (1), 1–11. https://doi.org/10.1038/s41598-019-55355-9.

(359) Vasilev, S.; Vodyashkin, A.; Vasileva, D.; Zelenovskiy, P.; Chezganov, D.; Yuzhakov, V.; Shur, V.; O'reilly, E.; Vinogradov, A. An Investigative Study on the Effect of Pre-Coating Polymer Solutions on the Fabrication of Low Cost Anti-Adhesive Release Paper. *Nanomaterials* **2020**, *10* (8), 1–12. https://doi.org/10.3390/NANO10081436.

(360) Ihalainen, P.; Määttänen, A.; Järnström, J.; Tobjörk, D.; Österbacka, R.; Peltonen, J. Influence of Surface Properties of Coated Papers on Printed Electronics. *Ind. Eng. Chem. Res.* **2012**, *51* (17), 6025–6036. https://doi.org/10.1021/IE202807V/SUPPL_FILE/IE202807V_SI_001.PDF.

(361) Guigo, N.; Forestier, E.; Sbirrazzuoli, N. Thermal Properties of Biobased Polymers: Furandicarboxylic Acid (FDCA)-Based Polyesters. *Adv. Polym. Sci.* **2019**, *283*, 189–217. https://doi.org/10.1007/12_2019_51.

(362) Murariu, M.; Da Silva Ferreira, A.; Alexandre, M.; Dubois, P. Polylactide (PLA) Designed with Desired End-Use Properties: 1. PLA Compositions with Low Molecular Weight Ester-like Plasticizers and Related Performances. *Polym. Adv. Technol.* **2008**, *19* (6), 636–646. https://doi.org/10.1002/PAT.1131.

(363) Carrasco, F.; Pagès, P.; Gámez-Pérez, J.; Santana, O. O.; Maspoch, M. L. Processing of Poly(Lactic Acid): Characterization of Chemical Structure, Thermal Stability and Mechanical Properties. *Polym. Degrad. Stab.* **2010**, *95* (2), 116–125. https://doi.org/10.1016/j.polymdegradstab.2009.11.045.

(364) Pyda, M.; Wunderlich, B. Reversing and Nonreversing Heat Capacity of Poly(Lactic Acid) in the Glass Transition Region by TMDSC. *Macromolecules* **2005**, *38* (25), 10472–10479. https://doi.org/10.1021/MA051611K/SUPPL_FILE/MA051611KSI20051014_091354.PDF.

(365) Huang, J.; Miller, P. F.; De Mello, J. C.; De Mello, A. J.; Bradley, D. D. C. Influence of Thermal Treatment on the Conductivity and Morphology of PEDOT/PSS Films. *Synth. Met.* **2003**, *139* (3), 569–572. https://doi.org/10.1016/S0379-6779(03)00280-7.

(366) Shi, H.; Liu, C.; Jiang, Q.; Xu, J. Effective Approaches to Improve the Electrical Conductivity of PEDOT:PSS: A Review. *Adv. Electron. Mater.* **2015**, *1* (4), 1500017. https://doi.org/10.1002/AELM.201500017.

(367) Wang, J.; Sun, J.; Gao, L.; Liu, Y.; Wang, Y.; Zhang, J.; Kajiura, H.; Li, Y. M.; Noda, K. Improving the Conductivity of Single-Walled Carbon Nanotubes Films by Heat Treatment. *J. Alloys Compd.* **2009**, *485* (1–2), 456–461. https://doi.org/10.1016/J.JALLCOM.2009.05.139.

(368) Hong, W. T.; Tai, N. H. Investigations on the Thermal Conductivity of Composites Reinforced with Carbon Nanotubes. *Diam. Relat. Mater.* **2008**, *17* (7–10), 1577–1581. https://doi.org/10.1016/J.DIAMOND.2008.03.037.

(369) Wang, G. F.; Tao, X. M.; Xin, J. H.; Fei, B. Modification of Conductive Polymer for Polymeric Anodes of Flexible Organic Light-Emitting Diodes. *Nanoscale Res. Lett.* **2009**, *4* (7), 613–617. https://doi.org/10.1007/S11671-009-9288-8/FIGURES/5.

(370) Wang, C. S.; Lee, C. Y.-C.; Arnold, F. E. Mechanical and Electrical Properties of Heat-Treated Ladder Polymer Fiber. *MRS Online Proc. Libr.* **1992**, *247*, 747. https://doi.org/10.1557/PROC-247-747.

(371) Gong, Q. M.; Li, Z.; Wang, Y.; Wu, B.; Zhang, Z.; Liang, J. The Effect of High-Temperature Annealing on the Structure and Electrical Properties of Well-Aligned Carbon Nanotubes. *Mater. Res. Bull.* **2007**, *42* (3), 474–481. https://doi.org/10.1016/J.MATERRESBULL.2006.06.023.

(372) Hou, Y. H.; Zhang, M. Q.; Rong, M. Z.; Yu, G.; Zeng, H. M. Improvement of Conductive Network Quality in Carbon Black-Filled Polymer Blends. *J. Appl. Polym. Sci.* **2002**, *84* (14), 2768–2775. https://doi.org/10.1002/APP.10574.

(373) Han, Z.; Fina, A. Thermal Conductivity of Carbon Nanotubes and Their Polymer Nanocomposites: A Review. *Prog. Polym. Sci.* **2011**, *36* (7), 914–944. https://doi.org/10.1016/J.PROGPOLYMSCI.2010.11.004.

(374) Radjabian, M.; Kish, M. H.; Mohammadi, N. Structure-Property Relationship for Poly(Lactic Acid) (PLA) Filaments: Physical, Thermomechanical and Shape Memory Characterization. *J. Polym. Res.* **2012**, *19* (6), 1–10. https://doi.org/10.1007/S10965-012-9870-0/FIGURES/11.

(375) Forestier, E.; Najafi, M.; Dussoni, S.; Maggiali, M.; Athanassiou, A.; Bayer, I. S. Characterization and Performance of Silicone Modified Polylactic Acid (PLA)-Graphene Nanoplatelet Ink Coatings for Flexible Elastomeric Substrates. *Prog. Org. Coatings* **2023**, *174*, 107251. https://doi.org/10.1016/J.PORGCOAT.2022.107251.

(376) Farah, S.; Anderson, D. G.; Langer, R. Physical and Mechanical Properties of PLA, and Their Functions in Widespread Applications — A Comprehensive Review. *Adv. Drug Deliv. Rev.* **2016**, *107*, 367–392. https://doi.org/10.1016/j.addr.2016.06.012.

(377) Abd El-Rehim, H. A.; Hegazy, E. S. A.; Ali, A. M.; Rabie, A. M. Synergistic Effect of Combining UV-Sunlight-Soil Burial Treatment on the Biodegradation Rate of LDPE/Starch Blends. *J. Photochem. Photobiol. A Chem.* **2004**, *163* (3), 547–556. https://doi.org/10.1016/j.jphotochem.2004.02.003.

(378) Jun, C. L. Reactive Blending of Biodegradable Polymers: PLA and Starch. *J. Polym. Environ.* **2000**, *8* (1), 33–37. https://doi.org/10.1023/A:1010172112118.

(379) Mort, R.; Olson, E.; Thurber, H.; Jiang, S.; Vorst, K.; Curtzwiler, G. Waterborne Polyurethane/Acrylic Adhesive Blends from Physaria Fendleri Oil for Food Packaging

Applications. *Sustain.* **2022**, *14* (14), 8657. https://doi.org/10.3390/su14148657.

(380) Zhou, X.; Li, Y.; Fang, C.; Li, S.; Cheng, Y.; Lei, W.; Meng, X. Recent Advances in Synthesis of Waterborne Polyurethane and Their Application in Water-Based Ink: A Review. *J. Mater. Sci. Technol.* **2015**, *31* (7), 708–722. https://doi.org/10.1016/J.JMST.2015.03.002.

(381) Cataldi, P.; Ceseracciu, L.; Marras, S.; Athanassiou, A.; Bayer, I. S. Electrical Conductivity Enhancement in Thermoplastic Polyurethane-Graphene Nanoplatelet Composites by Stretch-Release Cycles. *Appl. Phys. Lett.* **2017**, *110* (12), 121904. https://doi.org/10.1063/1.4978865.

(382) Sethi, D.; Ram, R.; Khastgir, D. Electrical Conductivity and Dynamic Mechanical Properties of Silicon Rubber-Based Conducting Composites: Effect of Cyclic Deformation, Pressure and Temperature. *Polym. Int.* **2017**, *66* (9), 1295–1305. https://doi.org/10.1002/PI.5385.

(383) Mohanraj, G. T.; Chaki, T. K.; Chakraborty, A.; Khastgir, D. Measurement of AC Conductivity and Dielectric Properties of Flexible Conductive Styrene–Butadiene Rubber-Carbon Black Composites. *J. Appl. Polym. Sci.* **2007**, *104* (2), 986–995. https://doi.org/10.1002/APP.25561.

(384) Das, N. C.; Chaki, T. K.; Khastgir, D. Effect of Axial Stretching on Electrical Resistivity of Short Carbon Fibre and Carbon Black Filled Conductive Rubber Composites. *Polym. Int.* **2002**, *51* (2), 156–163. https://doi.org/10.1002/PI.811.

(385) Bayer, I. S. MEMS-Based Tactile Sensors: Materials, Processes and Applications in Robotics. *Micromachines* **2022**, *13* (12), 2051. https://doi.org/10.3390/mi13122051.

(386) Orts Mercadillo, V.; Chan, K. C.; Caironi, M.; Athanassiou, A.; Kinloch, I. A.; Bissett, M.; Cataldi, P. Electrically Conductive 2D Material Coatings for Flexible and Stretchable Electronics: A Comparative Review of Graphenes and MXenes. *Adv. Funct. Mater.* **2022**, *32* (38), 2204772. https://doi.org/10.1002/adfm.202204772.

(387) Jin, F. L.; Li, X.; Park, S. J. Synthesis and Application of Epoxy Resins: A Review. *J. Ind. Eng. Chem.* **2015**, *29*, 1–11. https://doi.org/10.1016/j.jiec.2015.03.026.

(388) May, C. A. Introduction to Epoxy Resins. *Epoxy Resins* **2018**, 1–8. https://doi.org/10.1201/9780203756713-1.

(389) Li, Y. D.; Jian, X. Y.; Zhu, J.; Du, A. K.; Zeng, J. B. Fully Biobased and High Performance Epoxy Thermosets from Epoxidized Soybean Oil and Diamino Terminated Polyamide 1010 Oligomers. *Polym. Test.* **2018**, *72*, 140–146. https://doi.org/10.1016/j.polymertesting.2018.10.010.

(390) Jian, X. Y.; An, X. P.; Li, Y. D.; Chen, J. H.; Wang, M.; Zeng, J. B. All Plant Oil Derived Epoxy Thermosets with Excellent Comprehensive Properties. *Macromolecules* **2017**, *50* (15), 5729–5738. https://doi.org/10.1021/acs.macromol.7b01068.

(391) Zhang, C.; Garrison, T. F.; Madbouly, S. A.; Kessler, M. R. Recent Advances in Vegetable Oil-Based Polymers and Their Composites. *Prog. Polym. Sci.* **2017**, *71*, 91–143. https://doi.org/10.1016/J.PROGPOLYMSCI.2016.12.009.

(392) Xing, C.; Matuana, L. M. Epoxidized Soybean Oil-Plasticized Poly(Lactic Acid) Films Performance as Impacted by Storage. *J. Appl. Polym. Sci.* **2016**, *133* (12). https://doi.org/10.1002/app.43201.

(393) Zeng, R. T.; Wu, Y.; Li, Y. D.; Wang, M.; Zeng, J. B. Curing Behavior of Epoxidized Soybean Oil with Biobased Dicarboxylic Acids. *Polym. Test.* **2017**, *57*, 281–287. https://doi.org/10.1016/J.POLYMERTESTING.2016.12.007.

(394) Montarnal, D.; Capelot, M.; Tournilhac, F.; Leibler, L. Silica-like Malleable Materials from Permanent Organic Networks. *Science (80-.).* **2011**, *334* (6058), 965–968. https://doi.org/10.1126/science.1212648.

(395) Denissen, W.; Winne, J. M.; Du Prez, F. E. Vitrimers: Permanent Organic Networks with Glass-like Fluidity. *Chem. Sci.* **2016**, *7* (1), 30–38. https://doi.org/10.1039/c5sc02223a.

(396) Zhang, B.; Kowsari, K.; Serjouei, A.; Dunn, M. L.; Ge, Q. Reprocessable Thermosets for Sustainable Three-Dimensional Printing. *Nat. Commun. 2018 91* **2018**, *9* (1), 1–7. https://doi.org/10.1038/s41467-018-04292-8.

(397) Tellers, J.; Pinalli, R.; Soliman, M.; Vachon, J.; Dalcanale, E. Reprocessable Vinylogous Urethane Cross-Linked Polyethylene: Via Reactive Extrusion. *Polym. Chem.* **2019**, *10* (40), 5534–5542. https://doi.org/10.1039/c9py01194c.

(398) Blumenthal, T.; Meruga, J.; Stanley May, P.; Kellar, J.; Cross, W.; Ankireddy, K.; Vunnam, S.; Luu, Q. N. Patterned Direct-Write and Screen-Printing of NIR-to-Visible Upconverting Inks for Security Applications. *Nanotechnology* **2012**, *23* (18), 185305. https://doi.org/10.1088/0957-4484/23/18/185305.

(399) Philip, B.; Jewell, E.; Worsley, D. The Impact of Solvent Characteristics on Performance and Process Stability of Printed Carbon Resistive Materials. *J. Coatings Technol. Res.* **2016**, *13* (5), 911–920. https://doi.org/10.1007/s11998-016-9802-8.

(400) Hatala, M.; Gemeiner, P.; Hvojnik, M.; Mikula, M. The Effect of the Ink Composition on the Performance of Carbon-Based Conductive Screen Printing Inks. *J. Mater. Sci. Mater. Electron.* **2019**, *30* (2), 1034–1044. https://doi.org/10.1007/s10854-018-0372-7.

(401) Zhang, K.; Li, T.; Zhang, T.; Wang, C.; Wang, C.; Wu, M. Adhesion Improvement of UV-Curable Ink Using Silane Coupling Agent onto Glass Substrate. *http://dx.doi.org/10.1080/01694243.2012.746159* **2013**, *27* (13), 1499–1510. https://doi.org/10.1080/01694243.2012.746159.

(402) Zhang, Y.; Cen, Q.; Xu, X.; Li, W.; Zhao, Y.; Li, W.; Liu, Q.; Chen, M.; Guo, N.; Wu, W.; Sun, S. The Effect of PVAc in Silver Ink for Adhesion and Conductivity of Conductive Pattern. *J. Mater. Res. Technol.* **2022**, *18*, 4277–4284. https://doi.org/10.1016/J.JMRT.2022.04.095.

(403) Lux, F. Models Proposed to Explain the Electrical Conductivity of Mixtures Made of Conductive and Insulating Materials. *J. Mater. Sci.* **1993**, *28* (2), 285–301. https://doi.org/10.1007/BF00357799/METRICS.

(404) Vieira, L. de S.; dos Anjos, E. G. R.; Verginio, G. E. A.; Oyama, I. C.; Braga, N. F.; da Silva, T. F.; Montagna, L. S.; Passador, F. R. A Review Concerning the Main Factors That Interfere in the Electrical Percolation Threshold Content of Polymeric Antistatic Packaging with Carbon Fillers as Antistatic Agent. *Nano Sel.* **2022**, *3* (2), 248–260. https://doi.org/10.1002/nano.202100073.

(405) Li, J.; Ma, P. C.; Chow, W. S.; To, C. K.; Tang, B. Z.; Kim, J. K. Correlations between Percolation Threshold, Dispersion State, and Aspect Ratio of Carbon Nanotubes. *Adv. Funct. Mater.* **2007**, *17* (16), 3207–3215. https://doi.org/10.1002/adfm.200700065.

(406) Motaghi, A.; Hrymak, A.; Motlagh, G. H. Electrical Conductivity and Percolation Threshold of Hybrid Carbon/Polymer Composites. *J. Appl. Polym. Sci.* **2015**, *132* (13). https://doi.org/10.1002/app.41744.

(407) Azizi, S.; David, E.; Fréchette, M. F.; Nguyen-Tri, P.; Ouellet-Plamondon, C. M. Electrical and Thermal Phenomena in Low-Density Polyethylene/Carbon Black Composites near the Percolation Threshold. *J. Appl. Polym. Sci.* **2019**, *136* (6), 47043. https://doi.org/10.1002/app.47043.

(408) Yang, W.; Yu, S.; Sun, R.; Ke, S.; Huang, H.; Du, R. Electrical Modulus Analysis on the Ni/CCTO/PVDF System near the Percolation Threshold. *J. Phys. D. Appl. Phys.* **2011**, *44* (47), 475305. https://doi.org/10.1088/0022-3727/44/47/475305.

(409) Yang, W.; Wang, C.; Arrighi, V. An Organic Silver Complex Conductive Ink Using Both Decomposition and Self-Reduction Mechanisms in Film Formation. *J. Mater. Sci. Mater. Electron.* **2018**, *29* (4), 2771–2783. https://doi.org/10.1007/s10854-017-8205-7.

(410) Bhat, K. S.; Nakate, U. T.; Yoo, J. Y.; Wang, Y.; Mahmoudi, T.; Hahn, Y. B. Cost-Effective Silver Ink for Printable and Flexible Electronics with Robust Mechanical Performance. *Chem. Eng. J.* **2019**, *373*, 355–364. https://doi.org/10.1016/j.cej.2019.05.033.

(411) Zhang, J.; Ahmadi, M.; Serra, M.; Jimenez-Pique, E.; Llanes, L.; Fargas, G. Integration of Conductive Silver Sensors on Zirconia Ceramics by Screen-Printing for Monitoring Strain under Applied Load. *Ceram. Int.* **2022**. https://doi.org/10.1016/J.CERAMINT.2022.12.005.

(412) Merilampi, S.; Laine-Ma, T.; Ruuskanen, P. The Characterization of Electrically Conductive Silver Ink Patterns on Flexible Substrates. *Microelectron. Reliab.* **2009**, *49* (7), 782–790. https://doi.org/10.1016/j.microrel.2009.04.004.

(413) Yao, S.; Zhu, Y. Nanomaterial-Enabled Stretchable Conductors: Strategies, Materials and Devices. *Adv. Mater.* **2015**, *27* (9), 1480–1511. https://doi.org/10.1002/adma.201404446.

(414) Rogers, J. A.; Someya, T.; Huang, Y. Materials and Mechanics for Stretchable Electronics. *Science (80-.).* **2010**, *327* (5973), 1603–1607. https://doi.org/10.1126/science.1182383.

(415) Suikkola, J.; Björninen, T.; Mosallaei, M.; Kankkunen, T.; Iso-Ketola, P.; Ukkonen, L.; Vanhala, J.; Mäntysalo, M. Screen-Printing Fabrication and Characterization of Stretchable Electronics. *Sci. Rep.* **2016**, *6*. https://doi.org/10.1038/srep25784.

(416) Ayode Otitoju, T.; Ugochukwu Okoye, P.; Chen, G.; Li, Y.; Onyeka Okoye, M.; Li, S. Advanced Ceramic Components: Materials, Fabrication, and Applications. *J. Ind. Eng. Chem.* **2020**, *85*, 34–65. https://doi.org/10.1016/j.jiec.2020.02.002.

(417) Wang, C.; Xia, K.; Zhang, Y.; Kaplan, D. L. Silk-Based Advanced Materials for Soft Electronics. *Acc. Chem. Res.* **2019**, *52* (10), 2916–2927. https://doi.org/10.1021/acs.accounts.9b00333.

(418) O'Connor, M. P.; Zimmerman, J. B.; Anastas, P. T.; Plata, D. L. A Strategy for Material Supply Chain Sustainability: Enabling a Circular Economy in the Electronics Industry through Green Engineering. *ACS Sustain. Chem. Eng.* **2016**, *4* (11), 5879–5888. https://doi.org/10.1021/acssuschemeng.6b01954.

Appendices

Appendix A

synthesizing cross-linker DBEDT (diboronic ester dithiol)

REACTION:

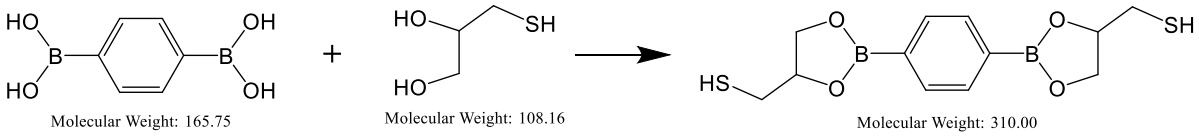

SUBSTRATE	MOLAR MASS	QUANTITY	MOL	MOL EQUIVALENT
Benzene-1,4-diboronic acid	165.75	20 g	120 mmol	1.0
Thioglycerol	108.16	25.96 g	240 mmol	2.0

Reaction procedure:

Benzene-1,4-diboronic acid (20.00 g, 120 mmol) and thioglycerol (25.96 g, 240 mmol) were dissolved in ethanol (500 mL). After 24 hours at room temperature, the solution was filtered and concentrated under reduced pressure to obtain the target compound as a white solid.